University of Tennessee, Knoxville
Trace: Tennessee Research and Creative Exchange

Masters Theses | Graduate School

12-2008

Moisture Degradation of CTD-403: Testing the Application of Cyanate Ester Insulations to Fusion Devices

Bradley Ian Morgan
University of Tennessee - Knoxville

Recommended Citation

Morgan, Bradley Ian, "Moisture Degradation of CTD-403: Testing the Application of Cyanate Ester Insulations to Fusion Devices. " Master's Thesis, University of Tennessee, 2008.
https://trace.tennessee.edu/utk_gradthes/471

This Thesis is brought to you for free and open access by the Graduate School at Trace: Tennessee Research and Creative Exchange. It has been accepted for inclusion in Masters Theses by an authorized administrator of Trace: Tennessee Research and Creative Exchange. For more information, please contact trace@utk.edu.

To the Graduate Council:

I am submitting herewith a thesis written by Bradley Ian Morgan entitled "Moisture Degradation of CTD-403: Testing the Application of Cyanate Ester Insulations to Fusion Devices." I have examined the final electronic copy of this thesis for form and content and recommend that it be accepted in partial fulfillment of the requirements for the degree of Master of Science, with a major in Mechanical Engineering.

Madhu S. Madhukar, Major Professor

We have read this thesis and recommend its acceptance:

J.A.M Boulet, John D. Landes

Accepted for the Council:
Carolyn R. Hodges

Vice Provost and Dean of the Graduate School

(Original signatures are on file with official student records.)

To the Graduate Council:

I am submitting herewith a thesis written by Bradley Ian Morgan entitled "Moisture Degradation of CTD-403: Testing the Application of Cyanate Ester Insulations to Fusion Devices." I have examined the final electronic copy of this thesis for form and content and recommend that it be accepted in partial fulfillment of the requirements for the degree of Master of Science, with a major in Mechanical Engineering.

Madhu S. Madhukar

Major Professor

We have read this thesis and
recommend its acceptance:

J.A.M Boulet

John D. Landes

Accepted for the Council:

Carolyn R. Hodges

Vice Provost and Dean of the Graduate School

(Original signatures are on file with official student records.)

MOISTURE DEGRADATION OF CTD-403:

TESTING THE APPLICATION OF CYANATE ESTER INSULATIONS TO FUSION DEVICES

A Thesis
Presented for the
Master of Science
Degree
The University of Tennessee, Knoxville

Bradley Ian Morgan
December, 2008

Copyright © 2008 by Bradley Ian Morgan
All rights reserved.

ACKNOWLEDGMENTS

I would like to first thank my mentor and guide, Dr. Madhukar. The opportunities that I have been given are because of him. He must also be recognized for all the conversations I have had with him ranging from moisture absorption mechanisms to the proper presentation of results, as well as motivating me to be concise in my work. I would also like to thank Dr. Landes and Dr. Boulet for their academic support and for serving on my thesis committee.

I am greatly appreciative for the help of Matthew Hooker, Jennifer Walsh, Samuel Grandlienard, and Kimiko Kano from Composite Technology Development, Inc. It was an honor working with each of them. The conclusions made in my research were all in part because of their guidance and suggestions. I appreciate the timely responses to all my emails. I could have in no way felt as confident in my work without their guidance and support.

The opportunity of working with UT and ORNL faculty at the Magnet Development Lab has been extraordinary. I am especially thankful to Bob Benson for supporting my research and allowing me the opportunity to work at the Magnet Development Lab. Thank you for your time and support.

Last but definitely not least, I would like to thank my parents. It would be impossible to express in words the gratitude I have for their love and guidance. I am who I am today because of them, and everything I have accomplished is because of their support.

ABSTRACT

The fusion devices currently being developed present several challenges for magnet designers. One challenge lies within the electrical insulation, which must be able to withstand extreme temperatures (both cryogenic and elevated temperatures), large shear and compressive stresses, high operating voltages, and high levels of incident radiation. To address the need for better performing insulation systems, Composite Technology Development, Inc. (CTD) has developed CTD-403, a cyanate ester resin with increased radiation resistance, ease of processing and fabrication, low moisture absorption characteristics, and high mechanical and electrical strength at cryogenic and elevated temperatures.

In this thesis, CTD-403 resin based insulation systems were tested under the operation guidelines of the Quasi-Poloidal Stellarator (QPS). Because the coils of QPS are water cooled, it is important to understand the effects of long term humidity exposure on the insulation. The effects of humidity on moisture absorption characteristics, dimensional stability, mechanical and electrical properties were characterized. Increasing the humidity level caused a corresponding increase in the saturation level, while increasing the temperature of exposure magnified these effects causing more pronounced non-Fickian behavior. The mechanical properties degraded with an increase in humidity level. Elevated temperature effects are more pronounced on the compressive properties than the tensile properties. The glass transition temperature was more greatly affected by elevated temperature exposure as opposed to increased humidity exposure, decreasing in both

instances. The dielectric strength decreases with increased humidity level and exposure time.

Based on these findings, the performance of cyanate ester resin based insulation systems is shown superior to that of traditional epoxy based resin systems in all performance measures. The degradation of the mechanical and electrical properties of the insulation from long term effects of humidity and elevated temperature exposure are shown to be within the performance criteria bounds, and the insulation is therefore recommended for use in current and future fusion programs.

TABLE OF CONTENTS

Chapter **Page**

Chapter **Page**

LIST OF TABLES

LIST OF FIGURES

Figure **Page**

Figure **Page**

List of Abbreviations

CE	Cyanate Ester
RH	Relative humidity
T_g	Glass transition temperature
M_t	Moisture content at time t
M_∞	Moisture content at saturation
M_o	Initial moisture content
ILSS	Interlaminar shear strength
CTD	Composite Technology Development, Inc.
DMA	Dynamic Mechanical Analysis
QPS	Quasi-Poloidal Stellarator
ORNL	Oak Ridge National Laboratory
D	Diffusion coefficient
D_c	Corrected diffusion coefficient
w	Measured and final weight of samples
w_d	Initial weight of samples
Cu	Copper
VPI	Vacuum pressure impregnation

CHAPTER I

INTRODUCTION

1.1 Energy Crisis

In the year 2008, energy consumption has reached an all time high with a large economic and environmental price. Environmental concerns were originally local in character, but the greenhouse effect has now widened to cover regional and global issues. The energy crisis has become a major political issue as well as the subject of international debate and regulation. Although oil extraction has become increasingly efficient with current technological advances, there is a struggle to provide oil due to costly and less productive methods such as deep sea drilling, as well as developing environmentally sensitive areas like the Arctic National Wildlife Refuge. The challenge arises to find clean renewable energy, reducing dependence on fossil fuels and other environmentally harmful sources in order to sustain the world's perpetual increase in energy consumption (Figure 1.1).

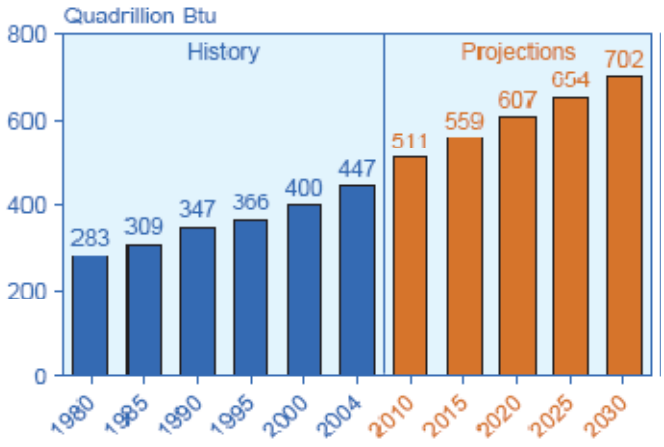

Figure 1.1 World Marketed Energy Consumption 1980- 2030 [1]

It is for these reasons that the principles of sustainable living and green energy are finally gaining popularity. Alternative power research such as hydrogen fuel, biodiesel, solar energy, geothermal energy, wind energy, tidal energy, fusion power, and fuel cell technology is growing. In the year 2008, hydroelectricity and nuclear power have shown to be the only significant alternatives to fossil fuels.

1.2 Nuclear Fission

According to the Energy Information Administration, nuclear power accounts for approximately 19 percent of the total electricity generated in the United States. A nuclear power plant operates the same way a fossil fuel plant does, with the exception of the heat source. Fissioning, or the splitting of uranium atoms, is the process that produces heat in a nuclear power plant. Compared to the electricity generated by burning fossil fuels, nuclear energy is clean. No air pollution or carbon dioxide is created by nuclear power plants, but there are many sources of radioactive waste in the fission cycle, and the problem of waste disposal is yet to be solved. Fission reactors also carry the danger of a nuclear accident, where runaway reactors and meltdowns are a reality.

1.3 Nuclear Fusion

Nuclear fusion reactions release 3 to 4 times the amount of energy than a fission reaction, and the output energy is 50-100 times greater than the energy needed to initiate the fusion reaction. This is due to a much greater amount of mass being transformed into energy in a fusion reaction. Fusion reactors use Deuterium and Tritium as fuel, which are in abundance on the earth. Deuterium is found in water and Tritium can be bred on site

using a Lithium reaction. The waste product is Helium, an inert gas that is harmless. Nuclear fusion also escapes the dangers of nuclear accidents, as the fuel is only inserted as needed, so should it become uncontrolled it simply dies out.

The key problem with fusion power is that the ignition temperatures for the reactions start at 100 million degrees Celsius. At this temperature, all gases ionize (electrons separate from nuclei) to form plasma. The main challenge in fusion reactors is the development, confinement, and sustenance of plasma [2].

1.3.1 Quasi-Poloidal Stellarator (QPS)

The Quasi-Poloidal Stellarator (QPS), as seen in Figure 1.2, is a very low aspect ratio stellarator experiment intended to test the novel confinement properties of Quasi-Poloidal symmetry [3]. Stellarators are a class of magnet fusion confinement devices

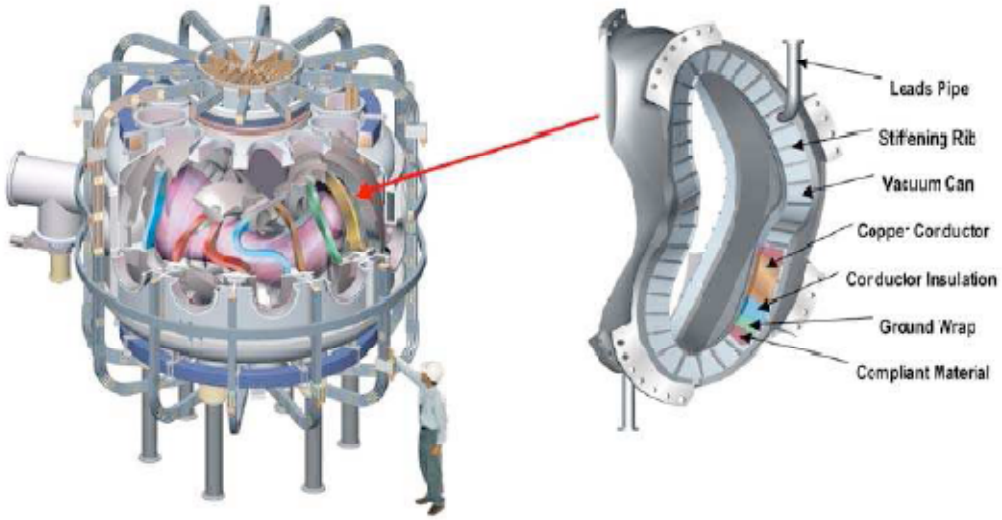

Figure 1.2 Construction concept for QPS compact stellarator device

characterized by three dimensional magnetic fields and plasma shapes and are one of the best developed classes of magnet fusion devices. QPS is currently in its early stages of development being investigated by Oak Ridge National Lab (ORNL) and the University of Tennessee. All of the QPS coil sets are water cooled and operate at or above room temperature.

1.4 Insulation Requirements

The design of QPS and other planned future fusion devices (Table 1.1) will demand that the electrical insulation used in the construction of the magnets reliably withstand a variety of challenging operational conditions. Requirements for fusion magnet insulation include the ability to withstand extreme temperatures (both cryogenic and elevated temperatures up to 150 degrees Celsius), large shear and compressive stresses, high operating voltages, and high levels of incident radiation (from 20 to 100 MGy) [4]. The primary mechanical stresses within fusion magnets are compressive stresses, normally held to 300-500 Mpa. In some instances, shear stresses are also developed, but usually held to 60 Mpa or less. Magnet insulation must also maintain its electrical integrity throughout its life, after exposure to high levels of radiation and mechanical stresses.

In addition to the challenging operating conditions, the insulation must also have a low viscosity and a long pot-life to enable efficient magnet fabrication. High viscosities can cause mold pressures that may be too high in both the mold and the injection unit. All of the QPS modular coils will be wound using a flexible copper conductor with an internal water-cooling line. These coils were originally designed to function between 40 and 65 degrees Celsius, but could operate at up to 100 degrees Celsius if the insulation system

Table 1.1 High-performance insulation requirements for various magnet systems.

Application	Insulation Requirements
ITER TF Coils	Very long pot life Radiation Resistance to >25 MGy
MAST	Operating temperatures to 150°C Radiation Resistance
QPS Modular Coils	Operating temperatures up to 150°C, Resistance to moisture/humidity
Large Hadron Collider (LHC) (CERN)	Radiation Resistance to >100 MGy
Medical Accelerators	Continuous operation at 50°C, Radiation Resistance to ~20 MGy

was capable of withstanding higher temperatures [5]. The conductor design provides for improved thermal performance of the machine, but the presence of the internal water cooling system necessitates that the insulation also be resistant to moisture and humidity, further adding to the requirements for the electrical insulation system.

1.5 Epoxy vs. Cyanate Ester Based Insulation Systems

To address the need for better performing insulation systems, Composite Technology Development, Inc. (CTD) has developed CTD-403, a cyanate ester resin with increased radiation resistance [1,6,7], ease of processing and fabrication, low moisture absorption characteristics, and high mechanical and electrical strength at cryogenic and elevated temperatures.

Epoxy polymers have been widely used for many important applications such as adhesives, reinforced plastic, insulating materials, and as a matrix for advanced

composite materials [8, 9] but are unsuitable for use in fusion magnets due to their relatively high dielectric loss and high propensity for water absorption, characterized by a 1-7% weight gain when exposed to humidity. Moisture absorption physically weakens the polymer (i.e. micro cracking, swelling, softening of the polymer, etc.) and may also chemically attack the polymer [10]. Epoxy resins have also been shown to degrade to unacceptable levels of performance when exposed to high levels of radiation, particularly the dose levels being considered for next generation fusion devices [1]. Additionally, the glass transition temperature (T_g) of epoxy insulations is much to low having operational temperatures of 50 to 65 degrees Celsius.

CTD-403, a cyanate ester based insulation developed by CTD, exhibits several desirable properties for use in magnet systems. CTD-403 is a thermosetting resin that displays improved strength and toughness at cryogenic and elevated temperatures as compared to typical epoxy based insulations. CTD-403 also displays high dielectric breakdown strength, excellent radiation resistance, a high glass transition temperature, and very good adhesion to both metals and glass fibers [11,6,12]. CTD-403 also has a lower viscosity and longer pot life that allows for lower impregnation temperatures and provides enhanced flexibility for the magnet fabricator. Therefore, the crosslinking reactions in CTD-403 will not advance at processing temperatures on the order of 50 degrees Celsius allowing the resin flow to remain uniform throughout the impregnation process thus yielding repeatable, highly uniform insulation [4].

1.6 Humidity Testing

This research focuses on the effects of humidity exposure in cyanate Ester resins. CTD-403 resin was used in testing, and QPS performance criteria were used as testing guidelines (fusion specific property measurements). The number of publications on moisture degradation of cyanate ester resins is small (a review of the current literature is found in Chapter 2), and in order to ensure long term use of CTD-403 in fusion devices, the performance criteria as outlined above must be validated through rigorous laboratory testing. Aging effects were studied using three constant humidity conditions. One elevated temperature condition was also studied. Three specimen types were used: neat (or unfilled) resin plates, S2-glass reinforced composites, and copper/insulation adhesive test specimens. Specimens involving a copper laminate were used because the resin is required to bond to the copper coils in magnet systems such as QPS. These specimens were included to examine how the interface behaved after long term exposure. The neat resin plates were used to identify the amounts of moisture absorption CTD-403 underwent throughout the test period. The moisture absorption as well as dimensional change for each composite was tracked over a 6 month aging period. The mechanical and electrical properties were also evaluated at five different periods throughout the aging process.

CHAPTER II

REVIEW OF LITERATURE

2.1 Overview

Epoxy resin R&D has provided a rich and high performing family of resin materials that have found extensive commercial and aerospace application. One drawback of epoxy resins is a tendency to absorb moisture both in the green or uncured and the cured stages [13]. This property of epoxy resins makes them unsuitable for use in the Quasi-Poloidal Stellarator (QPS) because the modular coils are to be wound using a flexible copper conductor with and internal water-cooling line, exposing the resin to high levels of moisture throughout its service life. Moisture absorption produces dimensional change and hence internal stresses. The absorbed water may also seek out and dissolve water soluble inclusions, thereby creating pockets of concentrated solutions which, by either chemical or physical means lead to loss of mechanical strength of the composite [14]. It is for this reason that cyanate ester (CE) polymer materials were developed. A CE matrix is far more moisture resistant than epoxies. Thus, they possess better electrical characteristics and are not subjected to the so called hot/wet T_g service temperature reduction. The lack of database and manufacturing experience inhibits the introduction of the cyanate materials in new systems [14]. This research provides a fundamental understanding of the moisture resistance of CE resins, specifically CTD-403, as well as the degradation that occurs in the mechanical and electrical properties from humidity/elevated temperature exposure.

2.2 Composite Materials

Composite materials are macroscopic combinations of two or more distinct materials having a discrete and recognizable interface separating them. The narrower definition of composites becomes more specific and can be restricted to those combinations of materials that contain high strength/stiffness fiber reinforcements supported by a high performance matrix material [13]. The fiber reinforcements of the composite predominately form the mechanical and physical properties, while the matrix is the adhesive binder that supports the fibers under compressive loads, provides shear capabilities in two dimensional fiber lay-ups, and transfers loads internally.

2.2.1 The Matrix

The matrix binds the fibers together by virtue of its cohesive and adhesive nature characteristics, and serves the purpose to transfer load to and between fibers, and to protect them from environments and handling. The matrix is the "weak link" in the composite; especially because resins do not presently exist that allow the utilization of the stresses that fibers are able to withstand [13]. The matrix plays a minor role in the tensile load-carrying capacity of a composite structure. However, the matrix serves the purpose of providing resistance to crack propagation and damage as well as influencing the compressive, interlaminar shear as well as in-plane shear properties of the composite. The matrix also provides lateral support against the possibility of fiber buckling under compressive loading thus influencing to a large extent, the compressive strength of the composite material. Finally, the processing and defects in a composite material depend strongly on the processing characteristics of the matrix. For example, for epoxy

polymers used as matrix in many aerospace composites, the processing characteristics include the liquid viscosity, the curing temperature and the curing time [15]. Most importantly for applications in fusion devices, the matrix generally determines the overall service temperature limitations of the composite as well as controlling its environmental resistance.

2.2.2 Cyanate Ester Based Polymer Materials

Cyanate esters are a relatively new class of thermosetting polymers that have become a popular replacement for other thermosets in the aerospace and microelectronics sectors because they possess a good combination of high temperature stability and excellent mechanical properties [16,17]. In addition, cyanate esters have excellent adhesive properties, are more resistant to moisture absorption than other thermosets (such as bismaleimides (BMIs) and epoxies), and have very low dielectric constants [16,17]. The greatest difference in processing between epoxies and cyanate esters is that cyanate esters require a relatively high curing temperature. Curing of cyanate esters is catalyzed by heat or a combination of heat and a catalyst, which is most commonly a carboxylate or chelate salt of a transition metal dissolved in an active hydrogen co-catalyst such as nonylphenol [16,18]. In a thermoset polymer (Figure 2.1), the molecules are chemically joined together by cross-links, forming a rigid, three-dimensional network structure. Once these cross-links are formed during the polymerization reaction (curing reaction), the thermoset polymer cannot be melted by the application of heat. However, if the number of cross links is low, it may still be possible to soften them at elevated temperatures.

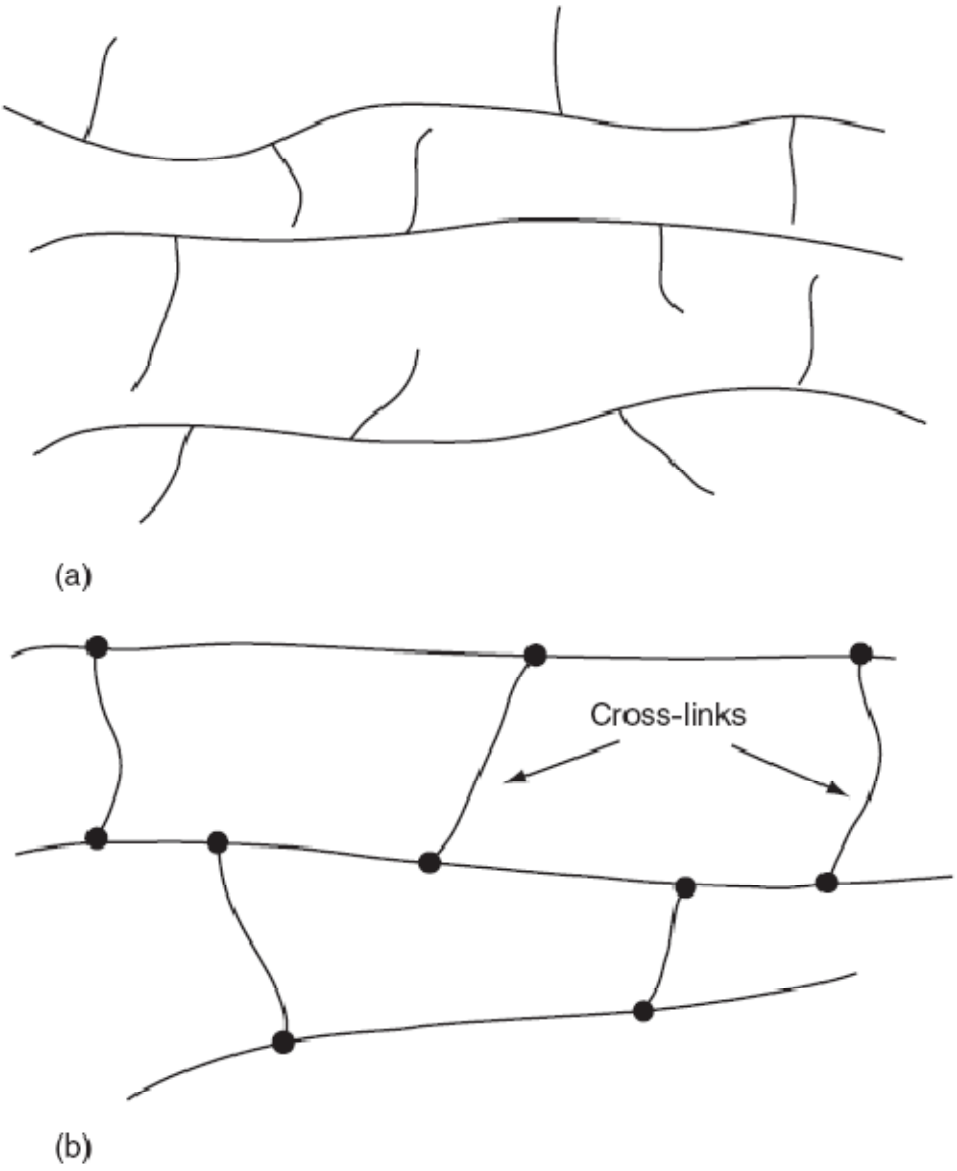

Figure 2.1 Schematic representation of (a) thermoplastic polymer and (b) thermoset Polymer [15].

2.2.3 Fibers

Fibers are the principal constituents in a fiber reinforced material. They occupy the largest volume fraction in a composite laminate and share the major portion of the load acting on a composite structure [15]. The fiber influences the following characteristics of a composite laminate:

1.) Density
2.) Tensile Strength and Modulus
3.) Compressive Strength and Modulus
4.) Fatigue Strength
5.) Electrical Conductivities
6.) Thermal Conductivities
7.) Cost

Figure 2.2 lists a number of commercially available fibers and their properties. Tensile properties listed are the average values reported by the fiber manufacturers. S2-glass fiber reinforcement of CTD-403 is tested in this research which will be covered in the next section. From Figure 2.2 it is seen that S-glass has slightly improved performance as compared to E-glass. The density of S-glass is also slightly lower when compared to E-glass.

Fiber	Typical Diameter (μm)[a]	Density (g/cm^3)	Tensile Modulus GPa (Msi)	Tensile Strength GPa (ksi)	Strain-to-Failure (%)	Coefficient of Thermal Expansion ($10^{-6}/°C$)[b]	Poisson's Ratio
Glass							
E-glass	10 (round)	2.54	72.4 (10.5)	3.45 (500)	4.8	5	0.2
S-glass	10 (round)	2.49	86.9 (12.6)	4.30 (625)	5.0	2.9	0.22
PAN carbon							
T-300[c]	7 (round)	1.76	231 (33.5)	3.65 (530)	1.4	−0.6 (longitudinal) 7–12 (radial)	0.2
AS-1[d]	8 (round)	1.80	228 (33)	3.10 (450)	1.32		
AS-4[d]	7 (round)	1.80	248 (36)	4.07 (590)	1.65		
T-40[c]	5.1 (round)	1.81	290 (42)	5.65 (820)	1.8	−0.75 (longitudinal)	
IM-7[d]	5 (round)	1.78	301 (43.6)	5.31 (770)	1.81		
HMS-4[d]	8 (round)	1.80	345 (50)	2.48 (360)	0.7		
GY-70[e]	8.4 (bilobal)	1.96	483 (70)	1.52 (220)	0.38		
Pitch carbon							
P-55[c]	10	2.0	380 (55)	1.90 (275)	0.5	−1.3 (longitudinal)	
P-100[c]	10	2.15	758 (110)	2.41 (350)	0.32	−1.45 (longitudinal)	
Aramid							
Kevlar 49[f]	11.9 (round)	1.45	131 (19)	3.62 (525)	2.8	−2 (longitudinal) 59 (radial)	0.35
Kevlar 149[f]		1.47	179 (26)	3.45 (500)	1.9		
Technora[g]		1.39	70 (10.1)	3.0 (435)	4.6	−6 (longitudinal)	

Figure 2.2 Properties of Selected Commercial Reinforcing Fibers [15].

2.2.4 Glass Reinforced Composite Materials

Glass fibers are the most common of all reinforcing fibers for polymeric matrix composites (PMC). The principal advantages of glass fibers are low cost, high tensile strength, high chemical resistance, and excellent insulating properties [15]. Some drawbacks of glass fibers are the relatively low tensile modulus and high density. Glass fibers also display a high sensitivity to abrasion during handling which frequently decreases their tensile strength, as well as a relatively low fatigue resistance. There are two types of glass fibers commonly used in fiber reinforced composite; E-glass and S-glass. E-glass has the lowest cost of all commercially available reinforcing fibers. S-glass has the highest tensile strength among all fibers in use. S-glass is much more expensive due to the compositional difference and higher manufacturing cost. A lower cost version of S-glass, called S-2 glass, is also available. S-2 glass is manufactured with less stringent nonmilitary specifications, but its tensile strength and modulus are similar to those of S-glass [15]. S2-glass is used as the fiber reinforcement in nuclear applications for many reasons, but most importantly it is boron free. Boron is added to glass melts because it reduces the viscosity and lowers the processing temperature. Boron is a neutron absorber, so in nuclear applications boron containing materials need to be minimized.

2.3 Hygrothermal Effect of Polymer Materials

Hygrothermal effects of polymers are extremely important because water and temperature are the most common factors reducing the performance of composites. Above all, sorbed moisture promotes material degradation, plasticization, swelling, and

lowered T_g of the composite matrix. Absorbed moisture plasticizes the resin matrix and lowers the strength of the composite in non-fiber dominated directions. A study on the physical properties of polytherimide performed by Merdas et al. [19] showed that water absorption affected important resin properties such as glass transition temperature, viscoelastic behavior of the polymer resin, and tensile properties. T_g decreased with exposure to moisture absorption, indicating that water significantly affected plasticizing. The tensile properties of the polyetherimide were seen to decrease with water absorption.

A study performed by Y.Z. Wan et al. [20] on the moisture sorption and mechanical degradation of carbon-epoxy composites showed a reduction of mechanical properties of three dimensional and unidirectional composites after moisture uptake. The 3D composites demonstrated lower losses of mechanical properties (flexural strength, flexural modulus, and shear strength) than the unidirectional composites after reaching saturation, indicating the 3D composites were less sensitive to moisture attack as a result of a lower effective interface area. The losses of the mechanical properties were found to be mainly dominated by the interface failure. It was also found that the unidirectional and 3D composites moisture absorption process could be described by Fick's second law of diffusion (Fick's law is described in sections below). The resemblance between the two composites suggested that the complex structure of the 3D fabric did not change the moisture diffusion pattern, except that the 3D composites showed a lower diffusion rate.

2.3.1 Moisture Absorption Kinetics

Moisture transport in polymer systems is related to the availability of molecular-sized holes in the polymer-water affinity [21]. The availability of holes is dependent upon the

polymer microstructure and crosslink density, which are functions of degree of cure, stoichiometry, molecular chain stiffness, and cohesive energy density of the polymer. Because the moisture is filling the free volume, referred to as unbound molecules, it does not cause dimensional change of the polymer. However, swelling and plasticizing of the polymer is induced by bound molecules (water molecules attaching themselves to the polymer chain via hydrogen bonding) disrupting the interchain hydrogen bonding. Fickian diffusion in polymers is an ideal case of moisture transport, corresponding to free diffusion of moisture without interference of polymer chain rearrangement, i.e., structural relaxation [22].

Moisture induced property degradation tends to correlate well with the extent of absorbed moisture in the polymer matrix. For most practical applications, changes in the percentage of moisture content, M, can be measured gravimetrically, or as changes in weight or mass of the polymer specimen [22]. This is expressed as

$$M = \frac{w - w_d}{w_d} * 100 \tag{2.1}$$

where w is the weight or mass of the material at any time, t, and w_d is the weight or mass of the dry material.

Fick's second law can describe the classical limiting case of diffusion with a constant diffusion coefficient or diffusivity (tendency to become equalized by spreading), D. Fick's second law assumes that water is driven to penetrate the material by the water

concentration gradient. For the one dimensional case of diffusion through an infinite plate of thickness h, the equation is as follows,

$$\frac{\partial M}{\partial t} = D * \frac{\partial^2 M}{\partial x^2} \tag{2.2}$$

where M is the moisture concentration and t is time. The diffusion of moisture into glass polymers generally follows this law when the moisture transport is completely controlled by diffusion, that is, when diffusion mechanisms related to degradation, molecular relaxation, or insufficient curing, for example, are not active [22]. The diffusion coefficient often exhibits temperature dependence that follows an Arrhenius relationship given by,

$$D(T) = D_0 \exp\left(-\frac{A_0}{RT}\right) \tag{2.3}$$

where D_0 is a pre-exponential factor, A_0 is the activation energy for diffusion, R is the universal gas constant, and T is the temperature measured on an absolute scale.
In the initial stages of absorption where $M_t / M_\infty < ½$ and assuming a constant diffusion coefficient, D, Eq. 2.2 can be shown to be approximated by the following (Crank, 1956).

$$\frac{M_t}{M_\infty} = \frac{4}{h} * \sqrt{\frac{Dt}{\pi}} \tag{2.4}$$

Equation 2.4 can be further reduced to

$$M_t = kt^{1/2} \tag{2.5}$$

where

$$k = \frac{4M_\infty}{h} * \sqrt{\frac{D}{\pi}} \tag{2.6}$$

This notation is convenient because k represents the initial slope of the M_t vs. $t^{1/2}$ curve hence D can be calculated. Solving for the diffusion coefficient explicitly,

$$D = \pi \left(\frac{kh}{4M_\infty}\right)^2 \tag{2.7}$$

where

$D =$ the diffusion coefficient,

h = sample thickness

$k =$ initial linear segment of diffusion profile, and

$M_\infty =$ moisture content at equilibrium, independent of time.

If the specimens used to determine the diffusion coefficient are of finite dimensions, a correction for the effect of diffusion through the edges can be made according to

$$D_c = D(1 + \frac{h}{L} + \frac{h}{w})^{-2} \tag{2.8}$$

where

h = sample thickness

L = sample length, and

w = sample width.

The entire moisture-time diffusion profile has been simplified by Shen and Springer [23] to

$$\frac{M_t}{M_\infty} = 1 - \exp\left[-7.3\left(\frac{Dt}{h^2}\right)^{0.75}\right]. \tag{2.9}$$

If the simple Fickian model fails, such as when saturation is not achieved or when two plateaus are noticed in the absorption curve, a more complex Langmuir type model can be applied. Another case for the Langmuir model is when it is found that the absorption depends on the specimen thickness. The Langmuir model assumes absorption to be in two phases, one free to diffuse and the other trapped and not so free to move in the absorbing medium [24]. In addition to the diffusion coefficient and saturation level used in the simple free-phase diffusion model, two other parameters are introduced. α represents the probability of a trapped water molecule being released and γ represents the probability of a free molecule being trapped. The two equations 2.10 and 2.11 represent the model.

$$D\frac{\partial^2 n}{\partial x^2} = \frac{\partial n}{\partial t} + \frac{\partial N}{\partial t} \tag{2.10}$$

$$\frac{\partial N}{\partial t} = \gamma n - \alpha n \tag{2.11}$$

Here, N respresnts the number density of bound molecules, and n represents the number density of mobile molecules. This model can be used to fit the experimental data if necessary. Figure 2.3 displays some typical classes of non-Fickian sorption.

2.3.2 Effects of Moisture Absorption on Composite Performance

Moisture effects on composites have been studied for decades. In a composite, the effects of moisture are predominately seen to reduce matrix dominated properties, such as transverse strength, fracture toughness, and impact resistance.

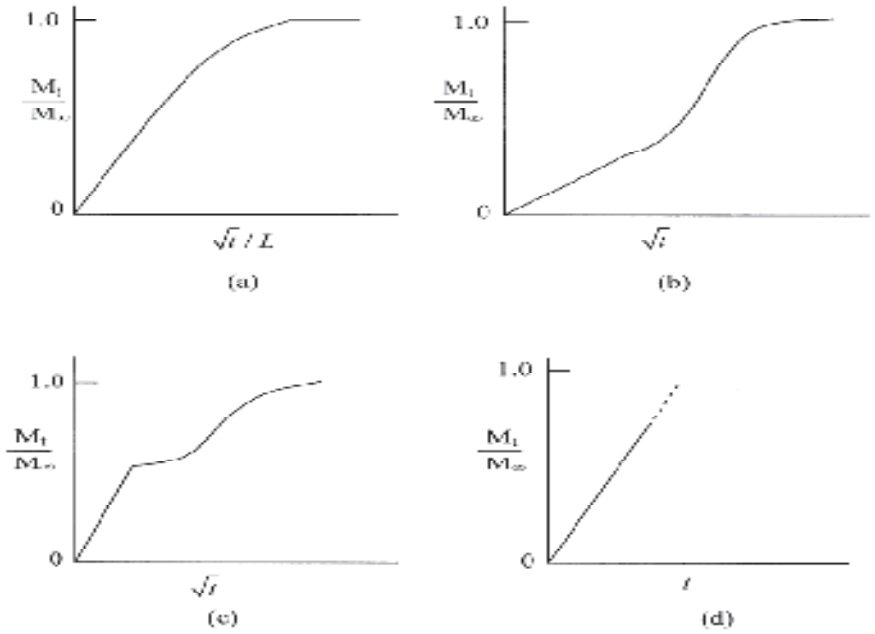

Figure 2.3 Different classes of non-Fickian sorption: (a) classical, (b) sigmoidal, (c) two-step, (d) Case II [25].

When water is absorbed by the matrix, it acts as a plasticizer softening the material and reducing some useful mechanical properties [13]. Lowering of the glass transition temperature is seen to occur in epoxy and polyimide resins with an increase in moisture absorption. Typically, moisture is absorbed in the composite until a saturation level is reached. Mechanical properties degrade in relation to the amount of moisture absorbed, with no further deterioration after saturation is reached. Thermoset composites are much more vulnerable to degradation when compared with thermoplastic composites, because of their characteristically higher moisture absorption trends [26].

Strength reductions in polyester laminates have been found to be 10-15%, while epoxy resins are less vulnerable. The hydrolytic degradation of epoxy results from the scission of the polymer chain, by which also decreases the molecular weight. A vast amount of research can be found on the effects of moisture absorption in epoxy based composites, but very little is found when dealing with the newer cyanate ester counterpart.

Moisture absorption also produces swelling in the resin (volumetric changes), causing dimensional changes. The volumetric change can be computed from the following relationship:

$$\frac{\Delta V(t)}{V_0} = \frac{\rho_m}{\rho_w} M \tag{2.12}$$

where

ρ_m = Matrix Density,

ρ_ω = Water Density ($\approx 1\ kg/mm^2$), and

M = Moisture Content at Time t.

The dilatational strain corresponding to this volumetric change in the resin can be calculated as follows:

$$\varepsilon_m = \frac{1}{3}\frac{\Delta V}{V_0} = \frac{1}{3}\frac{\rho_m}{\rho_w} M = \beta_m M \tag{2.13}$$

where $\beta_m = \frac{1}{3}\frac{\rho_m}{\rho_w}$ and is termed the swelling coefficient. One difficulty in representing the dilatational strain in this manner is that a certain amount of moisture absorbed fills free volume as well as micro cracks in the resin, and in turn does not need to be accounted for when considering volumetric changes [15]. To account for this, the following formulas can be used:

$$\begin{aligned} \varepsilon_m &= o\ for\ M < M_0 \\ &= \beta_m (M - M_0) for\ M > M_0 \end{aligned} \tag{2.14}$$

Here, M_0 is coined the threshold moisture concentration, i.e. the amount of moisture in the free volume as well as micro voids present in the resin. For a variety of cast-epoxy resins, the measured swelling coefficient ranges from 0.26 to 0.33 and the threshold moisture concentration is in the range of 0.3%–0.7%. Dimensional stability must be modeled and accounted for when designing systems with tight enclosures such as QPS. An expansion in the insulation would impose stresses on the system which could ultimately lead to system failure. The dilatational expansion of the matrix around the fiber also reduces the residual stresses at the fiber-matrix interface which were caused by curing shrinkage, altering the performance characteristics of the composite, and possible relieving the mechanical interlocking between the fiber and matrix [15].

In this research, dimensional changes will be measured in order to achieve more accurate results, as opposed to calculated using equations 2.13 and 2.14. Comparing the measured volumetric changes with the volumetric change as defined in Eq. 2.12 can be used as an indicator of the percentage of moisture settling in micro voids.

The superior electrical insulation properties of CTD-403 have been validated through laboratory testing, but the application specific performance (QPS) of the insulation is yet to be validated. For applications in QPS, the insulation must maintain its electrical integrity throughout its life, after exposure to high levels of radiation as well as high levels of humidity. Current magnets typically utilize fiberglass reinforced epoxy composite insulation. These materials provide sufficient electrical insulation, suitable mechanical properties, flexible processing, and reasonable cost. However, epoxy resins degrade to unacceptable levels when exposed to high levels of radiation, particularly dose

levels considered for next generation fusion devices [27, 28]. Epoxy resins have also been shown to have dimensional instability when exposed to humidity. CTD-403 has been shown to provide improved electrical properties over traditional epoxy insulations, but these properties must not degrade when exposed to humidity for long periods of time.

2.3.3 Effects of Temperature on Composite Performance

When dealing with a polymeric matrix composite, matrix dominated properties are more affected by elevated temperatures. Thermal softening causes a decrease in a polymer specimen's modulus and strength with increasing temperature. For this reason, off axis properties of unidirectional laminates are more greatly affected by elevated temperatures, whereas a randomly oriented discontinues fiber composite would see equally reduced strength and modulus in all directions.

The immediate effects of temperature are important, but for purposes of this research the focus will reside mainly on thermal aging due to long term exposure at elevated temperatures without load, which can cause deterioration in the properties of a polymer matrix composite. Studies show [29,30] that properties of the matrix as well as the matrix/fiber interface determine how the composite will act when exposed to elevated temperatures for long periods of time. Kerr and Haskins [29] performed a thermal aging study on carbon-epoxy composites at 121°C. No degradation in mechanical properties was seen in the first 10,000 hours. Matrix degradation began between 10,000 and 25,000 h and was severe after 50,000 h.

2.4 Similar Studies

The topic of modeling and predicting moisture absorption levels of composite materials is one of much controversy. Furthermore, very few hygrothermal studies have been performed on cyanate ester resins. An article titled "Mechanisms of moisture absorption by cyanate ester modified epoxy resin matrices: the clustering of water molecules" by Sunil K. Karad et al. [31] concludes that clustering of water due to the cohesive energy of water occurs in cyanate ester/epoxy blends. The effect of non-random mixing whereby water-clustering is said to occur is an important factor for non-Fickian solutions, determining the concentration of moisture that a polymer will absorb.

Rodriquez et al. [32] suggested that polymers with a strong interaction with water (such as epoxy matrix resins) have negligible degrees of water clustering, while the more hydrophobic polymers (such as cyanate ester matrix resins) exhibit a higher degree of clustering. The absorption of water by epoxies can be attributed to the affinity of the functional groups, which are highly polar, to water molecules [32]. Generally, the more polar the resin, the higher the equilibrium moisture concentration [32]. For the case of the cyanate ester/epoxy blend, clustering was seen to occur at relative humidity values of 40 percent and above. Brown [33] proposed a method of interpreting the sorption of water into certain polar polymers, in which the conventional Flory-Huggins solution theory and cluster theory are combined. Karad et al. [31] concluded that at low relative humidities, the sorption data can be described by the dual-mode sorption model but at high relative humidities, the dual theory can no longer describe the sorption data.

Lee et al. [34] performed a study on the water absorption in cyanate esters and showed that water absorption was low when exposed to high humidity. The study also concluded that the moisture profiles followed Fick's law in the early stage of moisture absorption, followed by Non-Fickian behavior after prolonged exposure to high humidity. A similar study by Cinquin et al. [35] on the water absorption in cyanate esters found that moisture absorption followed Langmuir's law. It was further determined that moisture absorption curves of these materials followed Fick's second law of diffusion. Kasehagen et al. [36] found that hydrolosis of cyanate ester caused blistering of the network, producing gaseous products such as carbon dioxide, alcohol, etc. and lowered the T_g and strength of the matrix. Shimp and Ising [37] found that the class of cyanate ester resin homopolymers absorbs less than 3% of moisture by weight over a period of 6 months as compared to up to 7% by the competing resins such as epoxies, BMI, and condensation polyimides.

This research focuses on identifying the moisture absorption mechanisms of the CTD-403/S2 glass insulation composite created by Composite Technology Development, Inc. in order to validate its use in magnet systems such as QPS that require water cooled conductors. The degradation of the mechanical and electrical properties (from moisture absorption) of the composite are also studied, as well as the dimensional stability of the composite. A last focus is to test the degradation of the copper foil interface, verifying that the resin will not lose its adhesion properties to copper coils in the magnet systems after long term exposure. This will be validated using standard short beam shear tests.

CHAPTER III

METHODOLOGY

3.1 Overview

In order to validate the application specific use of CTD-403 insulation for fusion devices, humidity testing was performed. Three sample types as well as three humidity levels were used in order to accurately identify the mechanisms of moisture absorption seen in CTD-403 as well as develop a general understanding of how humidity levels affect the absorption trends. A fourth test was performed using elevated temperature, in order to identify the effects of temperature on moisture absorption kinetics, as well as mechanical and electrical properties of the specimens. Humidity testing was performed over a six month period, tracking the weight gain and dimensional changes of each specimen at set increments over the aging process. Mechanical and electrical testing was also performed over the aging period, and due to its destructive nature was necessary to use multiple batches of specimens. The testing setup and procedure is outlined in the following section. All mechanical and electrical testing was performed by Composite Technology Development, Inc.

3.2 Specimen Types

For purpose of this research, three specimen types were used: S2-glass-reinforced composites (composite insulation specimens), copper/insulation adhesive test specimens, and neat resin plates. A sample cure profile for CTD-403 is seen in Figure 3.1.

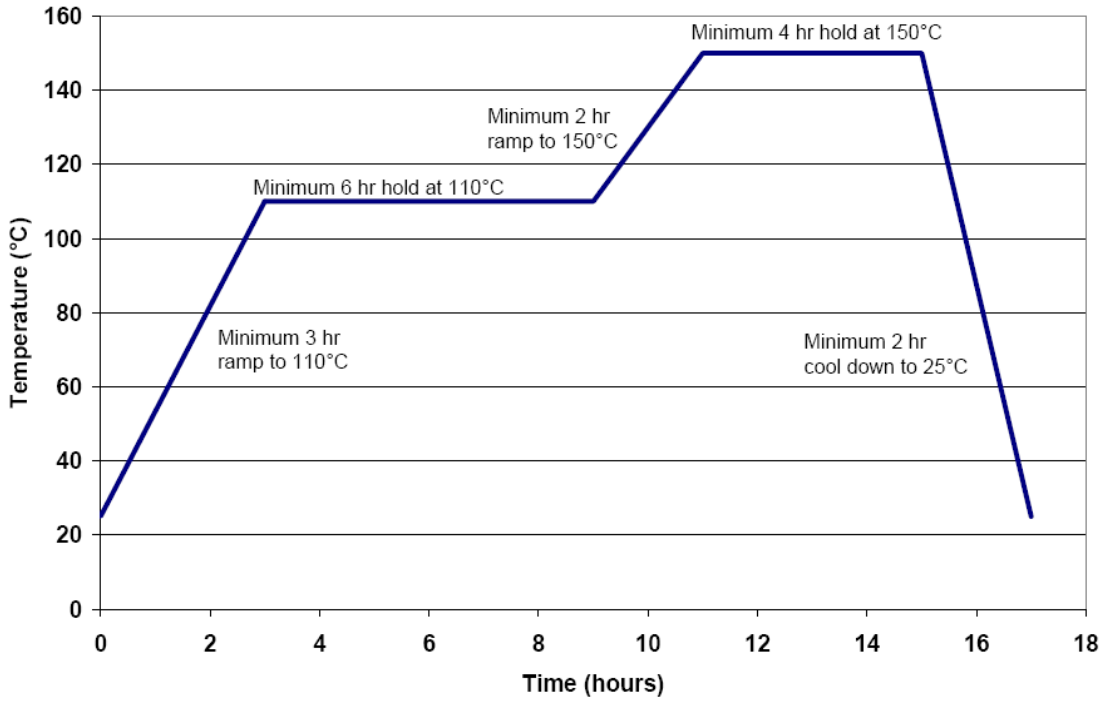

Figure 3.1 Cure Profile for CTD-403 (Max Temp 150°C)

The S2-glass-reinforced composites use an eight harness satin weave, having nominal fiber volume fractions of 50%. All specimen types were machined at Composite Technology Development, Inc.

The composite insulation specimens were machined by placing S2-glass plies in a closed mold under vacuum pressure of less than 200mTorr for at least three hours at 50°C. This initial bake (Figure 3.2) of the fiberglass reinforcement was performed to remove all the air from the mold and fabric. This was followed by degassing the CTD-403 resin under vacuum for 45-60 minutes at 50°C. The de-gassed resin was then transferred into the mold to impregnate the woven textiles. After completion of the vacuum pressure impregnation (VPI) process, the laminate was cured at a peak temperature of 175°C for four hours.

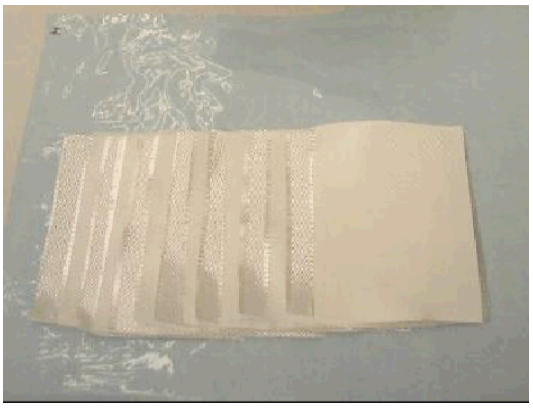

Initial Bake Out

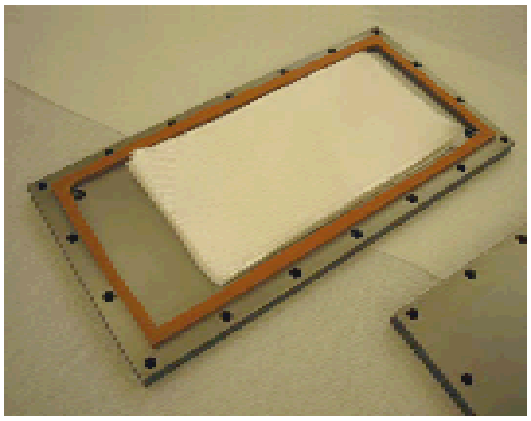

Assemble for Impregnation

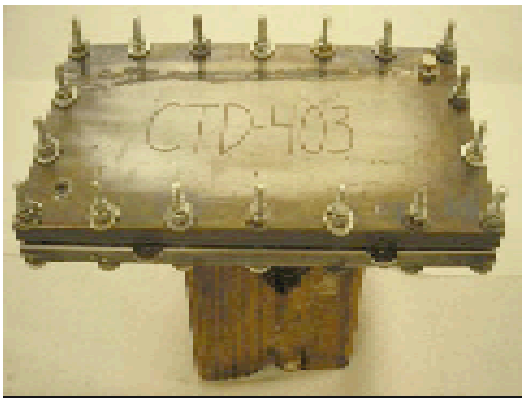

Prepared Mold Post Impregnation

Cured Laminate

Figure 3.2 Machining the Composite Insulation Specimens

The S2 glass plies are comprised of an eight harness satin weave. The 'harness' number is used to designate the total number of fibers crossed and passed under, before the fiber repeats the pattern. Satin weaves are very flat, have good wet out and a high degree of drape. The low crimp gives good mechanical properties. The high harness number and nature of the weave allows the fibers to be woven in close proximity causing a tight weave.

For the copper/insulation specimens, flat plate laminates were fabricated using a lay-up that included a 0.18-mm-thick copper foil positioned at the center of the S2-glass plies (Figure 3.3). CTD previously used this design to evaluate the effect of incident irradiation on the adhesive shear strength of the copper/insulation bond. That study showed that the insulation remained strongly adhered to the copper after exposure to high levels of radiation. These specimens will be used to evaluate the effect of humidity/temperature on the adhesive shear strength of the copper/insulation interface.

The neat resin plates were produced by degassing CTD-403 resin under vacuum for 45-60 minutes at 50°C. The de-gassed resin was then introduced into closed molds maintained at 50°C. The process is similar to that described for the fiber-reinforced composites, except the resin will not be reinforced with S2 glass. The plates were also cured using the same ramp and soak program as the fiber-reinforced composite plates. The neat resin specimens were used for DMA testing, that is to determine the effects of T_g the exposure had on the cured resin.

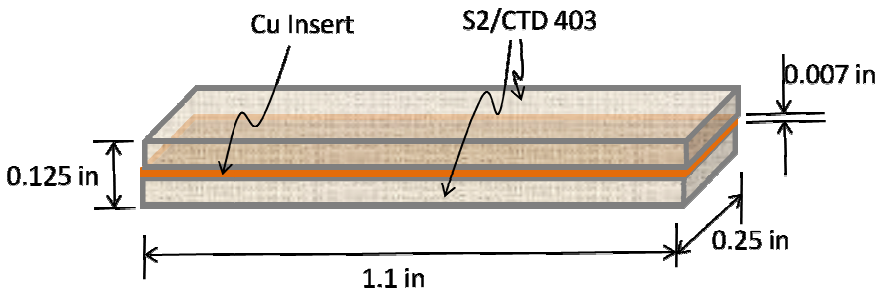

Figure 3.3 Copper/insulation specimens

3.3 Experimental Procedure

ASTM E 104-02 [38] (Standard Practice for Maintaining Constant Relative Humidity by Means of Aqueous Solutions) in conjunction with ASTM D5229/D 522M-92 [39] (Standard Test Method for Moisture Absorption Properties and Equilibrium Conditioning of Polymer Matrix Composite Materials) was used in this research to generate environments of known relative humidity. The method recommends using saturated aqueous solutions in contact with an excess solid phase of a specific salt to maintain a constant relative humidity in sealed aging jars. One-gallon, wide-neck glass jars were used with rubber gasket and clamp lids to expose the specimens to the constant humidity environment. A perforated platform was designed to mount inside the jar, providing a place to rest the specimens (Figure A.1). The platform was mounted inside the jar using a silicon sealant bead, approximately one-fourth of the distance from the bottom of the jar.

Three relative humidity conditions were generated: 79%, 85%, and 97%. These were chosen in accordance with the ASTM standard, where it was recommended that

ammonium chloride, potassium chloride, and potassium sulfate be used to generate the 79%, 85%, and 97% RH environments (at room temperature), respectively. Distilled water was used to saturate the salt solutions. A fourth jar was kept in an oven at a temperature of 75°C and RH of 79%. Each jar was monitored using a humidity gauge (HS-2000D with an RS232 evaluation kit) to ensure correct humidity levels throughout the six month aging period.

3.3.1 Exposure Specifics

The specimens were removed after periods of ten days, 30 days, two months, four months, and six months. At each aging period, the weight and dimensional change of each specimen was noted. Short-beam-shear, dielectric, DMA, and compression tests were also performed at each of the five aging periods. Due to the destructive nature of the mechanical and electrical tests, it was necessary to track the specimens in groups. Testing began with 420 specimens, and at each aging interval 85 specimens were removed. Each of the 85 specimens' weight and dimensional change was measured at each aging period, at which point the mechanical/electrical tests were performed.

Table 3.1 and 3.2 outline the testing configurations. For each test performed, a group of three or more specimens was used in order to track specimen deviation and formulate more meaningful averages. Specimens were kept thin in order to speed up saturation time, as well as minimize edge effects.

Table 3.1 Testing Configurations for 79% RH, 85% RH, and 79% RH 75°C Environments.

Matrix - CTD-403			
Fiber	**Dimensions (L x W x H) (in)**	**# of Samples/aging period**	**Tests Performed**
S2-Glass	1.1 x 0.25 x 0.125	4	Weight Gain, Dimensional Stability, Short-Beam-Shear
S2-Glass	0.25 x 0.25 x 0.125	4	Weight Gain, Dimensional Stability, Compression
S2-Glass	1.0 x 1.0 x 0.02	3	Weight Gain, Dimensional Stability, Dielectric
S2-Glass w/Cu Interface	1.1 x 0.25 x 0.125	4	Weight Gain, Dimensional Stability, Short-Beam-Shear
Neat Resin	2.2 x 0.5 x 0.125	2	Weight Gain, Dimensional Stability, DMA

Table 3.2 Testing Configuration for 97% RH Environment.

Matrix - CTD-403			
Fiber	**Dimensions (L x W x H) (in)**	**# of Samples/aging period**	**Tests Performed**
S2-Glass	1.1 x 0.25 x 0.125	4	Weight Gain, Dimensional Stability, Short-Beam-Shear
S2-Glass	0.25 x 0.25 x 0.125	4	Weight Gain, Dimensional Stability, Compression
S2-Glass	1.0 x 1.0 x 0.02	3	Weight Gain, Dimensional Stability, Dielectric
S2-Glass w/Cu Interface	1.1 x 0.25 x 0.125	4	Weight Gain, Dimensional Stability, Short-Beam-Shear
Neat Resin	2.2 x 0.5 x 0.125	2	Weight Gain, Dimensional Stability, DMA
S2-Glass	1.1 x 0.25 x 0.125	4	Weight Gain, Dimensional Stability, Short-Beam-Shear

3.4 Testing Descriptions

The following section describes procedures followed for each test performed in this research. For each experiment, groups of four specimens were used and tracked individually. In the results section, each value represents an average of four individual specimens in order to achieve more accurate results. Each property was evaluated at the specified time increments for each of the four environmental conditions.

3.4.1 Weight Gain

Weight gain testing was performed on all specimens as outlined in Tables 3.1 and 3.2. In addition, early stage moisture absorption tests were performed. This included tracking the weight changes at three, six, and eight days in addition to the previously mentioned intervals. As previously defined, composite insulation specimens, copper/insulation specimens, as well as neat resin specimens were tested. Room temperature specimens were held at 22°C ± 2°C. The elevated temperature samples were held at 75°C ± 2°C. Initial weights of the specimens were measured using an analytical balance with 0.01 mg resolution. At each aging period, the specimens were removed from their respective environments and wiped dry of any excess moisture. Then, the specimens were left in the ambient temperature and humidity condition for 3-5 minutes before reweighing with the same analytical balance (0.01 mg resolution). Specimens were handled wearing latex gloves to avoid moisture absorption from the skin. The moisture absorption percentage in the resin is measured using equation 2.1. The procedure outlined here is in accordance with ASTM E 104-02 [38].

3.4.2 Moisture Induced Swelling

Samples used for moisture diffusion studies were also used to measure moisture induced swelling. The initial thickness, length, and width were measured and recorded using a micrometer with an accuracy of 0.001 in. At each aging interval, samples were removed from their respective environments and measured with the same micrometer in order to estimate the amount of moisture induced swelling.

3.4.3 Short Beam Shear Testing

As outlined in Tables 3.1 and 3.2, composite insulation specimens (CTD-403/S2 glass) as well as copper/insulation specimens were subjected to short beam shear testing. The exposed samples were cut into dimensions of approximately 1.1 x 0.25 x 0.25 inches. The machined specimens were also measured with a micrometer before and after testing in order to generate more accurate results for the apparent interlaminate shear strength (ILSS) as well as flexural modulus. SBS testing was conducted at 25°C in accordance with ASTM test standard D2344. SBS testing provides the ILSS as well as the flexural modulus, utilizing specimens of small span-depth (L/h) ratio in a three point bend test. This produces failure between the laminae, i.e. cracking along a horizontal plane between the laminae [40]. Additionally, SBS tests will be used to assess the adhesive shear strength of copper/insulation interfaces. The ILSS (Eq. 3.1) is calculated using the maximum load at failure (P).

$$\tau_{xz} = \frac{3P}{4wh} \tag{3.1}$$

The flexural modulus is also calculated knowing the span length (S) in testing as well as the slope (m) of the linear portion (within elastic limit) of the load vs. displacement curve using the following equation.

$$F = \frac{S^3 m}{4wh^3} \tag{3.2}$$

The flexural modulus is used as an indication of a material's stiffness when flexed, and the data is often used to select materials for parts that will support loads without flexing. If the flexural modulus is not sufficiently high buckling becomes probable. ILSS depends primarily on the matrix properties and fiber-matrix interfacial shear strengths rather than the fiber properties. The ILSS can be improved by increasing the matrix tensile strength as well as the matrix volume fraction [15]. Fabrication defects, such as internal micro cracks and dry strands, reduce the ILSS [15]. Figures 3.4 and 3.5 depict the three point bend test used in SBS testing.

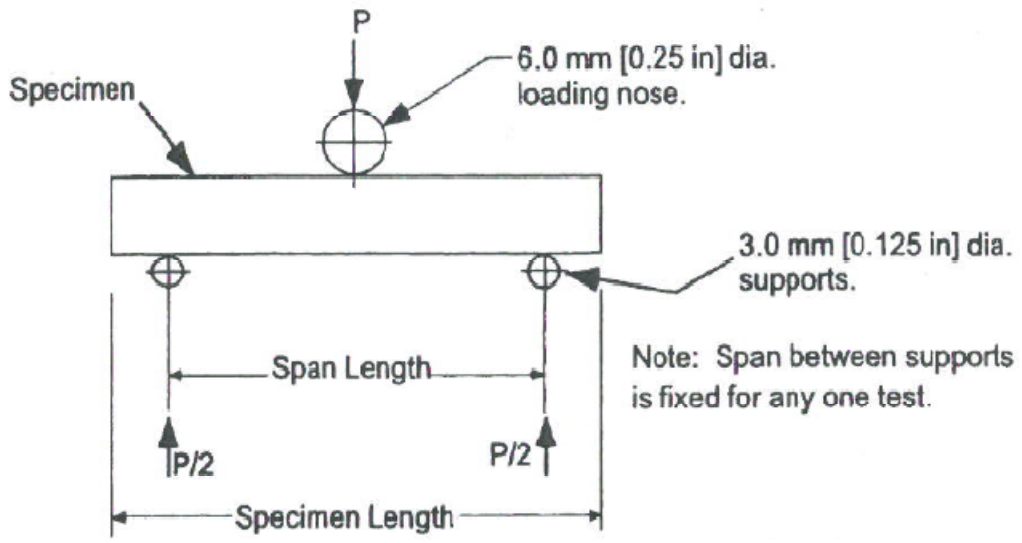

Figure 3.4 Horizontal Shear Load Diagram [40].

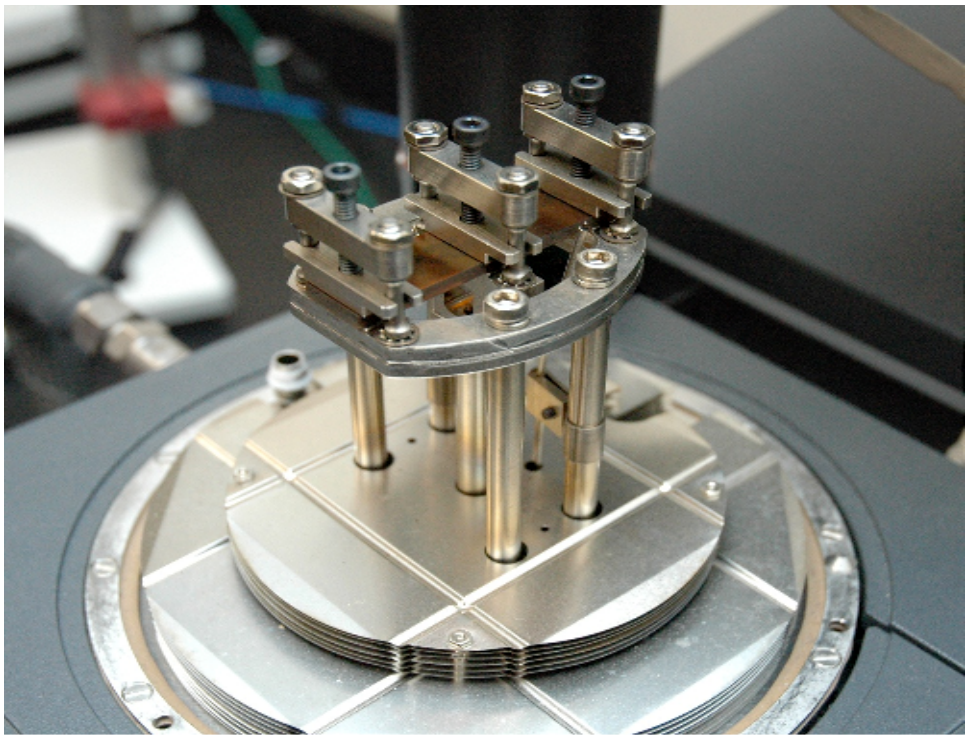

Figure 3.5 Three-point loading fixture with neat-resin test specimen.

3.4.4 Compression Testing

Compression tests were performed on composite insulation specimens of dimensions 0.25 x 0.25 x 0.125. Testing was performed at 25°C by placing the specimens between two platens and applying a mechanical load in the through thickness direction, normal to the glass plies. This type of loading is what the insulation will experience in most fusion applications. As described by ASTM D635 [41], the compressive stress is calculated by dividing the failure load by the specimens loading area. An extensometer was also used in order to accurately measure the deflection experienced by the specimen. This enabled the calculation of the compressive modulus (elastic modulus) by capturing the slope of the linear portion of the stress vs. strain curve.

3.4.5 Dielectric Breakdown Testing

Wafer shaped composite insulation specimens (1.0 x 1.0 x 0.02 in.) were used to measure the dielectric breakdown strength of the composite insulation specimens using a method adapted from ASTM D149-81 [42] and D3755-79 [43]. Dielectric strength is defined as the ratio of the voltage that will produce a rupture in an insulation to the thickness of the insulation. The dielectric breakdown on the insulation is the maximum voltage it can experience without failure of its insulating properties. Dielectric breakdown, in most laminates, typically results in localized oxidation and the destruction of the material's electrical characteristics, or in this case the insulation properties of the composite. Moisture decreases the dielectric strength of a polymer because water is a small mobile molecule carrying a permanent dipole [44].

Examination on a molecular level shows that there are different modes of dielectric breakdown. Electrochemical breakdown is characterized by the release of a trapped ion in the resin when subjected to a voltage stress. The ion causes a disturbance in the surrounding resin molecules, manifesting itself as the release of electrons which disturbs other molecules until it propagates to such an extent as to produce an electrical current through the resin. Thermal breakdown is caused by low resistivity conduction paths. Upon being subjected to a voltage stress, the low resistivity paths allow for current flow which imparts heat to the specimen and in turn disturbs the surrounding molecules. This disturbance propagates until breakdown occurs. If air is trapped in the resin or between the resin and the test electrode, streamer breakdown can occur. The entrapped air becomes ionized causing chemical damage to the resin until breakdown occurs. If the

above mentioned breakdowns do not occur, there is an ultimate voltage stress the resin can withstand. This is described as intrinsic breakdown, and occurs when the voltage stress reaches such a level that the electrons are stripped away from molecules until a current flow is produced [45].

The tests were performed at 25°C with the specimens immersed in a dielectric fluid. Specimens were placed between two electrodes where a voltage was applied until dielectric breakdown occurred. It has been found that the dielectric strength of homogeneous solids varies approximately as the reciprocal of the square root of the thickness [45, 46]; therefore the dielectric strength constant ($kV/mm^{1/2}$) was also calculated for future comparisons between resins. The dielectric constant is a dimension-less parameter that is based on a capacitance measurement.

3.4.6 Dynamic Mechanical Analysis (DMA)

Neat resin specimens of dimension 2.2 x 0.5 x 0.125 inches were used for DMA testing. DMA measurements were used to characterize the modulus of the neat resin specimens as a function of temperature between 25°C and 300°C, providing data to describe the viscoelastic properties of the material as a function of temperature. Specifically, the loss modulus (viscous contribution) and storage modulus (elastic contribution) of the material can be determined. The tests were performed with a strain controlled measurement technique, at an amplitude of 15 microns and a heating rate of 4°C/minute., maintaining a preload of 0.01 N.

Viscoelastic materials are characterized by a stress response out of phase between 0° and 90° of the strain input, where the phase angle of the response (tan Δ) describes the materials damping. This can also be expressed as the complex modulus, or the vector sum of the elastic and viscous (damping) contributions. Composite samples exhibit dramatic changes in their damping (loss) profiles and display characteristic peaks as they pass through the glass transition temperature range. The glass transition temperature of the specimens was determined to evaluate the effects of aging under humid conditions on this aspect of the insulation performance.

CHAPTER IV

RESULTS AND DISCUSSION

4.1 Gravimetric Analysis

4.1.1 Effects of Humidity

Figures 4.1-4.3 show the room temperature weight change profiles for neat resin, S2 glass reinforced composite, and S2 Glass composite with copper interface, respectively. Each data point represents the average weight change of four individual specimens. The plots were generated using the standard configuration, containing moisture concentration % on the vertical axis and time (square root of hours) on the horizontal axis. An example of specimen variation in weight change used to calculate the averages weight gain is displayed in Figures 4.4 and 4.5. Moisture concentration percentages were calculated using Eq. 2.1. As seen in Figures 4.1-4.3, the absorption plots are non-Fickian in that equilibrium moisture content was not reached. For calculation of diffusion coefficients, Eq. 2.7 was used. The initial slope of the moisture concentration plot was found as shown in Figures 4.6-4.8, which is used in solving for the diffusion coefficient. Since the specimens used to determine the diffusion coefficient were of finite dimensions, Eq. 2.8 was used as a correction for the effect of diffusion though the edges. Due to the non-Fickian trend, the moisture concentration after 4300 hours of conditioning was used as M_∞. Table 4.1 displays the results.

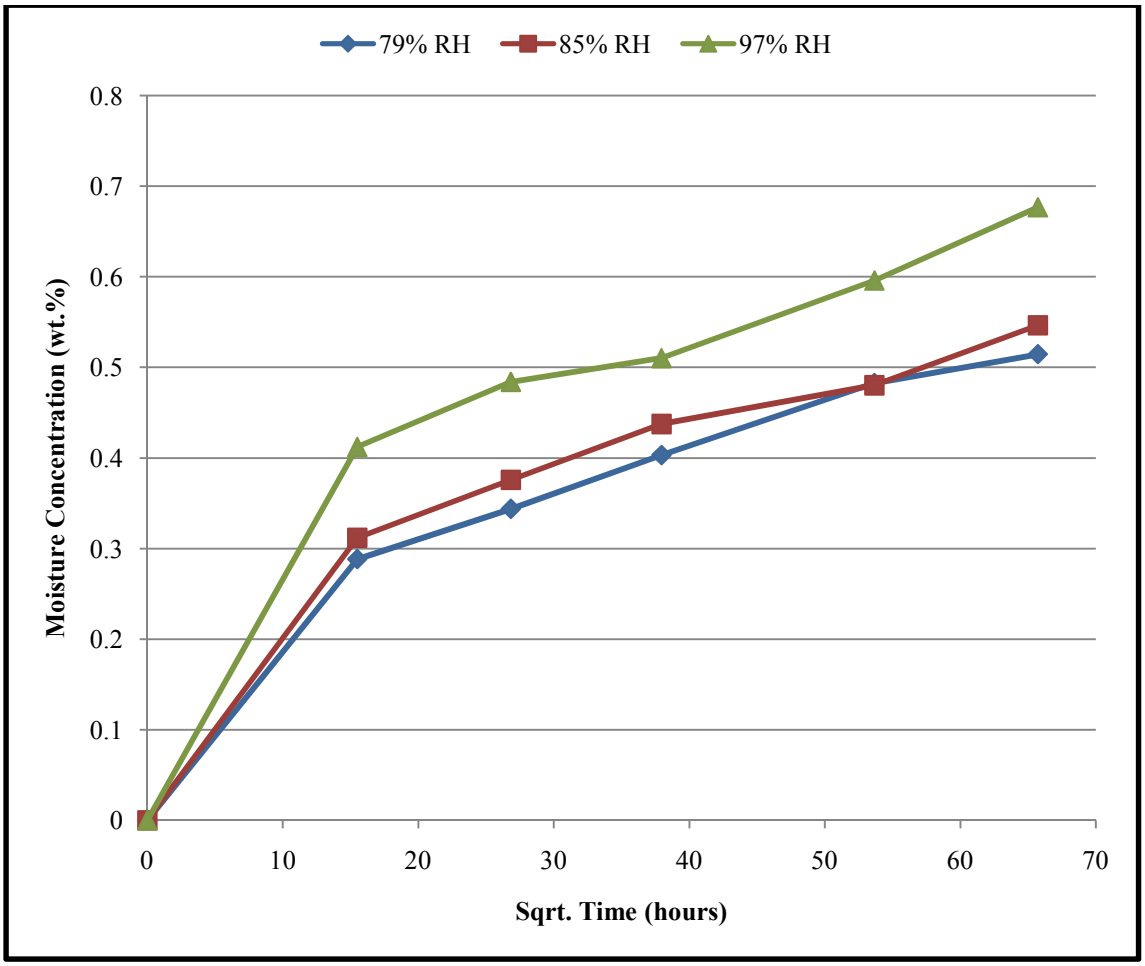

Figure 4.1 Neat resin moisture absorption curves at room temperature with square root of time. The curves compare the effects of three humidity levels on weight gain of neat resin cyanate ester (CTD-403) specimens.

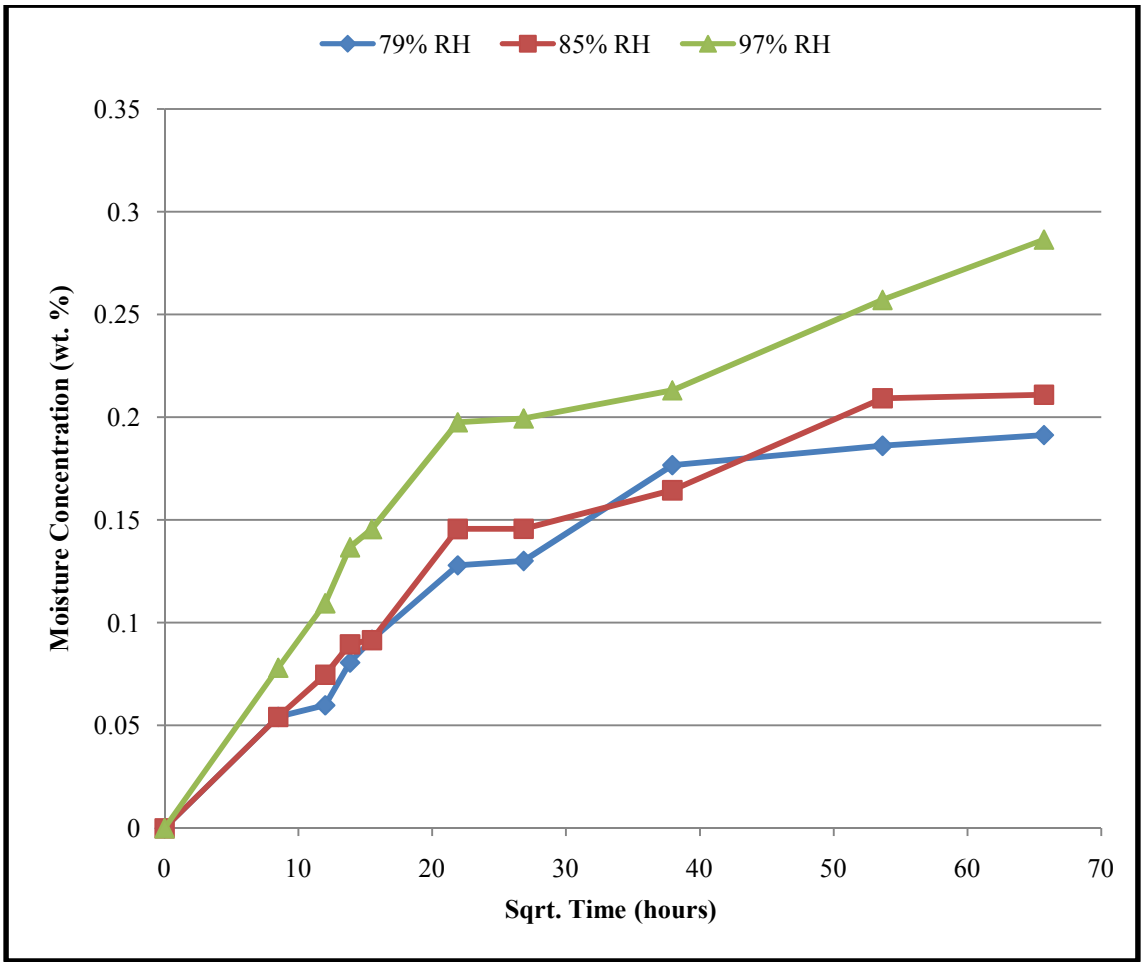

Figure 4.2 S2 glass reinforced composites moisture absorption curves at room temperature with square root of time. The curves compare the effects of three humidity levels on weight gain of CTD-403/S2 glass composite specimens.

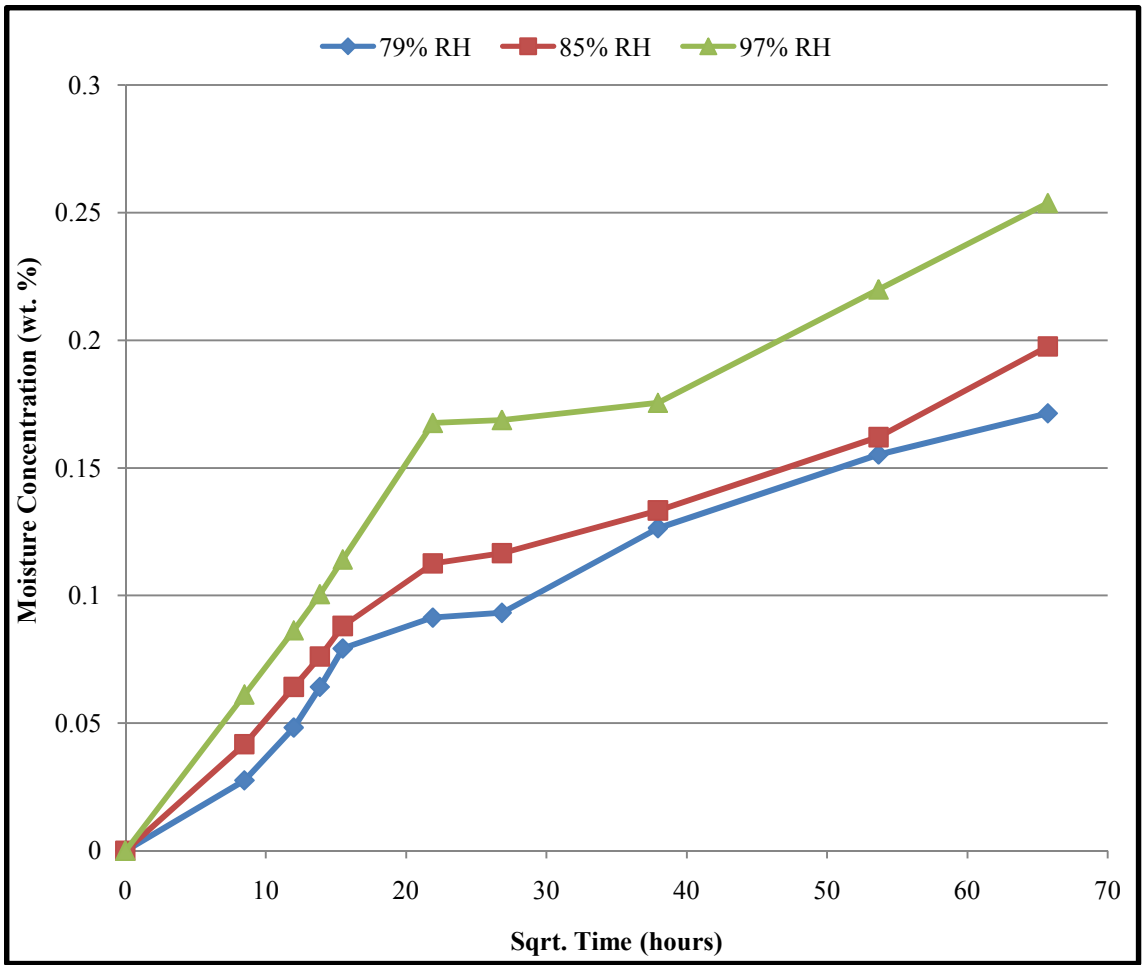

Figure 4.3 Copper/insulation composites moisture absorption curves at room temperature with square root of time. The curves compare the effects of three humidity levels on weight gain of CTD-403/S2 glass composite specimens with a copper Interface.

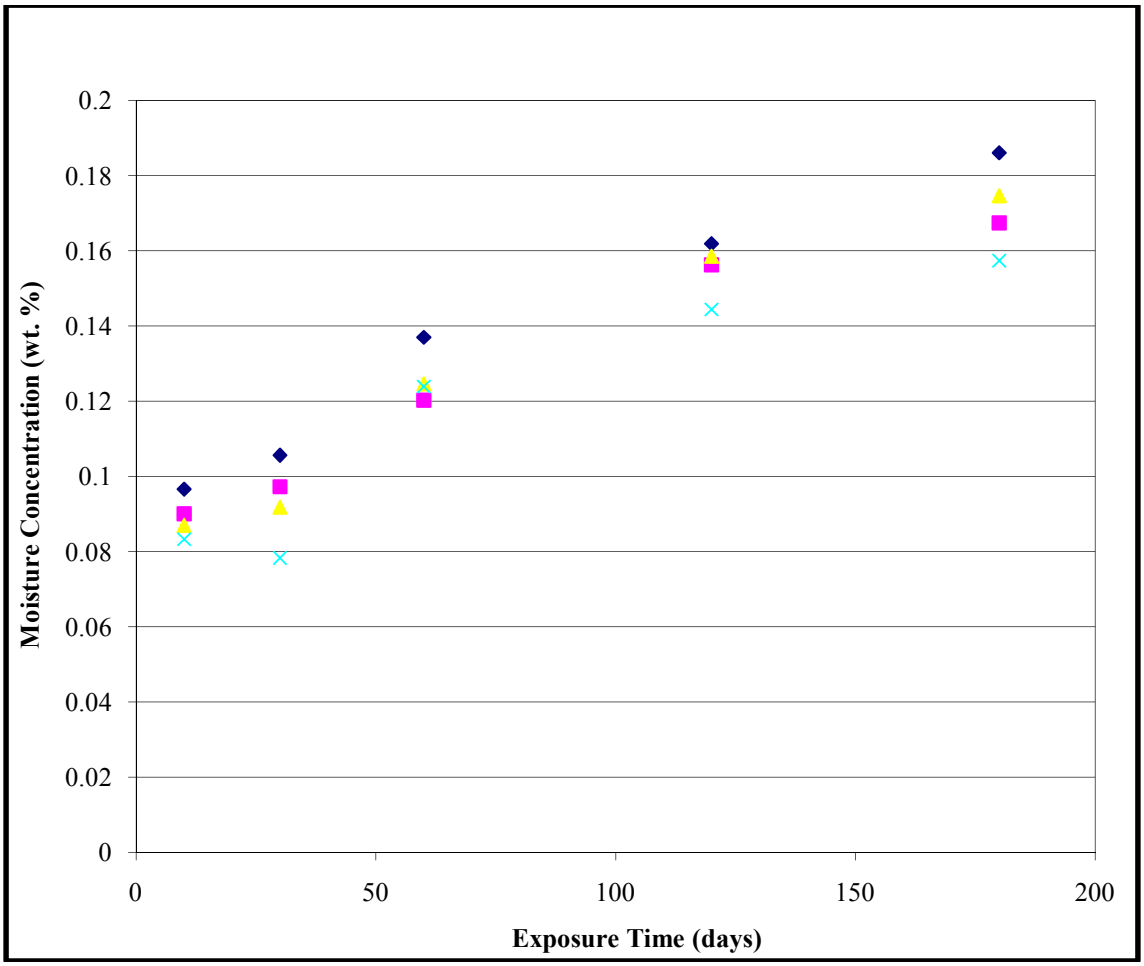

Figure 4.4 Copper/insulation composite moisture absorption specimen data scatter at room temperature with time. The points show the amount of data scatter seen at 79% RH on weight gain of CTD-403/S2 glass composite specimens with a copper Interface.

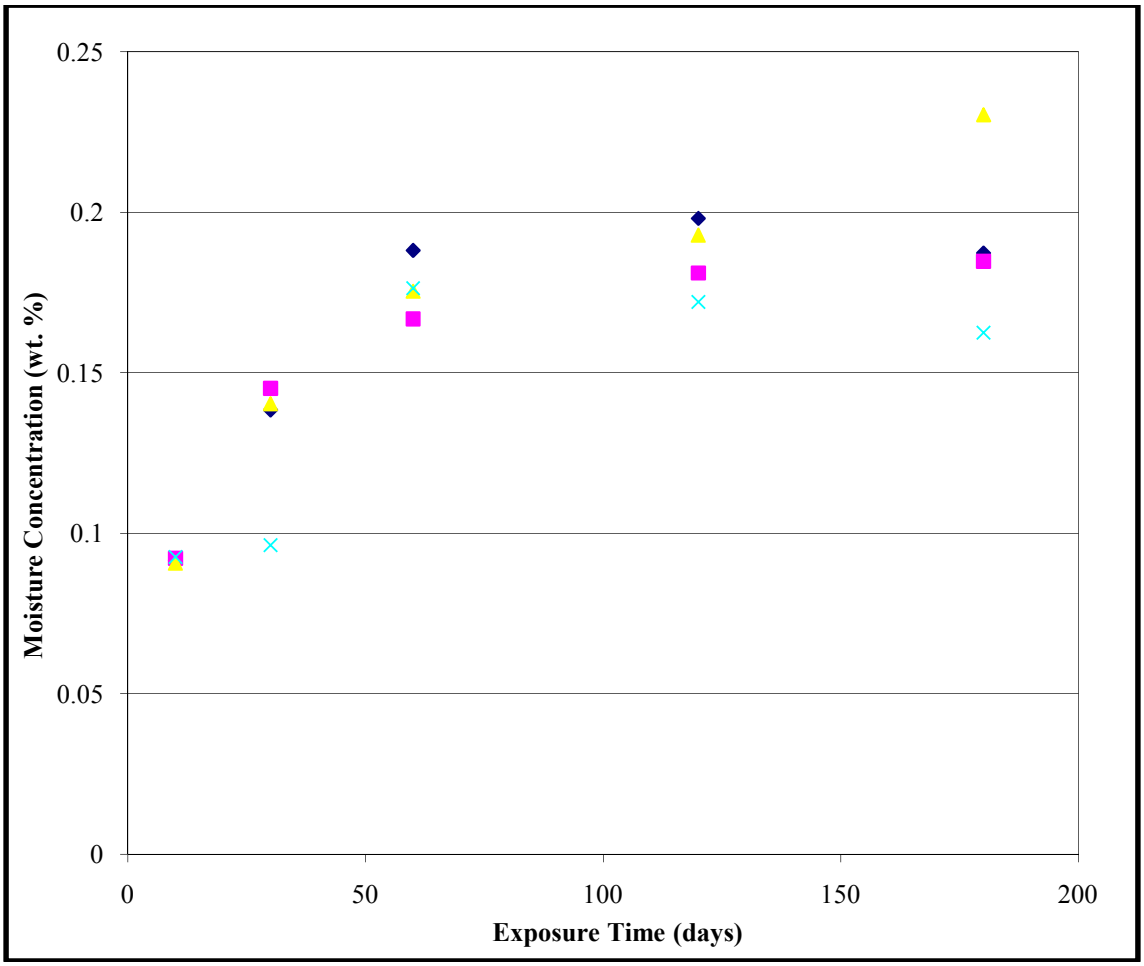

Figure 4.5 Insulation composite moisture absorption specimen data scatter at room temperature with time. The points show the amount of data scatter seen at 79% RH on weight gain of CTD-403/S2 glass composite.

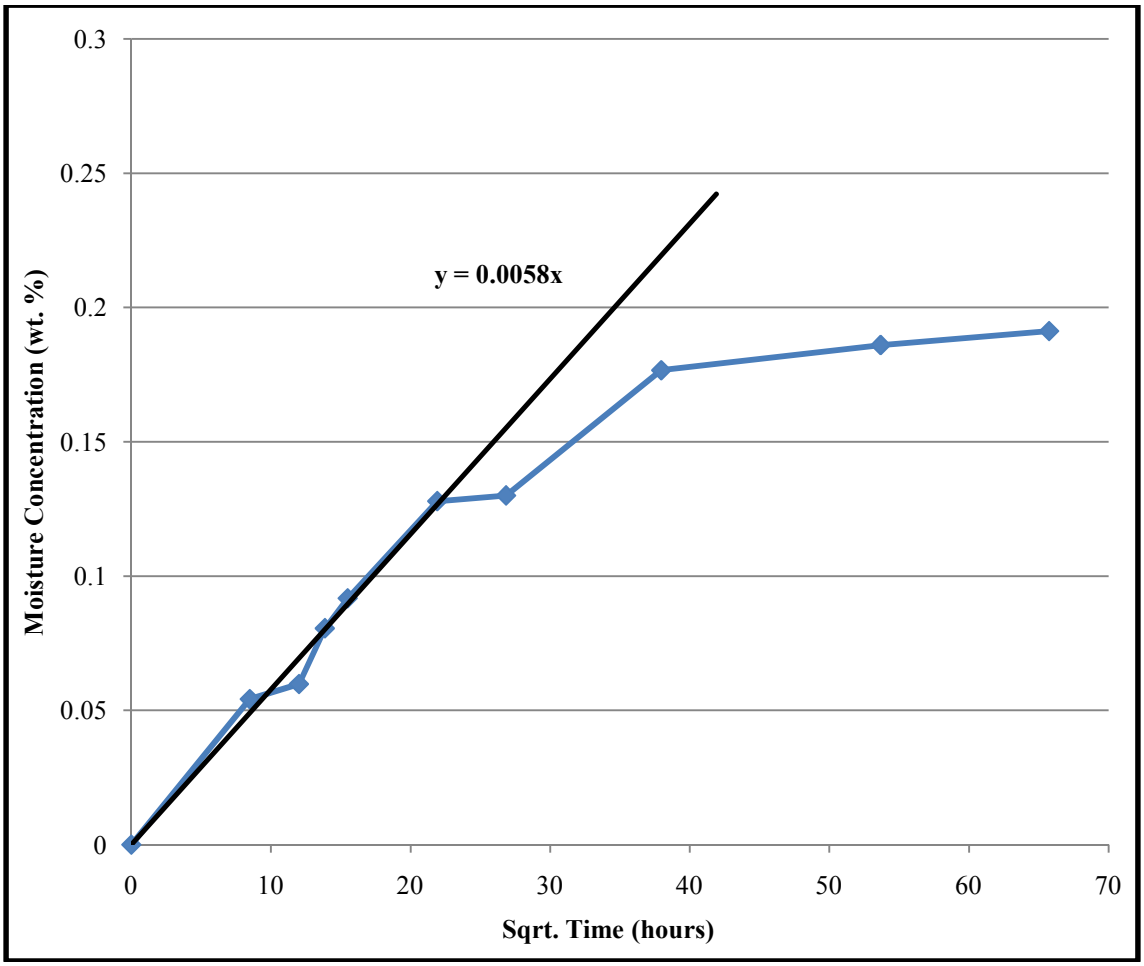

Figure 4.6 Insulation composite moisture absorption curve at room temperature and 79% RH with square root of time. The slope of the initial linear portion of the curve is used to calculate the diffusion coefficient.

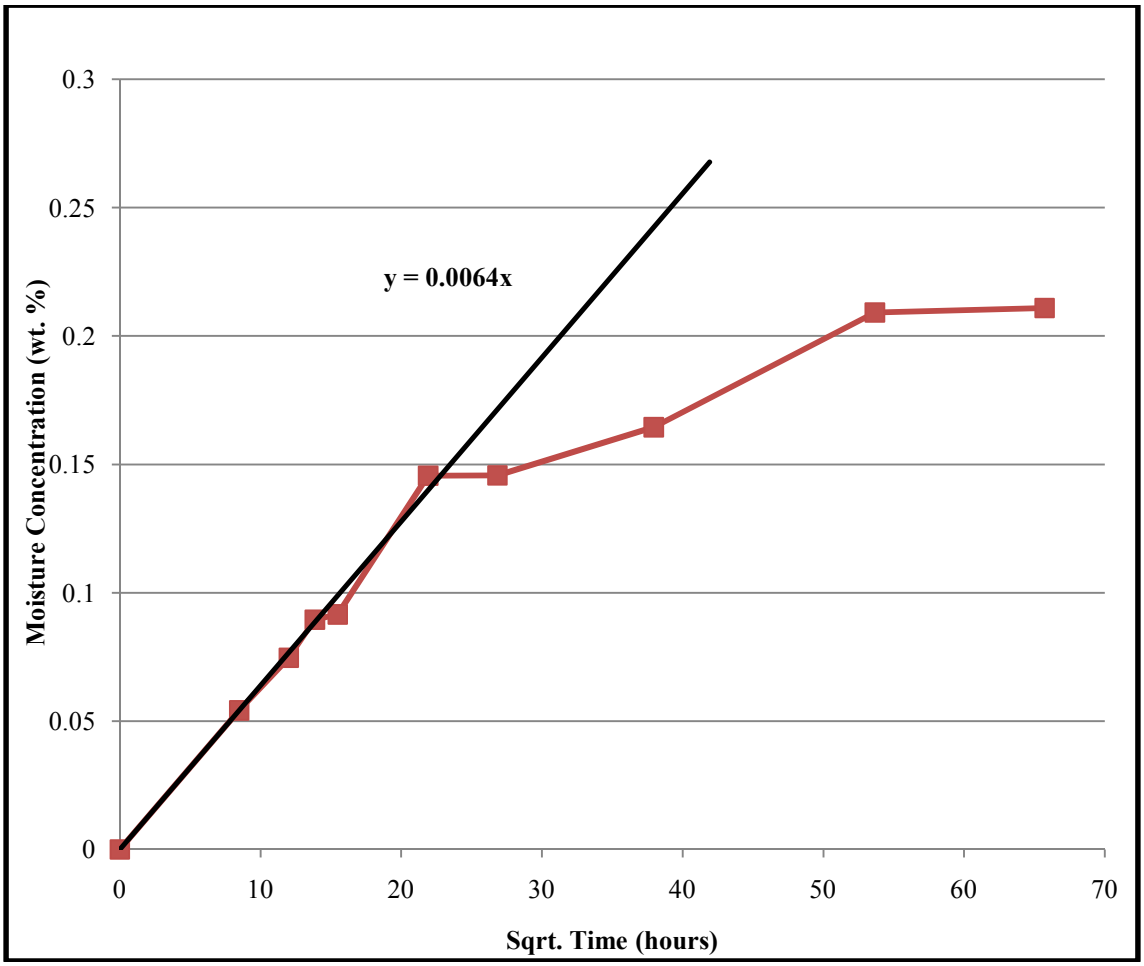

Figure 4.7 Insulation composite moisture absorption curve at room temperature and 85% RH with square root of time. The slope of the initial linear portion of the curve is used to calculate the diffusion coefficient.

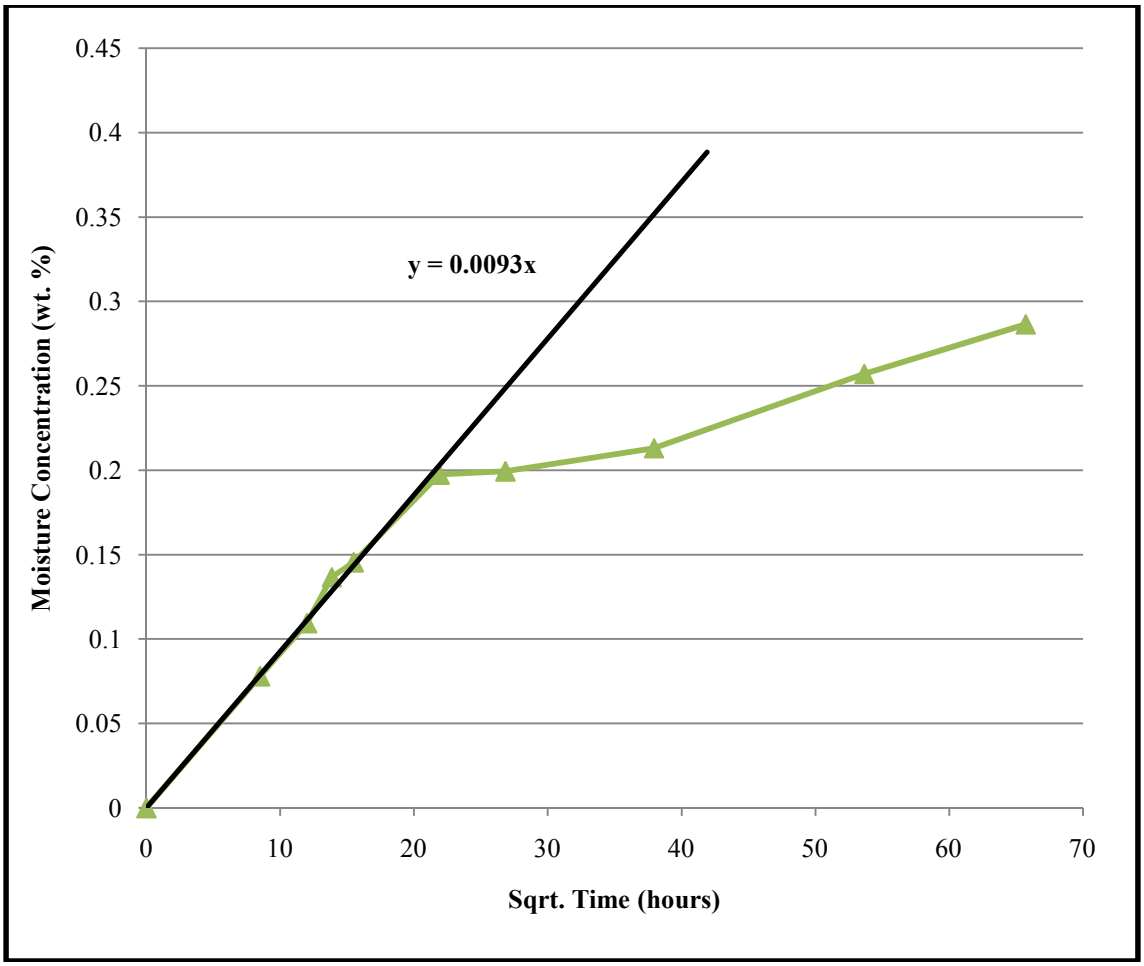

Figure 4.8 Insulation composite moisture absorption curve at room temperature and 97% RH with square root of time. The slope of the initial linear portion of the curve is used to calculate the diffusion coefficient.

Table 4.1 Apparent diffusion and corrected diffusion coefficients for room temperature samples at three humidity levels

Diffusion Coefficient $\left(x\ 10^{-10}\frac{in^2}{s}\right)$	79% RH		85% RH		97% RH	
	D	Dc	D	Dc	D	Dc
CTD-403/S2 Glass	7.83	3.01	7.84	3.02	8.98	3.445
CTD-403/S2 Glass w/CU Interface	5.87	2.26	5.90	2.27	7.25	2.78
Neat Resin	11.13	6.52	11.53	6.75	13.16	7.70

The samples exposed to higher levels of humidity exhibit increased moisture absorption over time. For many samples, the moisture absorption showed Fickian behavior but only during the initial stages of diffusion. The weight gain due to moisture increased proportionally to the square root of time, before beginning to settle off to a saturation level. However, instead of decreasing further towards zero like a typical Fickian curve, the rate of weight gain again began increasing. This type of behavior is known as two step non-Fickian absorption as depicted in Figure 2.3. In each of the Figures, none of the samples appear to be at a saturation level even after 4300 hours of exposure, although the lower relative humidity levels show signs of reaching saturation.

To minimize the effects of three-dimensional diffusion, the specimens were dimensioned to promote predominately one-dimensional diffusion through the length of the sample to experimentally determine the diffusivity. The diffusivity, D, is shown to be dependent on humidity which indicates non-Fickian diffusion. For the composite insulation specimens, a 14% increase is seen from 79% RH to 97% RH. A 23% and 18% increase is seen for the copper/insulation and neat resin specimens, respectively. The percents stated above are based on the corrected diffusion coefficient. The neat resin specimens were different dimensionally in order to be later used for DMA testing, so correcting for edge absorption is important when comparing specimens of different geometries. It should be noted that the error involved in calculating diffusivity could be large for samples exhibiting non-Fickian diffusion, because choosing an appropriate saturation level is difficult. Fickian curve fits for the insulation and neat resin specimens can be found in the appendix. A true Fickian absorption process should show no more than 2% deviation.

4.1.2 Effects of Specimen Type

Figures 4.9-4.11 show moisture absorption curves for each of the three humidity levels, effectively comparing specimen types. Once again, moisture concentration is plotted against the square root of time. For all three humidity levels, the copper/insulation specimens show the lowest weight gain percentage, followed by the insulation specimens, and then the neat resin specimens. The trends are once again non-Fickian in that saturation is not reached and the diffusion coefficients vary with humidity level. Generally, the diffusivity of a polymer does not depend on the moisture concentration of the surrounding environment for Fickian diffusion, although the moisture saturation level is often observed to depend on relative humidity [22]. The diffusion coefficient merely describes the initial rate of moisture absorption.

According to [15], the fiber diffusivity for glass, carbon, and boron fibers is negligible compared with the matrix diffusivity. As previously defined, the fiber-volume fraction for the S2 Glass composites is 50% by volume fiber. Interestingly enough, the moisture absorption for the neat resin specimens is a little over double that of the S2 glass specimens. Although the S2 glass does not retain moisture, it provides a barrier for diffusion of moisture through the matrix, thus slowing down the diffusion process and explaining the further reduction in moisture absorption.

The copper/insulation specimens incorporated a copper foil of thickness 0.007 inches as seen in Figure 3.3, having the same overall thickness as the insulation specimens (0.125 in.). The copper foil therefore reduces the volume of S2 glass insulation by

approximately 6%, explaining the reduction in moisture absorption when compared with the insulation specimens.

As reviewed in chapter 2, most research has observed the non-Fickian moisture absorption of cyanate ester materials, suggesting that non-Fickian water absorption is caused by chemical interaction or reaction of water molecules with the cyanate ester polymer network. These chemical interactions cause the sample to continue gaining weight even after the pseudo-saturation moisture level in the matrix is reached. This chemically absorbed water in the polymer network can be attributed to the non-Fickian two step behaviors as seen in Figures 4.9-4.11. The pseudo saturation level is seen in almost every case, followed by an increase in slope of the moisture absorption curves.

Tables 4.2-4.4 outline the numerical weight gain percentages for each of the three humidity levels. At the 6 month aging period, the neat resin samples saw an average weight gain of 0.58% for all three humidity levels. The insulation specimens averaged 0.23% weight gain and the copper/insulation specimens averaged 0.21% weight gain over the 6 month aging period. The moisture absorption percentages are extremely low when compared to 1-7% weight gain percentages seen by typical epoxy formulations. This is an initial indicator of improved electrical properties of cyanate ester resins as compared to epoxy resins.

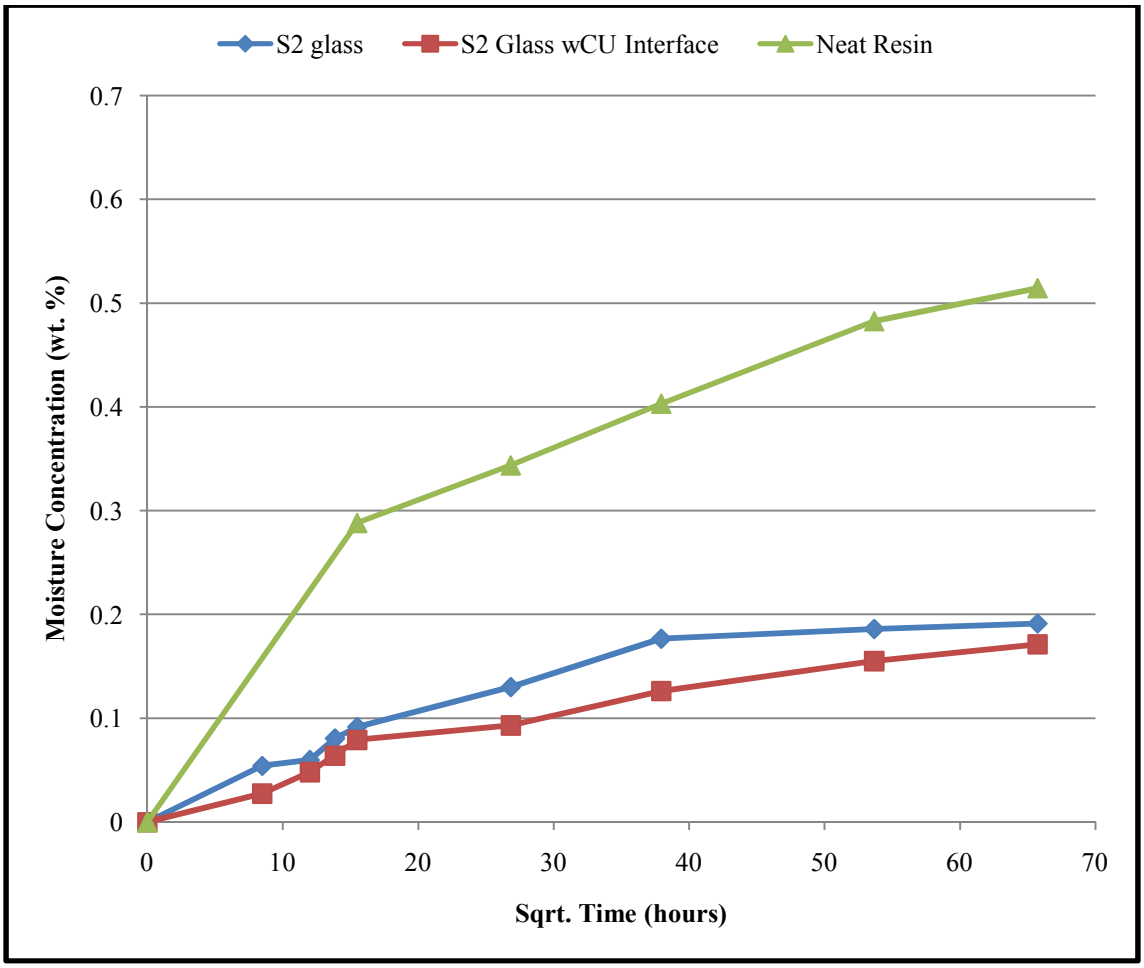

Figure 4.9 79% relative humidity moisture absorption curves at room temperature with square root of time. The curves compare the effects of specimen type on moisture absorption kinetics.

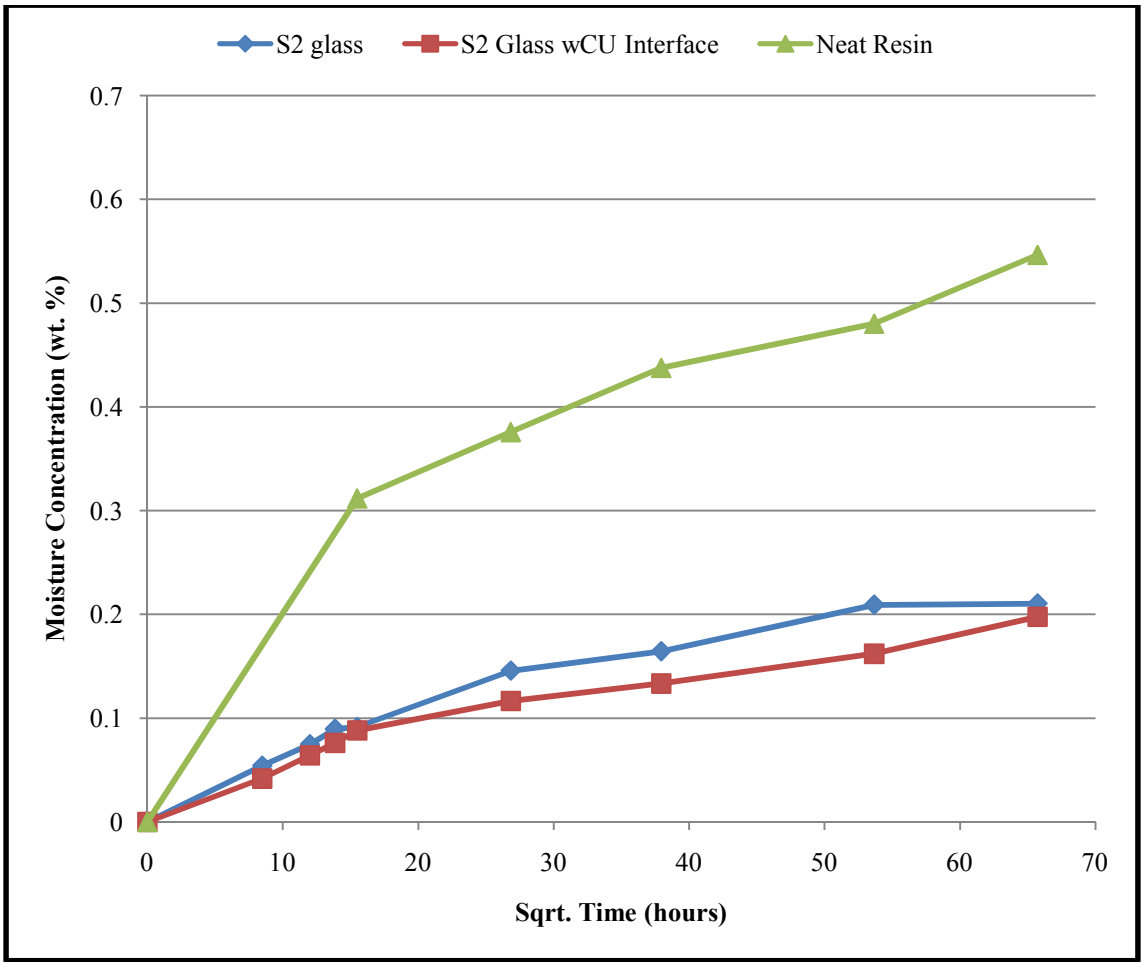

Figure 4.10 85% relative humidity moisture absorption curves at room temperature with square root of time. The curves compare the effects of specimen type on moisture absorption kinetics.

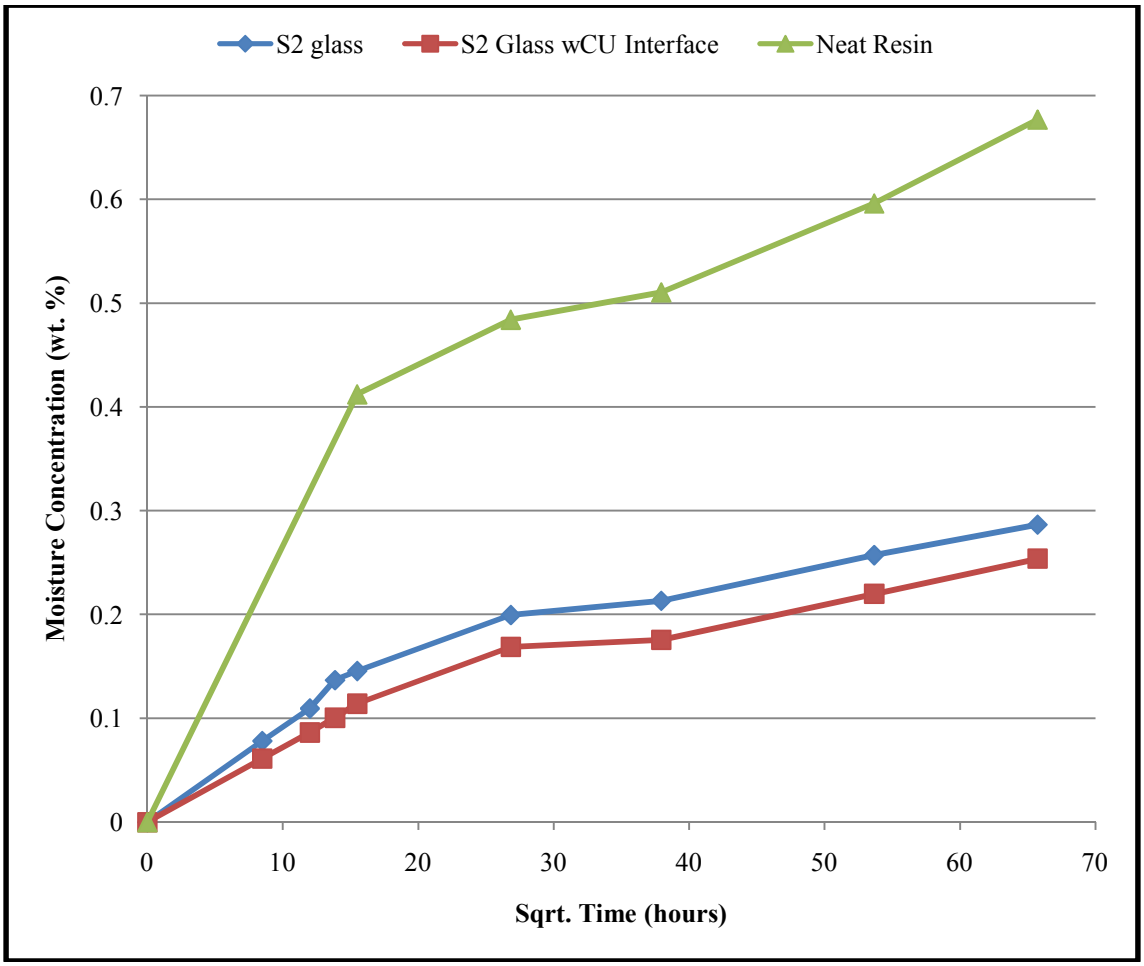

Figure 4.11 97% relative humidity moisture absorption curves at room temperature with square root of time. The curves compare the effects of specimen type on moisture absorption kinetics.

Table 4.2 Weight gain percentages for 79% relative humidity exposure samples.

Specimen Type	10 Days	30 Days	60 Days	120 Days	180 Days
	Mt	Mt	Mt	Mt	Mt
Neat Resin	0.288312	0.343796	0.403123	0.482751	0.514461
Insulation	0.091765	0.130049	0.176672	0.186054	0.191253
Copper/Insulation	0.079191	0.093214	0.12641	0.155228	0.171348

Table 4.3 Weight gain percentages for 85% relative humidity exposure samples.

Specimen Type	10 Days	30 Days	60 Days	120 Days	180 Days
	Mt	Mt	Mt	Mt	Mt
Neat Resin	0.311739	0.375699	0.437448	0.480095	0.546308
Insulation	0.091568	0.145717	0.164495	0.20924	0.210456
Copper/Insulation	0.088067	0.1166	0.133316	0.162057	0.197575

Table 4.4 Weight gain percentages for 97% relative humidity exposure samples.

Specimen Type	10 Days	30 Days	60 Days	120 Days	180 Days
	M_t	M_t	M_t	M_t	M_t
Neat Resin	0.412192	0.484104	0.510339	0.596034	0.676842
Insulation	0.145577	0.199374	0.213107	0.257109	0.286429
Copper/Insulation	0.114107	0.168729	0.175492	0.219902	0.253704

4.1.3 Effects of Temperature

Figures 4.12-4.14 show the temperature effects on the three specimen types by comparing the aging of room temperature specimens at 79% RH with the aging of elevated temperature (75°C) specimens at the same humidity level. Figure 4.15 compares the moisture absorption trends of the three specimen types at elevated temperature and 79% RH.

The curves once again show non-Fickian behavior. The elevated temperature is shown to dramatically increase the rate of moisture absorption, and after the 6 month aging period there is no sign of saturation. Unlike the room temperature curves, there is no pseudo-saturation point in the elevated temperature curves. All three specimen types display an almost linear moisture absorption curve, showing much greater non-Fickian behavior as compared with the room temperature samples. The saturation trends are comparable to the room temperature trends in that the neat resin samples show the greatest moisture absorption, followed by the insulation specimens and the copper/insulation specimens. The initial weight gain rates of the neat resin curves for elevated and room temperatures appear to be identical up until the 10 day period, but then quickly separate. The initial moisture uptake in the S2 glass and copper interface specimens do not show this trend, which indicates a larger initial temperature dependence of the composite specimen.

Comparing Figure 4.15 with Figures 4.9-4.11, the shape of the moisture absorption profile is seen to be unaffected by the elevated temperature, except for an upward shift in

the curves due to increased weight gain percentages and a slightly more linear trend. After six months of exposure, an average weight gain of 1.5%, 0.54%, and 0.45% is seen for neat resin, S2 glass, and S2 glass/copper specimens, respectively.

When comparing room temperature samples to the elevated temperature samples, a much larger deviation is seen between the neat resin specimens and the S2 glass specimens in the elevated temperature. For the elevated temperature case, there is a difference of almost 1% weight gain between the neat resin specimens and the S2 glass specimens, where the room temperature samples show less than a 0.4% difference. This increase of moisture absorption is seen because cyanate ester aged at elevated temperatures undergoes chain scission as described in section 2.2.2, forming products of low molecular weight and high mobility within the matrix. Moisture diffusion in a polymer is an energy activated process, and the diffusion coefficient depends strongly on temperature following the Arrhenius relationship shown in equation 2.3. At elevated temperatures, the required activation energy for diffusion of water molecules is attained much earlier as compared to the molecules at room temperature.

Table 4.5 outlines the numerical weight gain percentages for the elevated temperature samples at the five aging periods. Again, the initial moisture absorption is seen to be much greater when compared with the room temperature samples (Tables 4.2-4.4) due to the activation energy for diffusion being attained much earlier from the elevated temperatures.

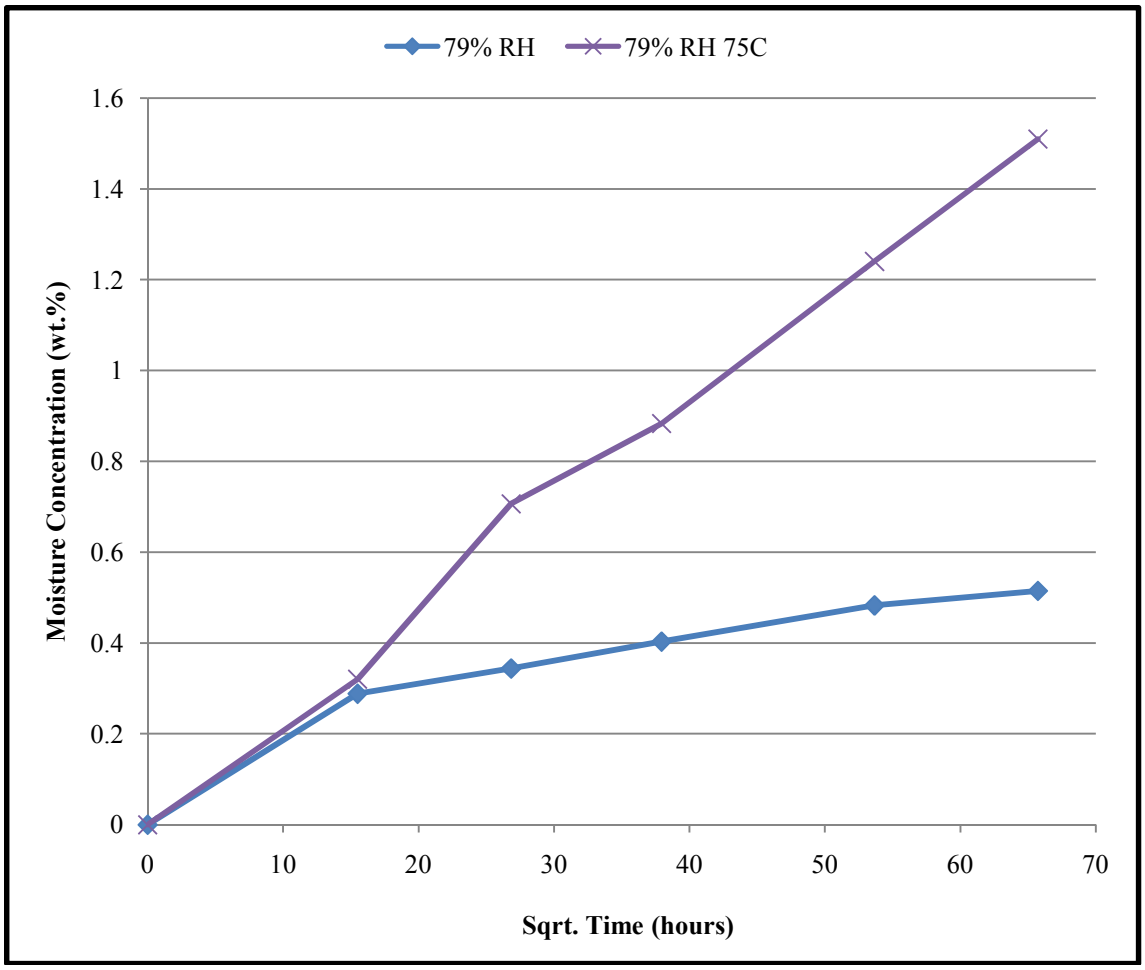

Figure 4.12 Neat resin 79% relative humidity moisture absorption curves at room and elevated temperature with square root of time. The curves show the temperature effects on weight gain of neat resin cyanate ester (CTD-403) specimens.

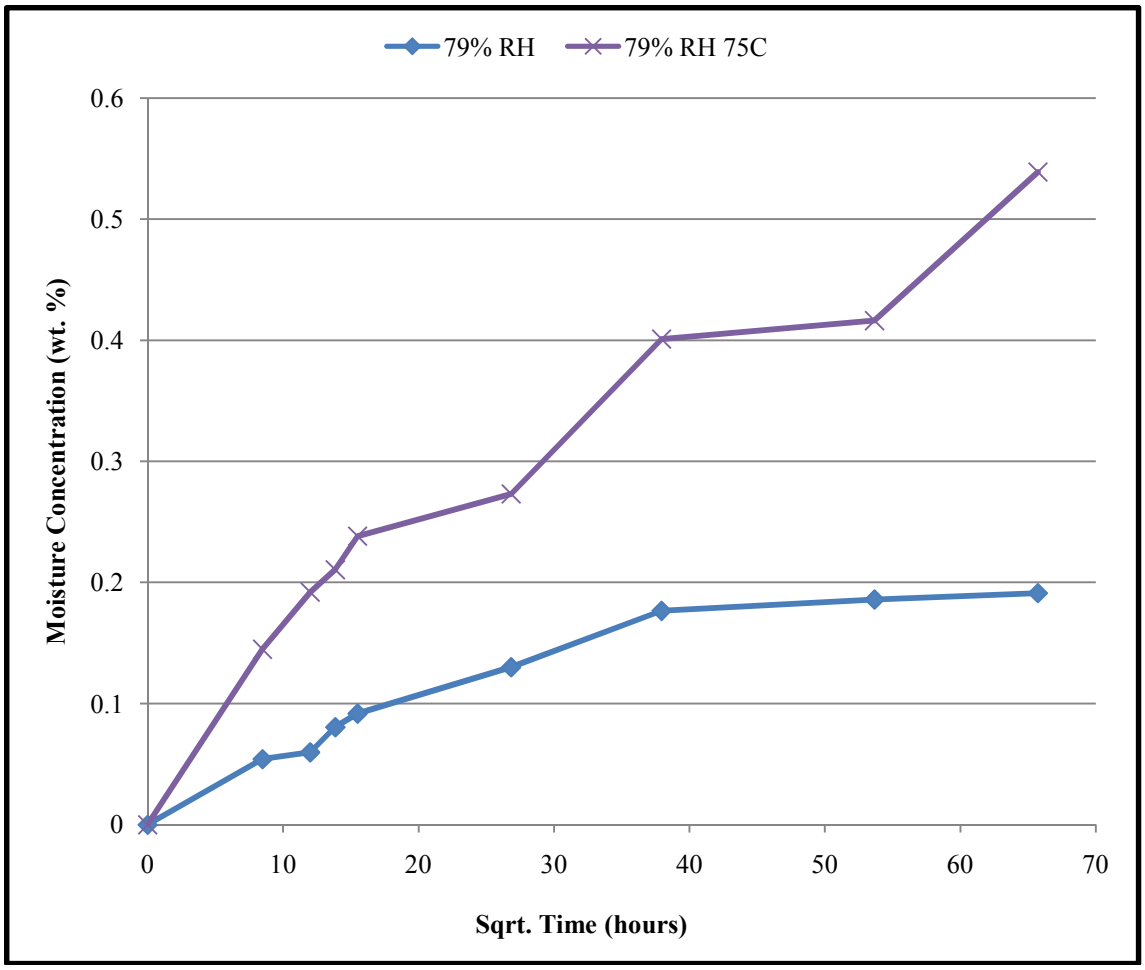

Figure 4.13 S2 glass insulation specimen 79% relative humidity moisture absorption curves at room and elevated temperature with square root of time. The curves show the temperature effects on weight gain of CTD-403/S2 glass specimens.

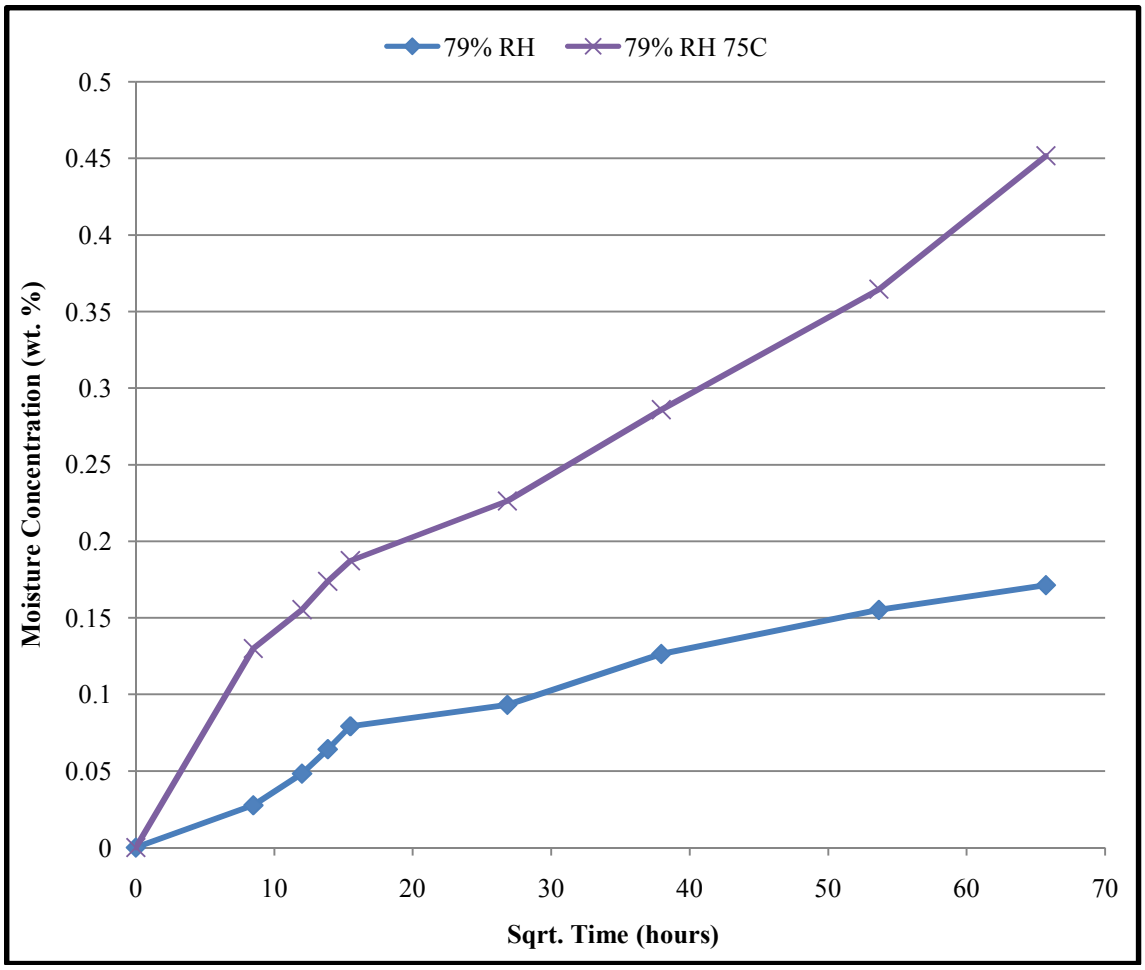

Figure 4.14 Copper/insulation specimen 79% relative humidity moisture absorption curves at room and elevated temperature with square root of time. The curves show the temperature effects on weight gain of S2 glass with copper foil specimens.

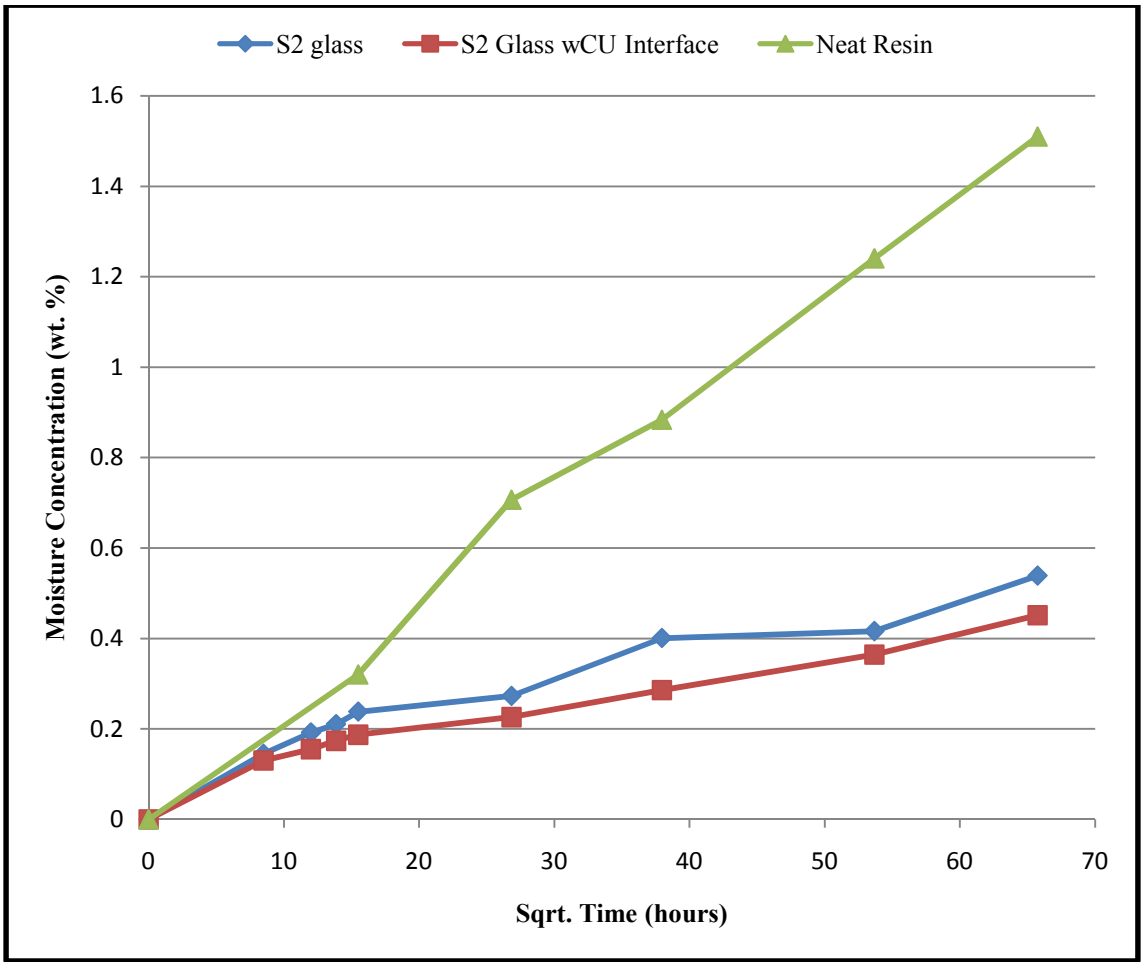

Figure 4.15 79% relative humidity moisture absorption curves at elevated temperature with square root of time. The curves compare the effects of specimen type on moisture absorption kinetics under elevated temperature conditions.

Table 4.5 Weight gain percentages for aging specimens at 79% RH and an elevated temperature of 75°C

Specimen Type	10 Days	30 Days	60 Days	120 Days	180 Days
	Mt	Mt	Mt	Mt	Mt
Neat Resin	0.32031	0.7068	0.88363	1.24061	1.50997
Insulation	0.23818	0.27305	0.40097	0.41614	0.53884
Copper/Insulation	0.18730	0.22626	0.28586	0.36459	0.45164

4.2 Moisture Induced Swelling

Table 4.6 shows the average percent dimensional increase in length, width, and height the specimens experienced after 6 months of aging. Table 4.7 shows the average percent volume increase in inches the specimens experienced after 6 months of aging.

At room temperature conditions, the copper/insulation and neat resin specimens showed the greatest average volume increase. The neat resin samples averaged approximately 1.15% volumetric increase where the copper/insulation specimens saw an increase of approximately 1.38%. The insulation specimens exhibited much greater dimensional stability, averaging around 0.5% volume increase at room temperature. The results show that the S2 glass fiber-matrix interface played a role in reducing swelling. The increase in swelling of the copper/insulation specimens as compared to the insulations specimens points to relaxation at the copper/matrix interface, which is verified by the abnormally large increase in height of the copper/insulation specimens for all RH/temperature conditions as seen in Table 4.6. The copper/insulation specimens were dominated by an increase in height, perpendicular to the copper foil interface, and reduced swelling in the directions parallel to the copper foil interface.

At the elevated temperature, the neat resin samples showed an average volumetric increase of 3.17%, where the insulation and copper insulation specimens showed an increase of 0.34% and 1.64%, respectively. The elevated temperature is seen to influence the neat resin samples much greater as compared to the other two specimen types. The insulation specimens showed the lowest percent volumetric increase at the elevated temperature condition, actually showing less than at room temperature. When compared

with the moisture absorption data, this information is interesting in the fact that the copper/insulation specimens showed the least moisture absorption and the greatest volumetric change. This type of phenomena is due to micro cracks and free volume in the matrix. The neat resin samples showed much greater moisture absorption when compared with the copper/insulation specimens, but approximately the same volumetric change. This indicates that the neat resin samples have a higher threshold moisture concentration, or contain more free volume as compared to the copper/insulation specimens.

4.3 Short Beam Shear Testing

The results of the short beam shear tests are extremely important because they give good indication of the interlaminar shear strength and most importantly assess the degradation trends of the copper/insulation interface as well as the fiber/matrix adhesion strength. The ILSS depends on matrix properties and fiber-matrix interfacial shear strengths rather than fiber properties. As previously described, poor adhesion of the insulation to copper conductors can be limiting design factors in these systems. It is for this reason the copper/insulation specimens were incorporated in this study. Short beam shear testing provides a method to test the adhesion strength of the copper foil interface by comparing the insulation specimens ILSS with the copper/insulation ILSS. The flexural modulus was also evaluated using the procedure as outlined in section 3.4.3 (Eq. 3.2). The flex modulus is used as an indicator of the materials stiffness when flexed, and the data is often used to select materials for parts that will support loads without flexing.

Table 4.6 Average percent dimensional increase after 6 months

Specimen	79% RH			85% RH			97% RH			79% RH 75C		
	L	W	H	L	W	H	L	W	H	L	W	H
Neat Resin	0.09	0.30	0.83	0.07	0.20	0.82	0.14	0.10	0.92	0.23	0.40	2.52
Insulation	0.08	0.40	0.60	0.09	0.10	0.20	0.09	0.02	0.40	0.14	0.20	0.01
Copper/Insulation	0.16	0.30	1.04	0.12	0.30	1.04	0.09	0.10	1.03	0.09	0.50	1.04

Table 4.7 Average percent volume increase seen after 6 months

Specimen	79%	85%	97%	79% 75C
Neat Resin	1.24	1.09	1.15	3.17
Insulation	0.52	0.39	0.49	0.34
Copper/Insulation	1.51	1.39	1.23	1.64

4.3.1 Effects of Humidity

Figures 4.16 and 4.17 show the room temperature humidity aging effects on the interlaminar shear strength (ILSS) for the insulation and copper/insulation specimens, respectively. Each data point represents the mean of four samples. The error bars represent the standard deviation of each sample set. On each of the following Figures the pre-exposure value for the respective property is also displayed as a single point on the vertical axis.

The insulation specimens show dependency on the relative humidity of the environment (Figure 4.16). As the humidity level is increased, further degradation of the ILSS is seen. The three curves follow similar trends, and after 4 months of aging the degradation of the ILSS are seen to stop at approximately 8 ksi for the 79% and 85% RH specimens, and at approximately 7 ksi for the 97% RH specimens. The pre-exposure value for these specimens was measured to be approximately 10.23 ksi, thus seeing an average reduction in ILSS of approximately 2.56 ksi at room temperature.

The copper/insulation specimens at room temperature show a similar trend as the insulation specimens. Once again, the higher humidity levels are seen to further degrade the ILSS with time. When compared with the insulation specimens, the copper/insulation specimens show to be less affected by changes in humidity at room temperature as seen when comparing Figures 4.16 and 4.17. After 4 months of aging, the specimens actually see an increase in ILSS, having values of approximately 8.3 ksi for the 79% and 85% RH environments and 8.1 ksi for the 97% RH environment. The pre-exposure value for the copper/insulation specimens was measured to be approximately 9 ksi, thus an average decrease of approximately 0.8 ksi was seen after 6 months.

The pre-exposure ILSS for the copper/insulation specimens was measured to be approximately 1 ksi lower than the insulation specimens, but these results show that the copper/insulation specimens see less of a decrease in ILSS when exposed to humid environments for extended periods of time. Specifically, the insulation specimens saw an average decrease in ILSS of approximately 2.56 ksi (75% retention) where the copper/insulation specimens saw a mere reduction of approximately 0.8 ksi (91% retention). The 97% RH environment is also shown to affect the insulation specimens much greater than the copper/insulation specimens. These are positive results showing that the copper foil/CTD-403 interface is not weakened by room temperature humidity exposure; in fact the copper foil is shown to help diminish the effects of humidity on the ILSS.

Figures 4.18 and 4.19 show the room temperature humidity aging effects on the flexural modulus for the insulation and copper/insulation specimens, respectively. The pre-exposure flexural modulus for the insulation specimens was measured to be approximately 2.6 Msi. Within the first ten days of exposure, the insulation specimens display an increase in flex modulus of approximately 0.3 Msi. This is due to the cyanate ester resin becoming more brittle. This increase in modulus results in a loss of strength. As exposure time increases, the modulus begins to decrease due to softening of the matrix and weakening of the fiber matrix interface. Similar to the ILSS, the flex modulus decreases at larger magnitude at the higher humidity levels. After 6 months of exposure, an average flex modulus of 2.56 Msi is seen for the room temperature specimens, a retention of 98.5%.

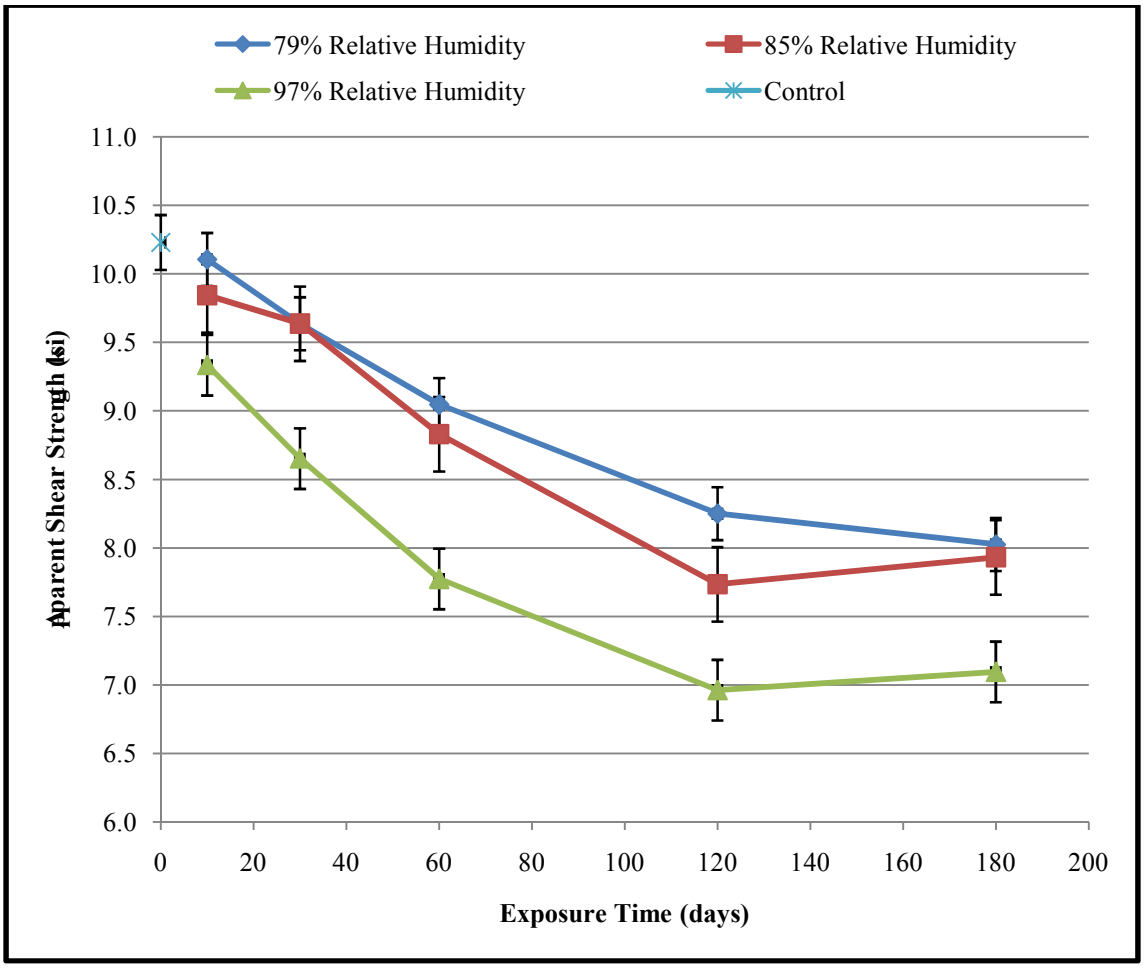

Figure 4.16 Interlaminar shear strength vs. time (days) for the insulation specimens aged at three humidity levels. The curves show the humidity effects on the ILSS of S2 glass/CTD-403 insulation specimens.

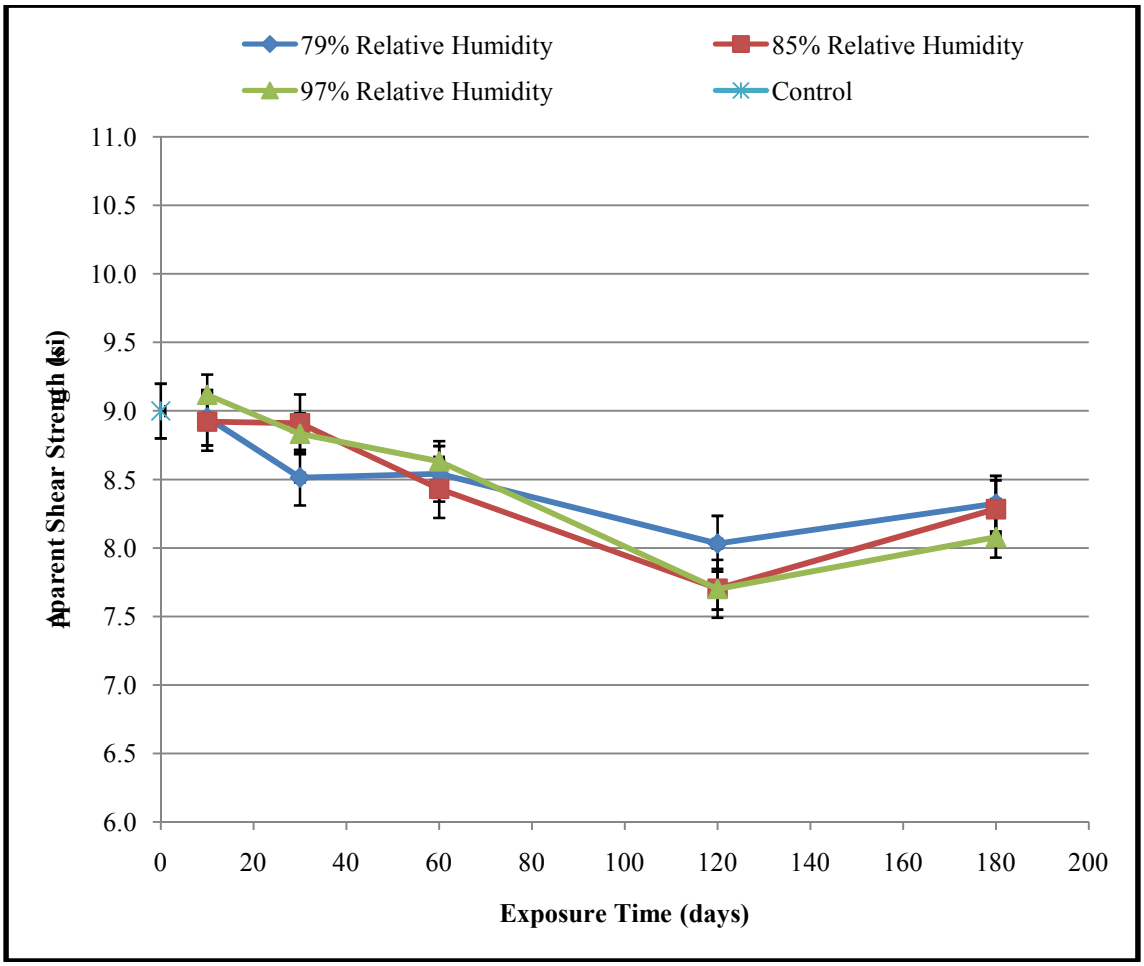

Figure 4.17 Interlaminar shear strength vs. time (days) for the copper/insulation specimens aged at three humidity levels. The curves show the humidity effects on the ILSS of S2 glass/CTD-403 with a copper foil interface specimens.

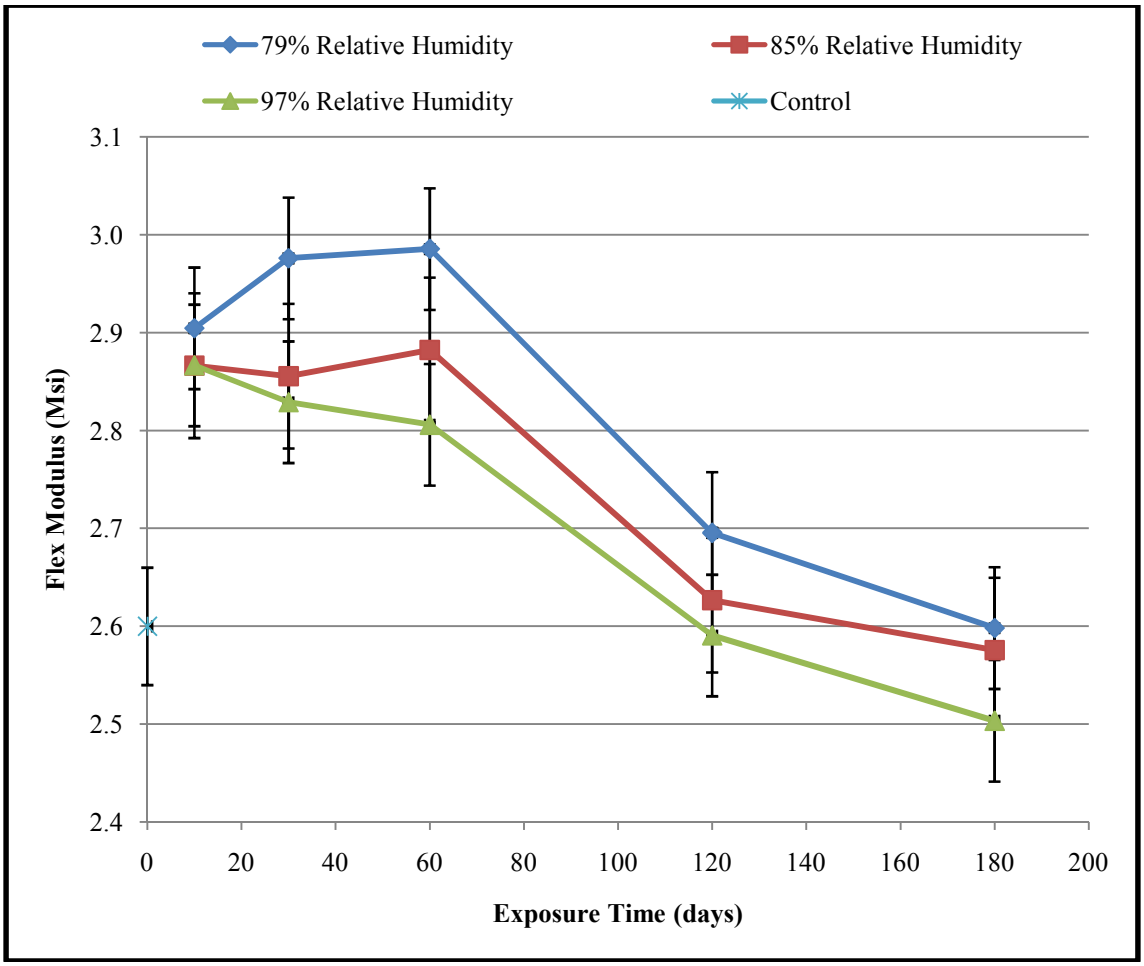

Figure 4.18 Flexural modulus vs. time (days) for the insulation specimens aged at three humidity levels. The curves show the humidity effects on the flex modulus of S2 glass/CTD-403 insulation specimens.

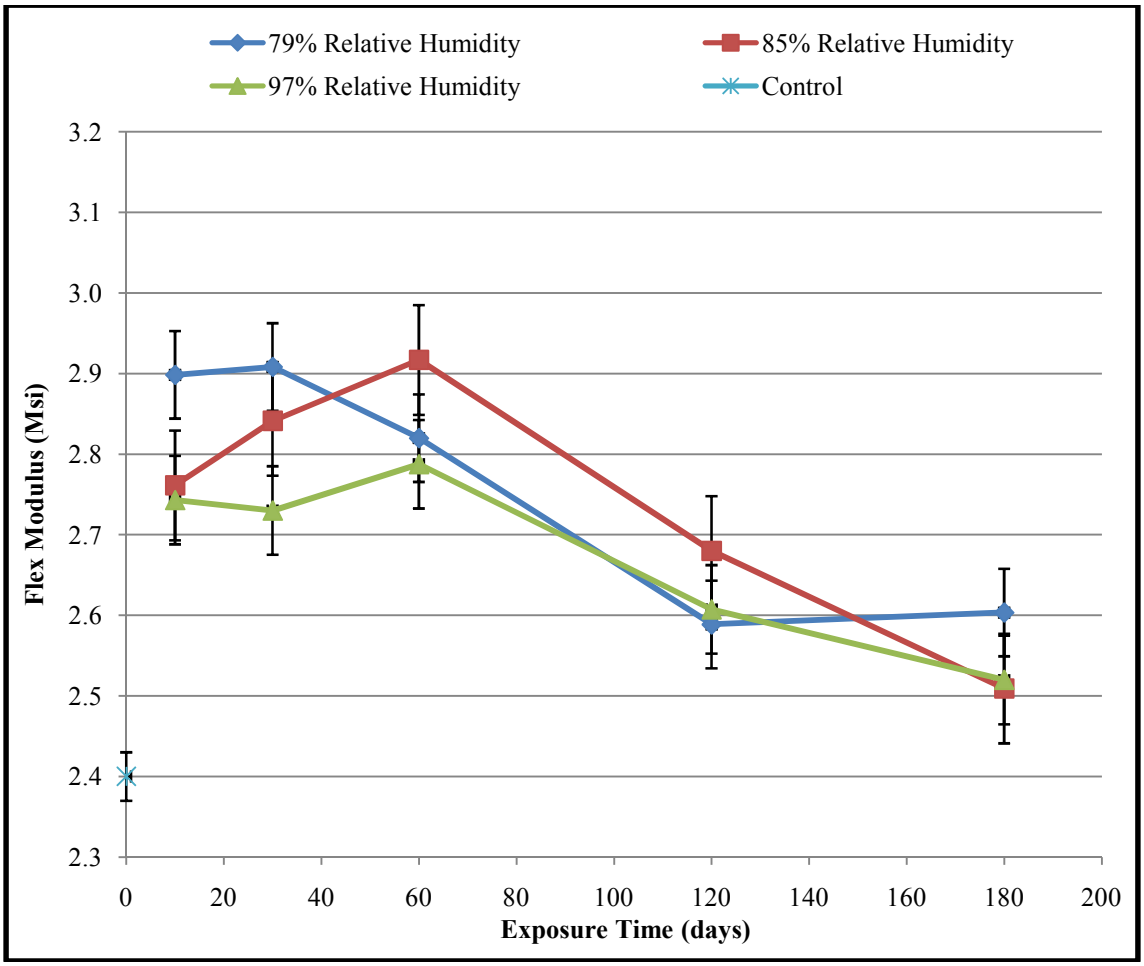

Figure 4.19 Flexural modulus vs. time (days) for the copper/insulation specimens aged at three humidity levels. The curves show the humidity effects on the flex modulus of S2 glass/CTD-403 with a copper foil interface specimens

The flexural modulus for the copper/insulation specimens (Figure 4.19) shows less of a trend when compared to the insulation specimens. The pre-exposure flex modulus was measured to be approximately 2.4 Msi. The same increase as the insulation specimens is seen in the first ten days of exposure, where once again the 79% RH specimens show the greatest initial increase. After six months of exposure, an average flex modulus of 2.54 Msi is seen for the copper/insulation specimens, actually seeing an increase of approximately 6% when compared with the pre-exposure flex modulus. A difference of 0.02 Msi is seen when comparing the average room temperature flex modulus of the two specimen types after 6 months of exposure. This again is a positive result indicating that the copper foil does not have a large effect on the modulus. The reductions in the modulus are also seen to be minimal.

4.3.2 Effects of Temperature

Figures 4.20 and 4.21 show the elevated temperature aging effects on the ILSS for the insulation and copper/insulation specimens, respectively. A constant relative humidity of 79% was used for both temperature conditions. The elevated temperature effects are shown to be minimal for the insulation specimens (Figure 4.20), showing an ILSS of 0.15 ksi less when compared to the room temperature insulation specimens after 6 months of aging. The ILSS for the copper/insulation specimens at elevated temperatures do not follow this trend. Figure 4.21 shows that after the first ten days of exposure the ILSS of the two conditions are approximately equal, but then the elevated temperature begins to significantly affect the ILSS. After 6 months of exposure, the ILSS of the room temperature specimens is at an average of 8.32 ksi, and the elevated temperature

specimens drop down to an average ILSS of 3.33 ksi. The fact that the insulation specimens were only slightly affected by elevated temperature conditions and the copper/insulation specimens were greatly affected by the elevated temperature conditions, points to a breakdown in the copper foil/matrix interface. The retention rate for the copper/insulation specimens at room temperature is found to be 92.5% as opposed to 37% for aging at 75°C.

Figures 4.22 and 4.23 show the elevated temperature aging effects on the flexural modulus for the insulation and copper/insulation specimens, respectively. For the insulation specimens, the elevated temperature is seen to slightly increase the flex modulus where for the copper/insulation specimens the elevated temperature is seen to slightly decrease the flexural modulus. In both cases, the flex modulus aged at elevated temperatures shows a retention rate above 90% after 6 months. When using coupon sized specimens for SBS testing as was performed in this research, a few things must be noted. As described in the methodology section, the specimens were machined in rectangular cross sections thus having a machined interface which allows for moisture and heat to travel along the copper/composite interface. In practice, this interface would not be directly exposed to humidity due to the insulation being wrapped around the conductor. Also, the resin flows into conductor strands during the impregnation process, creating a meshed interface. The above mentioned provides a means for the degradation of the copper/insulation interface, which is shown to occur at elevated temperature. Lastly, there are typically large compressive forces on the coils to minimize the shear forces within the insulation [47].

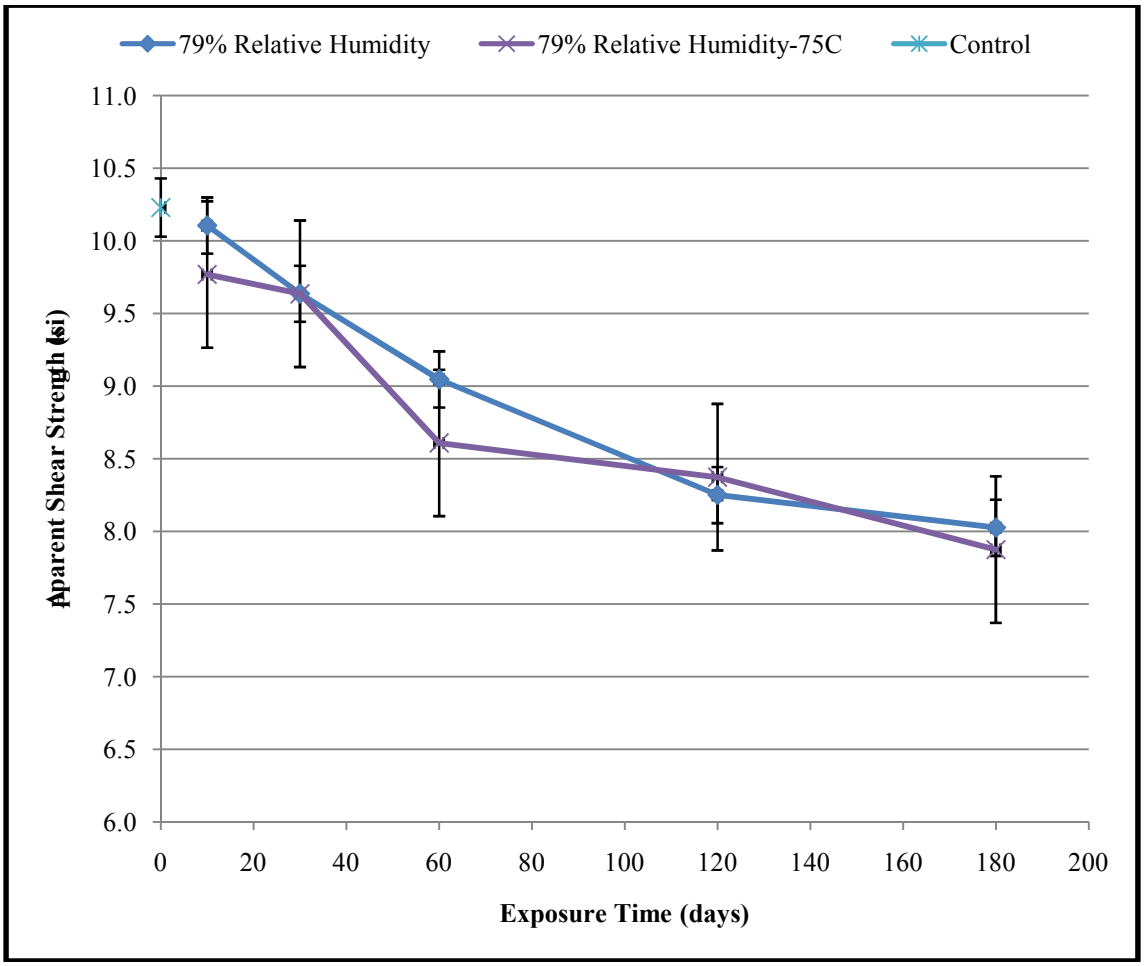

Figure 4.20 Interlaminar shear strength vs. time (days) for the insulation specimens aged at room and elevated temperatures. The curves show the elevated temperature effects on the ILSS of S2 glass/CTD-403 insulation specimens.

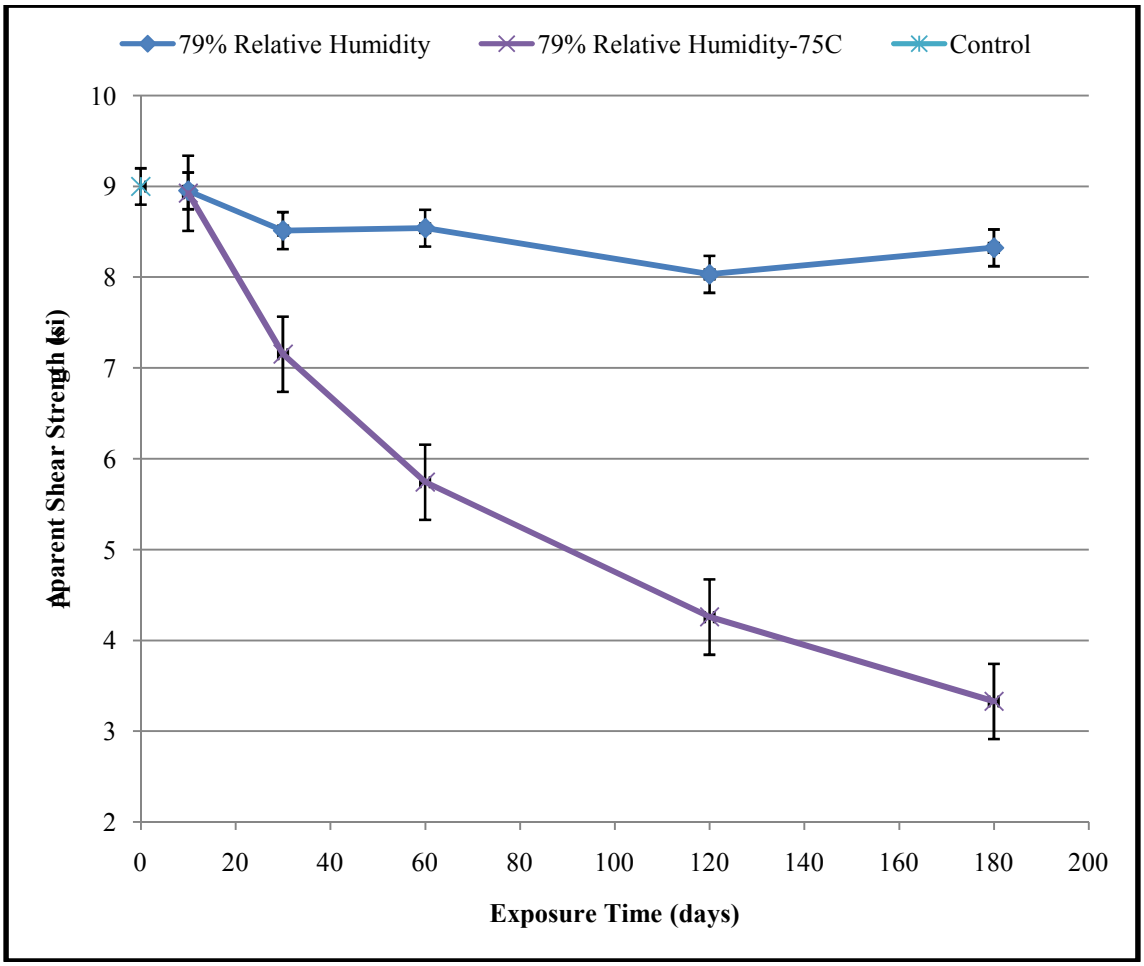

Figure 4.21 Interlaminar shear strength vs. time (days) for the copper/insulation specimens aged at room and elevated temperatures. The curves show the elevated temperature effects on the ILSS of S2 glass/CTD-403 with a copper foil interface specimens.

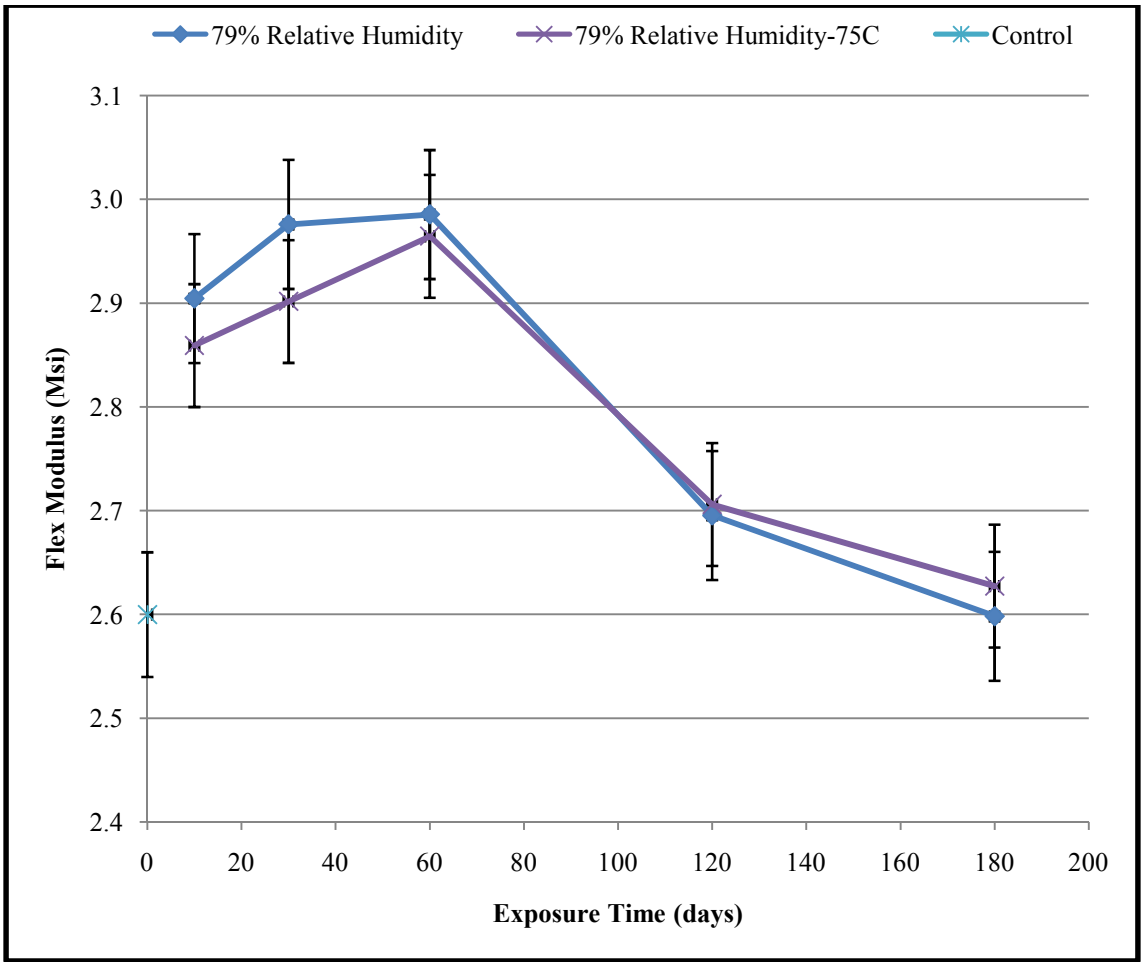

Figure 4.22 Flexural modulus vs. time (days) for the insulation specimens aged at room and elevated temperatures. The curves show the elevated temperature effects on the flex modulus of S2 glass/CTD-403 insulation specimens.

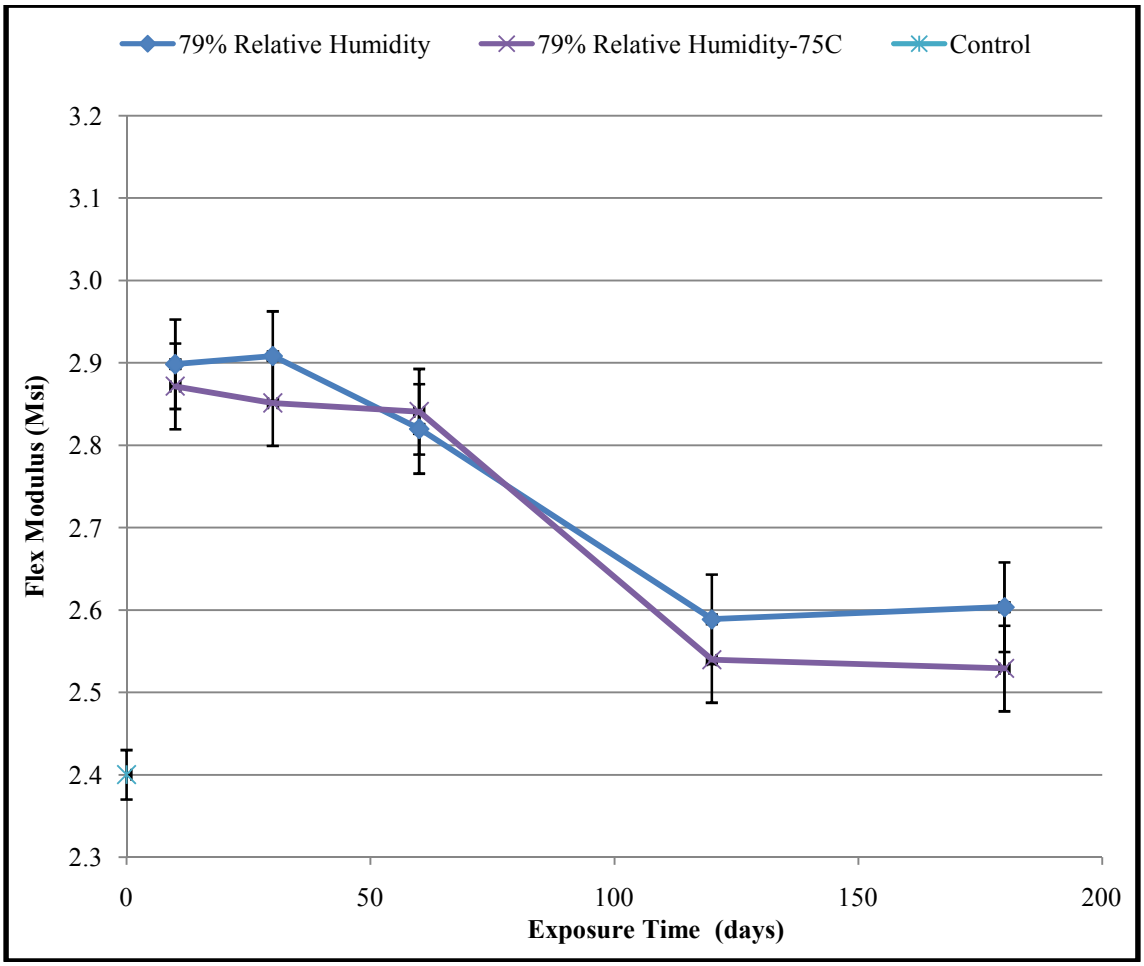

Figure 4.23 Flexural modulus vs. time (days) for the copper/insulation specimens aged at room and elevated temperatures. The curves show the elevated temperature effects on the flex modulus of S2 glass/CTD-403 with a copper foil interface specimens.

4.4 Compression Testing

The primary mechanical stresses within fusion or superconducting magnets are compressive stresses, normally held to 40-75 ksi [27]. The compression tests were performed in the through thickness direction, with the compressive forces applied normal to the fabric plies. As previously described, compressive strength as well as the compressive modulus was determined using an extensometer to accurately measure the deflection experienced by the specimen. The pre-exposure values for compressive strength and compressive modulus were determined to be 136 ksi and 1,218 ksi, respectively.

Figure 4.24 shows the results for the compressive strength average values for the four aging conditions, 79% RH, 85% RH, 97% RH, and 79% RH 75°C. The pre-exposure values are seen as a single point on the vertical axis, and the standard deviation of each sample set is represented by error bars. The room temperature specimens see a slight increase in compressive strength, at an average increase of approximately 3.5% after six months of exposure. The elevated temperature specimens are seen to have a retention rate greater than 90% for their compressive strength after six months of exposure. This decrease in compressive strength at elevated temperatures may be accounted for by a decrease in the radial compressing force due to a decrease in the residual thermal stress.

Compressive strength is generally characterized by the matrix properties, and tensile strength is generally characterized by the fiber properties. Under compression, the matrix simply acts as a housing for the fibers, where in tension the fiber/matrix interface is tested which makes the specimens more vulnerable to degradation. It is for these reasons that

the compressive strength is generally more stable than tensile properties as shown in comparison with the short beam shear testing results. When comparing the temperature effects of the compression specimens as opposed to the short beam shear specimens, the elevated temperature is seen to play a larger role on the compressive strength of the insulation when compared to the interlaminar shear strength. Once again, this is due to compressive properties of composites being dependant predominately on the matrix (temperature dependant), and the tensile properties being predominately dependant on the fiber of the composite (temperature independent).

Figure 4.25 shows the results for the compressive modulus average values for the four aging conditions. The compressive modulus for the room temperature specimens shows an average increase of 2.5% after 6 months of aging. The compressive modulus is seen to increase approximately 14% after 6 months of aging at 75°C. During the first month of aging, all four environmental conditions show the same initial increase in the compressive modulus. Past the first month of exposure, the room temperature specimens begin to settle back to their initial compressive modulus values where the elevated temperature specimens continue to see an increase in their compressive modulus. One possible cause for this increase in modulus is additional bond formation within the matrix due to the elevated temperatures. The increased modulus results in a more brittle fracture, effectively lowering the compressive strength of the insulation. Plots of specimen variation for the four each of the four environments can be found in the appendix.

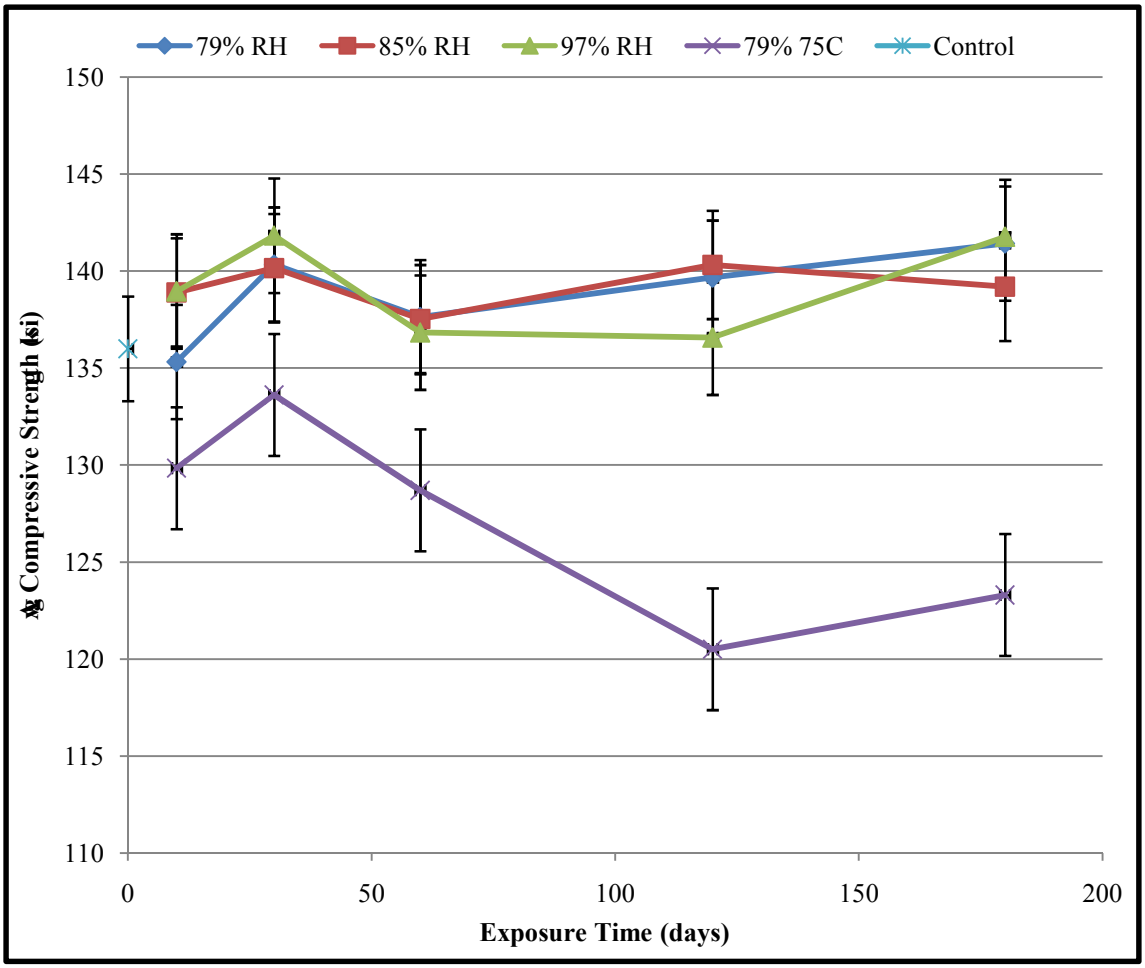

Figure 4.24 Insulation specimens average compressive strength (ksi) vs. time (days). The graph shows the aging effects of the four different environmental conditions on the compressive strength of S2 glass/CTD-403 composites.

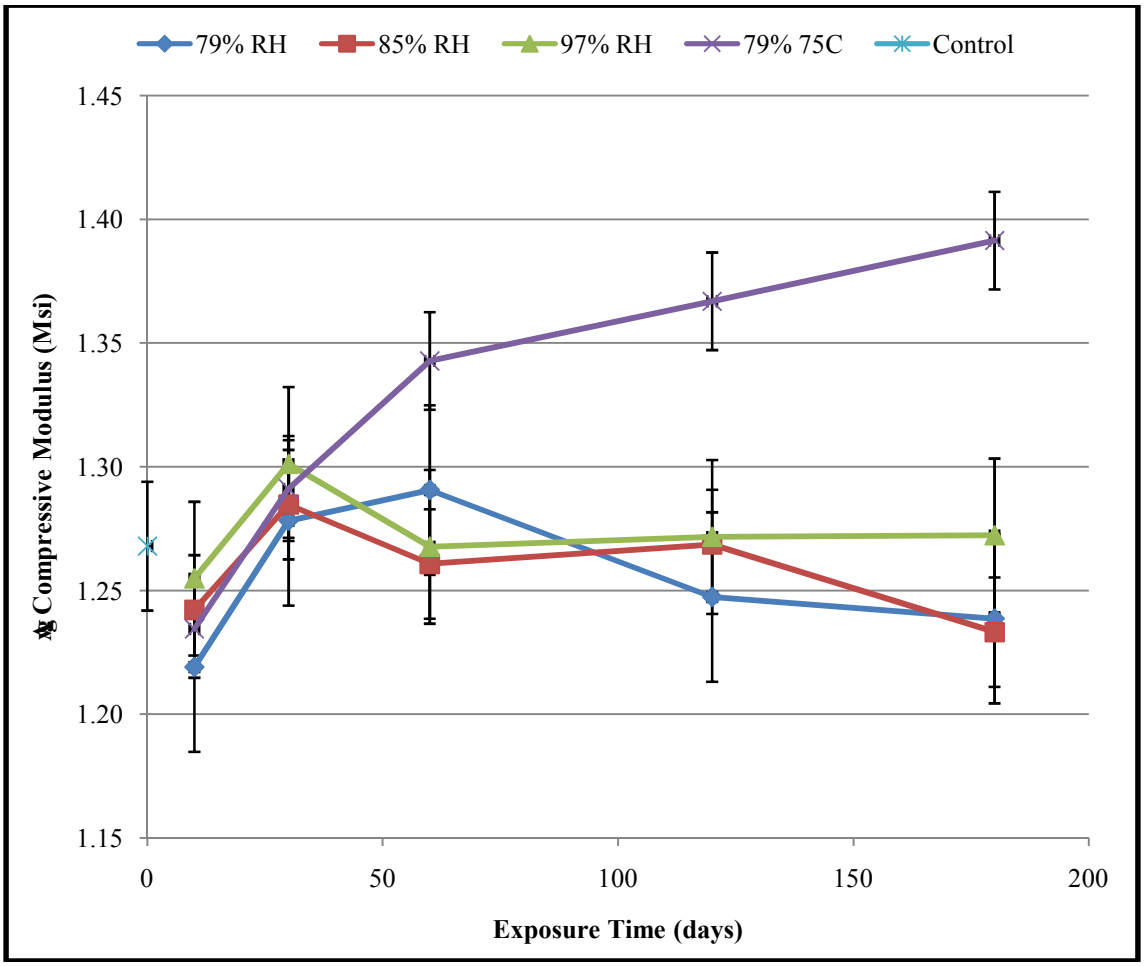

Figure 4.25 Insulation specimens average compressive modulus (Msi) vs. time (days). The graph shows the aging effects of the four different environmental conditions on the compressive modulus of S2 glass/CTD-403 composites.

4.5 Dielectric Breakdown Testing

Figures 4.26 and 4.27 show the humidity aging effects at room temperature for the average dielectric strength (kV/mm) and the average electrical strength constant (kV/mm^1/2), respectively. As outlined in Tables 3.1 and 3.2, insulation specimens were used for dielectric testing. The pre-exposed values for the dielectric strength and the electrical strength constant were determined to be 105 kV/mm and 74 kV/mm^1/2, respectively. The composites dielectric strengths were determined by dividing the experimentally determined breakdown voltage by the specimen thickness. As expected, the degradation trend of the dielectric strength is seen to be directly related to the amount of moisture absorption in the specimens (Figure 4.26). Dielectric strength retentions of 99%, 93%, and 90% are seen after six months of humidity exposure for the 79%, 85%, and 97% RH specimens, respectively. An average dielectric strength of 98.6 kV/mm is seen for all specimens at room temperature after six months of aging.

Figures 4.28 and 4.29 show the humidity aging effects an elevated temperature for the average dielectric strength (kV/mm) and the average electrical strength constant (kV/mm^1/2), respectively. The effects of temperature on the dielectric strength of the insulation are seen to be minimal. The specimens aged at 75°C have an average dielectric strength retention of 91% after six months of aging. As previously described, the room temperature specimens aged at the same RH as the elevated temperature specimens saw an average dielectric strength retention of 99%, equating to an 8% dielectric strength loss due to the elevated temperature. Overall, the 97% RH exposure specimens saw the greatest loss in dielectric strength after six months of aging.

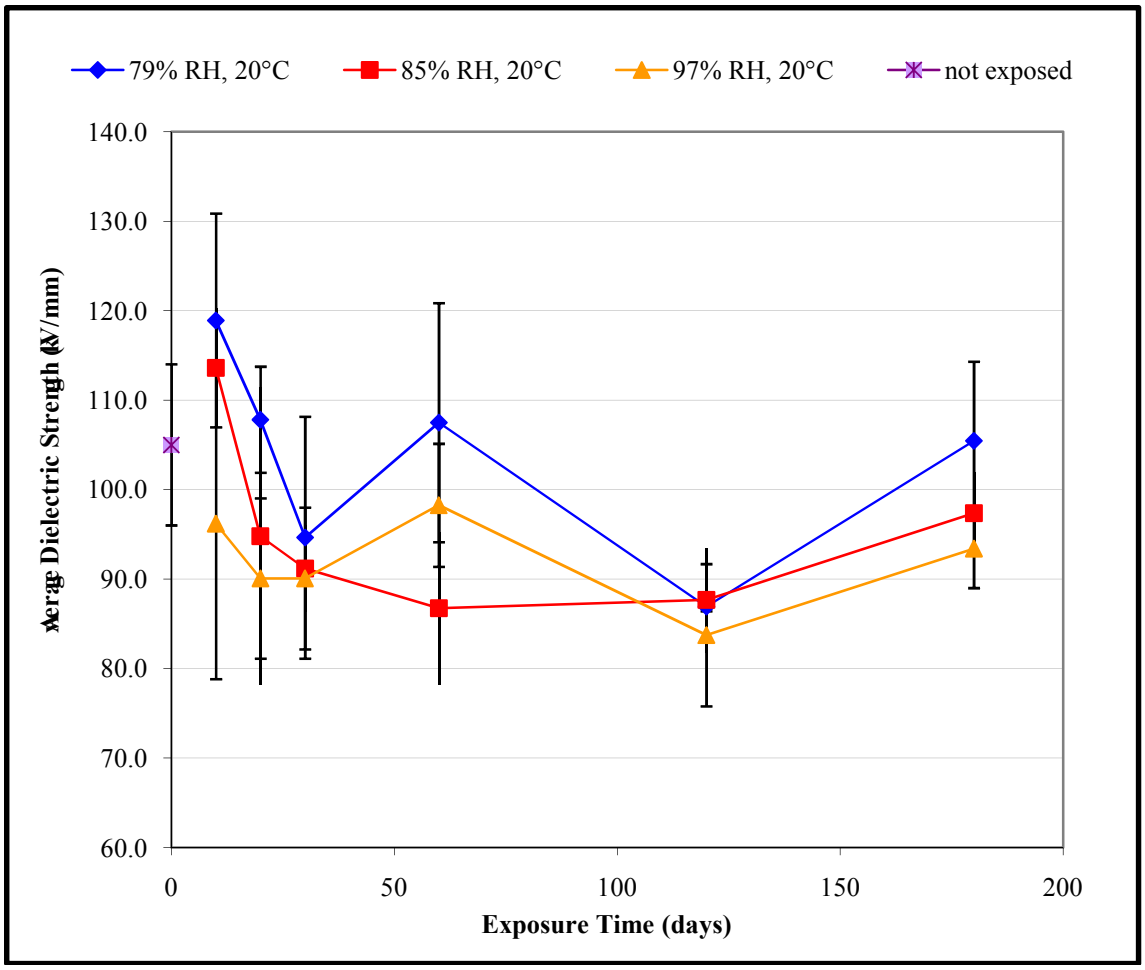

Figure 4.26 Average dielectric strength (kV/mm) for the insulation specimens at room temperature. The graph shows the humidity aging effects on the dielectric strength as a function of exposure time for the CTD-403/S2 glass composites.

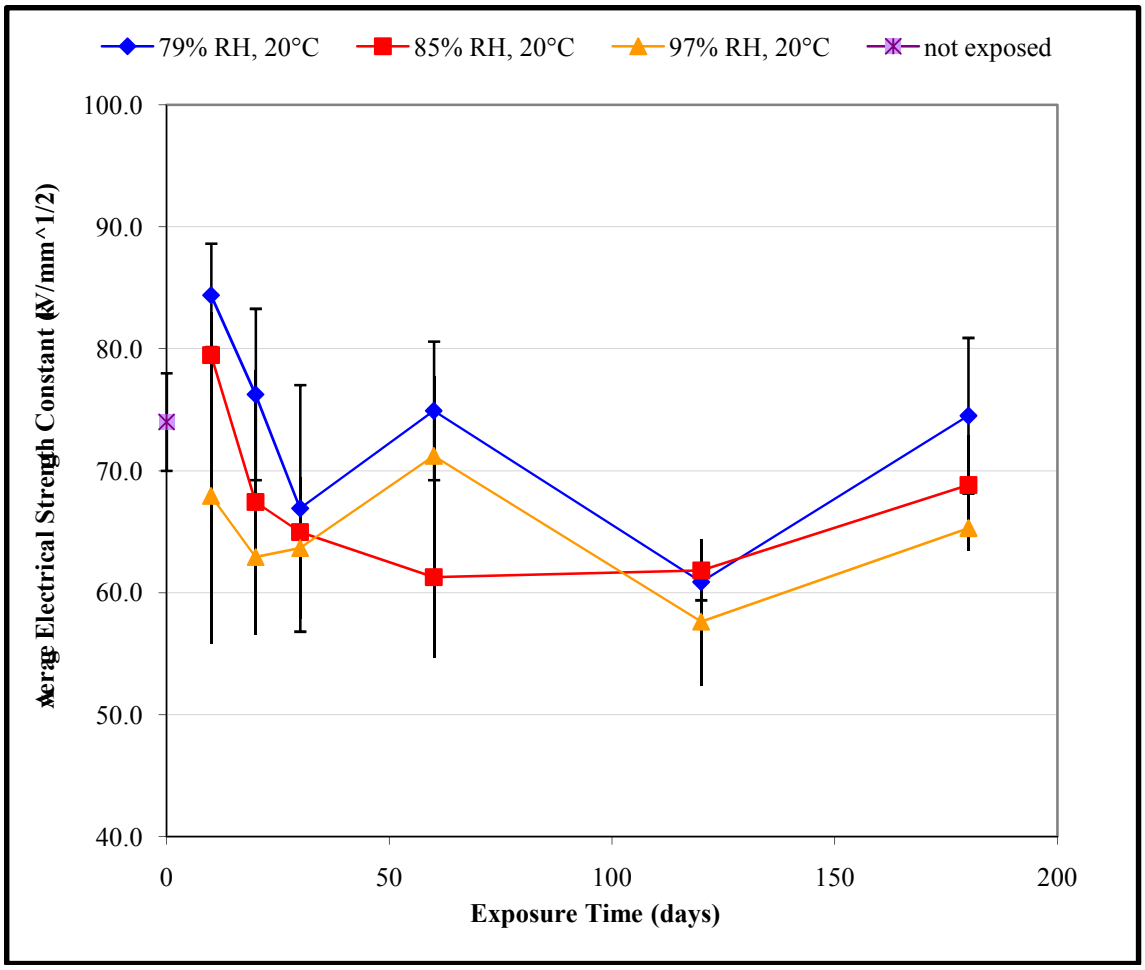

Figure 4.27 Average electrical strength constant (kV/mm^1/2) for the insulation specimens at room temperature. The graph shows the humidity aging effects on the electrical strength constant as a function of exposure time for the CTD-403/S2 glass composites.

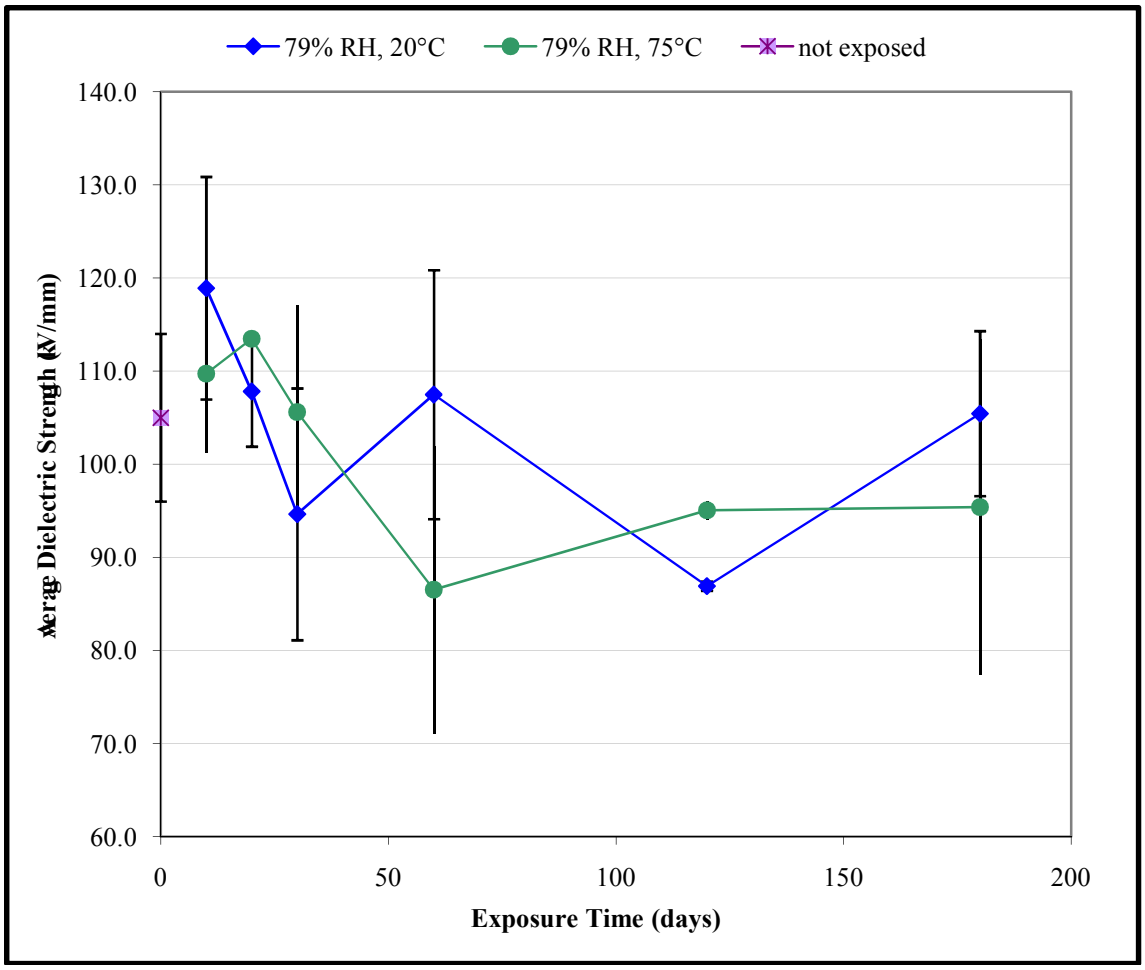

Figure 4.28 Average dielectric strength (kV/mm) for the insulation specimens at elevated temperatures. The graph compares the humidity/temperature aging effects on the dielectric strength as a function of exposure time for the CTD-403/S2 glass composites.

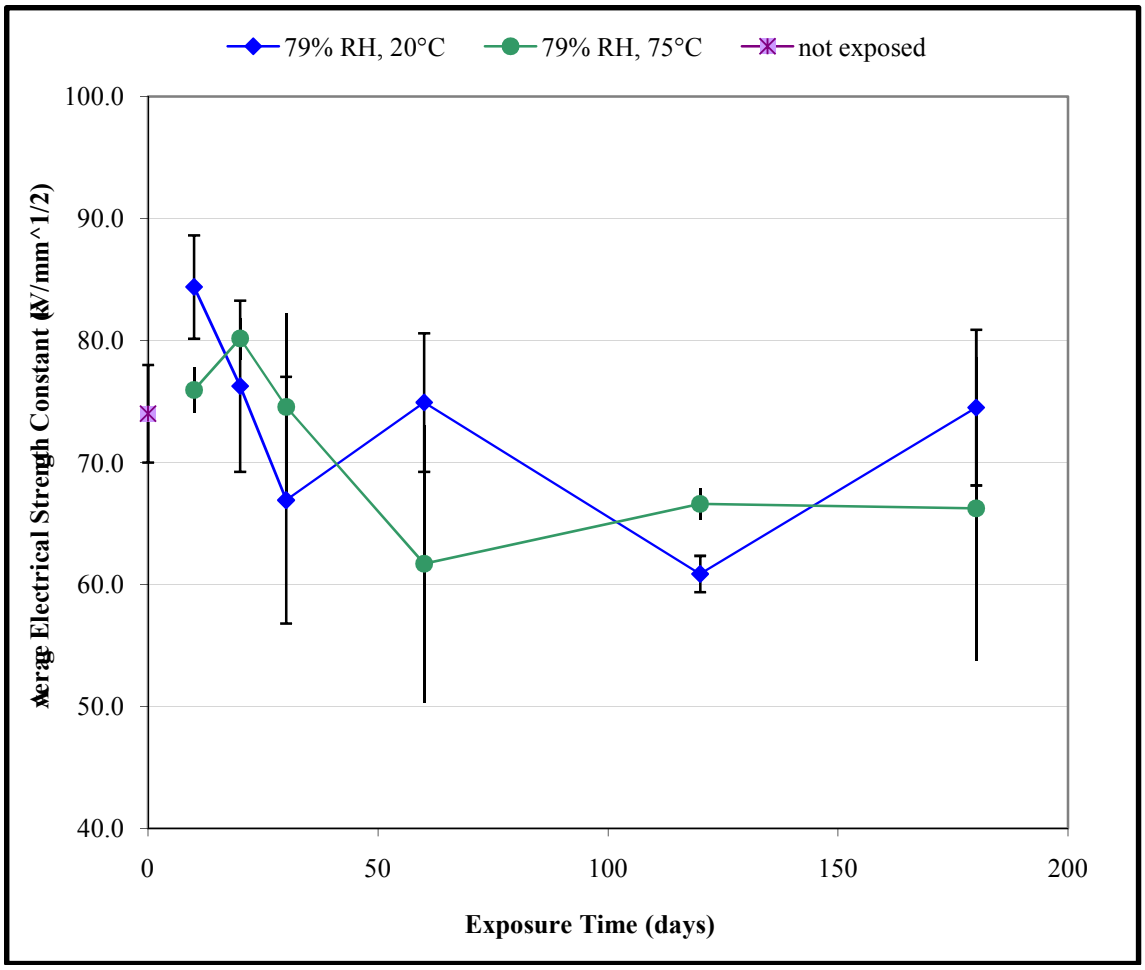

Figure 4.29 Average electrical strength constant (kV/mm^1/2) for the insulation specimens at elevated temperatures. The graph compares the humidity/temperature aging effects on the dielectric strength constant as a function of exposure time for the CTD-403/S2 glass composites.

4.6 Dynamic Mechanical Analysis

In order to characterize the modulus of the neat resin specimens as a function of temperature DMA testing was performed using TA instruments model Q800 DMA. The glass transition (T_g) was also determined to evaluate the effects of the various environmental conditions on this aspect of the insulation performance. An example output of the Q800 is seen in Figure 4.30. The storage modulus (MPa), loss modulus (MPa), and tan delta are plotted as a function of temperature. The temperature seen in this plot is not to be confused with exposure temperature. Testing was performed between 25°C and 300°C.

Glass transition temperatures are commonly defined one of two ways using DMA data. The "knee" of the storage modulus vs. temperature plot is a more conservative estimate while the maximum of the tan delta vs. temperature curve will most often yield higher results. For this reason, it is important to define the parameter used to identify T_g. The temperature values reported are considered accurate to ±2°C, according to the manufacturers accuracy rating of the thermocouple used to monitor and record the specimen temperature. In Figure 4.30, the knee of the storage modulus curve is seen to occur at approximately 195°C. The maximum value of the tan delta curve is seen to occur at approximately 232°C. Since T_g is being used for engineering design, that is, the determination of maximal end-use temperatures, the conservative estimate of T_g is warranted.

Figures 4.31 and 4.32 show the room temperature results of the DMA analysis, using the knee of the storage modulus curve and the maximum of the tan delta curve, respectively. It is seen that the results based on the storage modulus do in fact present a more conservative value for T_g. The glass transition temperature is seen to decrease with exposure time, decreasing with increased moisture absorption. The 6 month specimens unexpectedly see an increase in T_g. These results are most likely due to instrument technical difficulties restricting immediate testing of the specimens, allowing drying to occur. The pre-exposure storage modulus T_g and tan delta T_g were determined to be 191°C and 272°C, respectively.

Figures 4.33 and 4.34 show the elevated temperature results of the DMA analysis, using the knee of the storage modulus curve and the maximum of the tan delta curve, respectively. The specimens aged at 79% RH 75°C see an additional reduction in storage modulus T_g of approximately 1°C after 4 months of exposure when compared to the 79% RH room temperature specimens. Similarly, the tan delta T_g specimens see an additional reduction of approximately 30°C after 4 months of exposure. The elevated temperatures increase moisture absorption in the specimens which in turn decrease the T_g. The lowest T_g is seen to be approximately 186°C, after 6 months of exposure at 79% and 75°C. Different test methods and oscillation frequencies can result in different T_g values, so as a rule of thumb, the glass transition temperature should be at least 30°C higher than service temperature [13]. With most room temperature curing epoxies, the T_g is no more than 50-60°C. Table 4.8 provides a summary of the results. Glass transition temperatures for all specimens are well above the maximum end-use temperature of 150°C (QPS) after six months exposure.

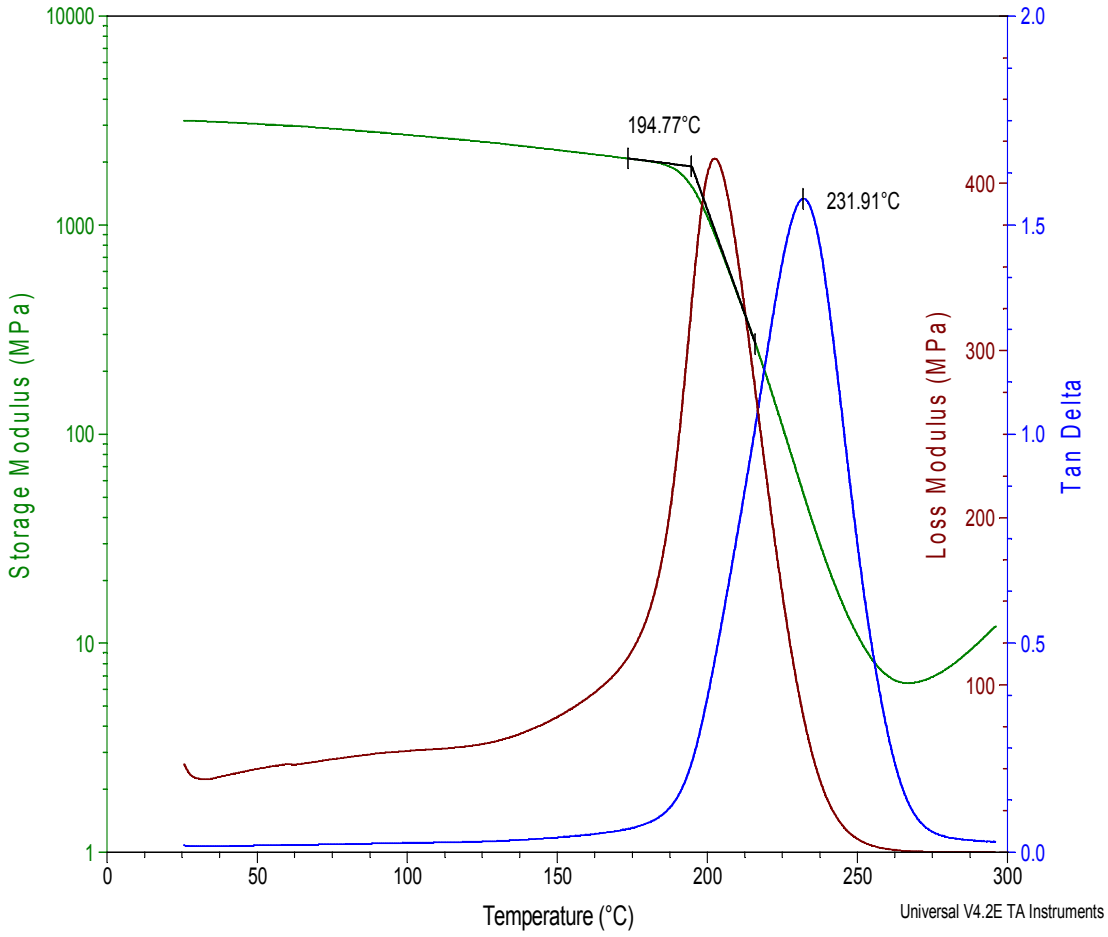

Figure 4.30 TA instruments model Q800 DMA output plot. The plot shows the storage modulus, loss modulus, and tan delta as a function of temperature.

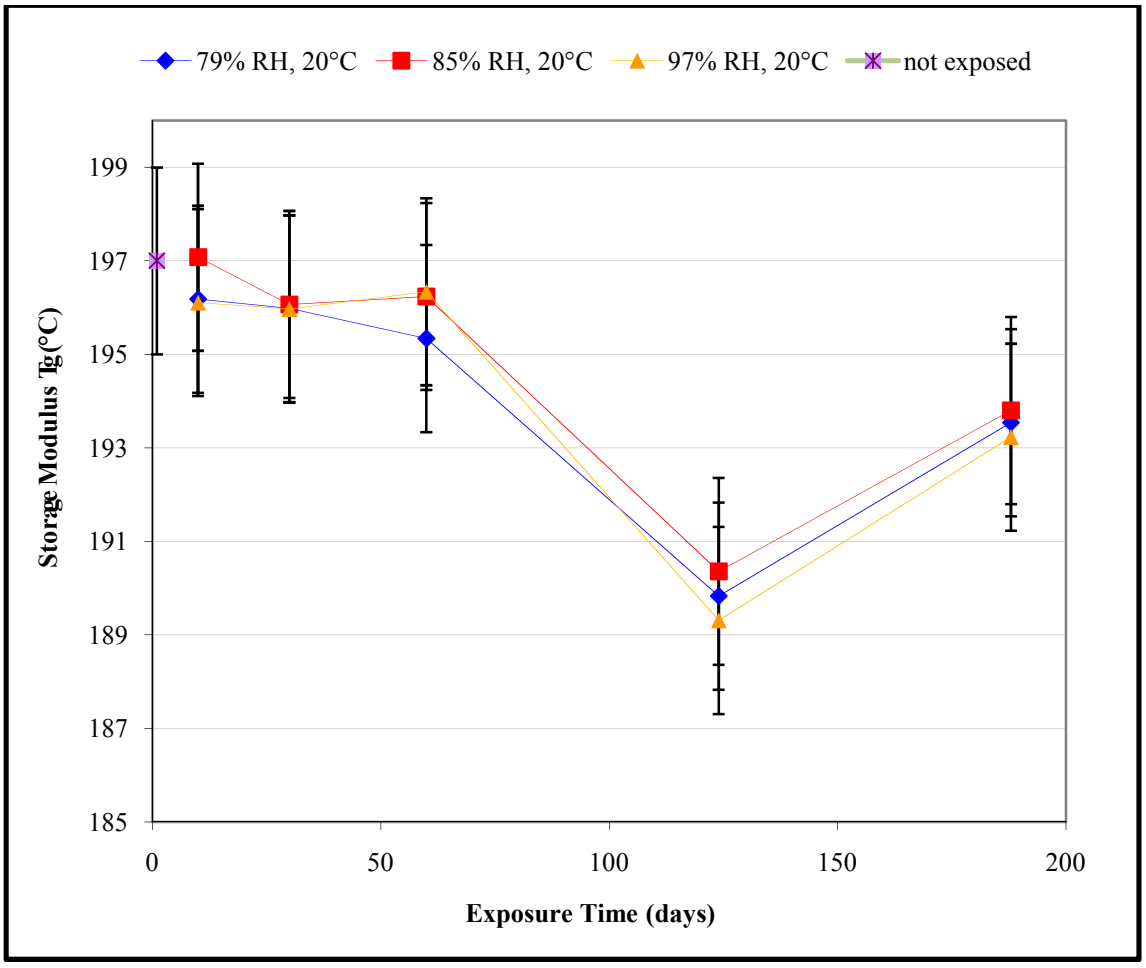

Figure 4.31 Average glass transition temperature vs. exposure time at room temperature. The plot shows the reduction of the storage modulus T_g on the neat resin specimens due to humidity exposure.

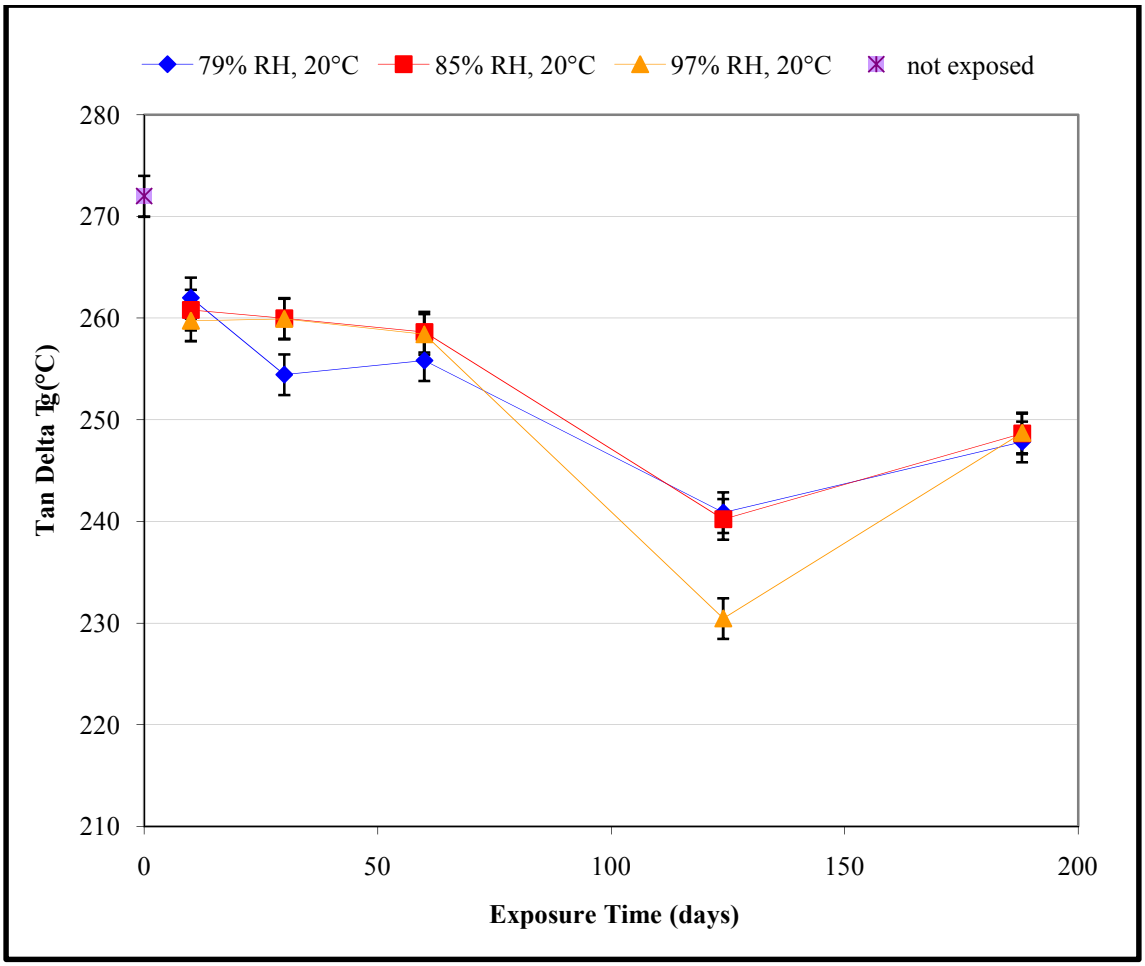

Figure 4.32 Average glass transition temperature vs. exposure time at room temperature. The plot shows the reduction of the tan delta T_g on the neat resin specimens due to humidity exposure.

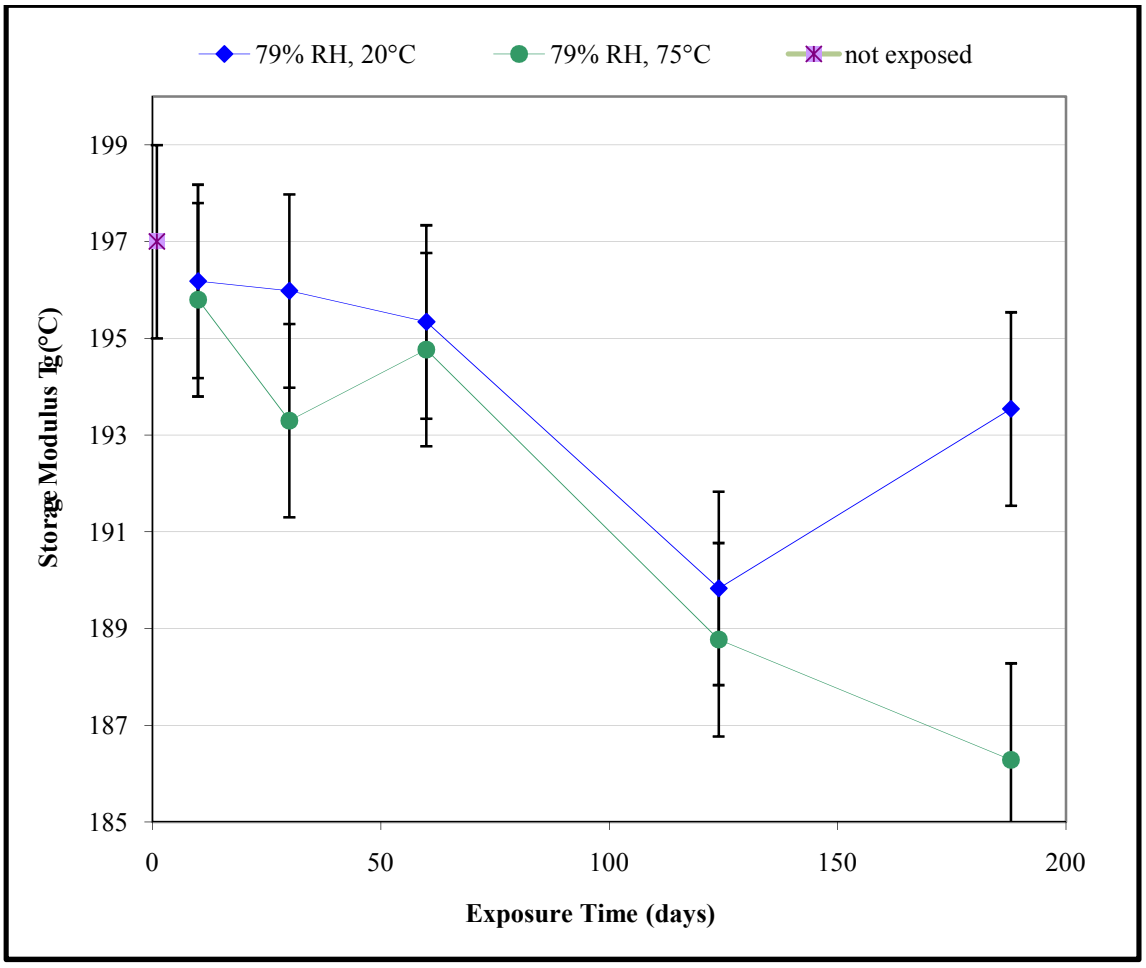

Figure 4.33 Average glass transition temperature vs. exposure time at an elevated temperature. The plot shows the reduction of the storage modulus T_g on the neat resin specimens due to humidity/elevated temperature exposure.

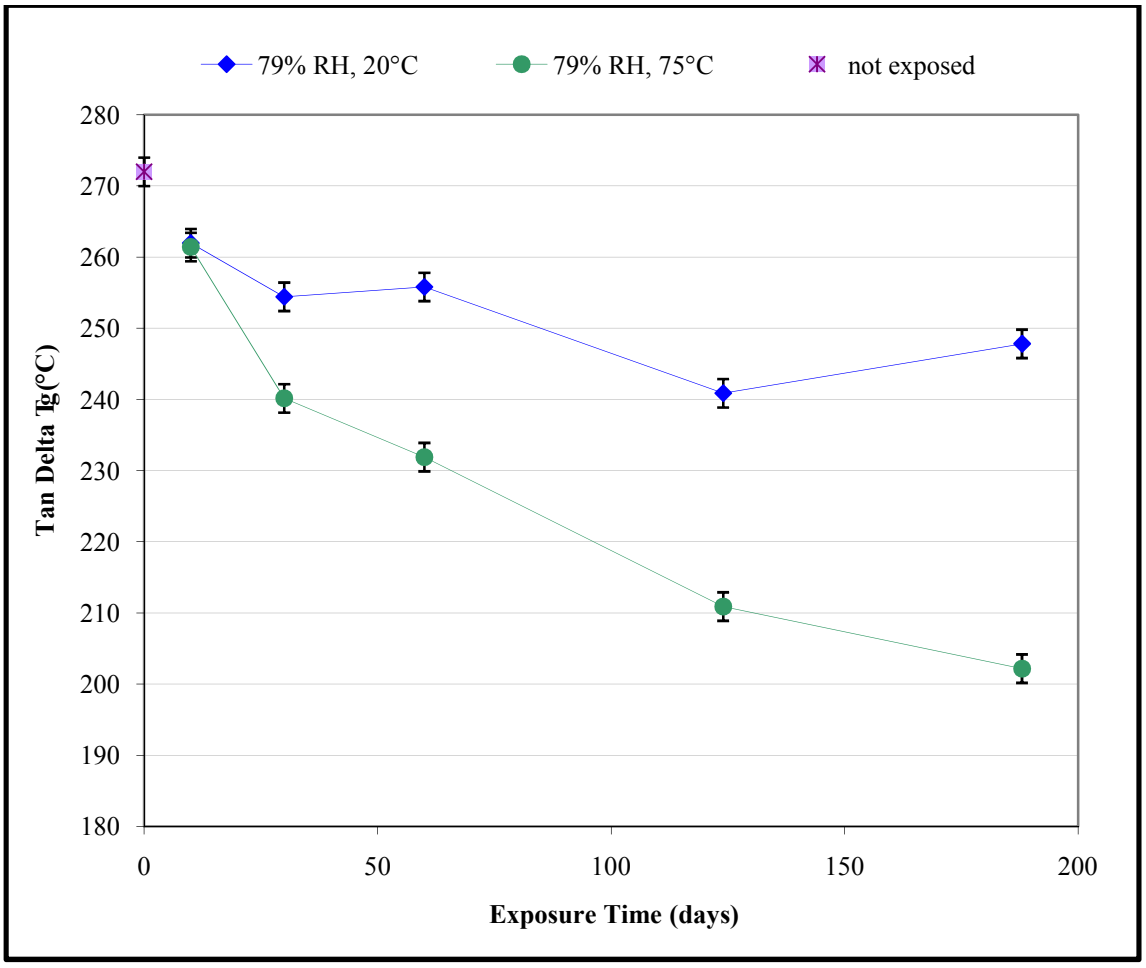

Figure 4.34 Average glass transition temperature vs. exposure time at an elevated temperature. The plot shows the reduction of the tan delta T_g on the neat resin specimens due to humidity/elevated temperature exposure.

Table 4.8 Summary of results after 6 months of exposure for three specimen types and four environmental conditions

Parameters	Neat Resin Specimens				Insulation Specimens				Copper/Insulation Specimens			
	79%	85%	97%	79% 75C	79%	85%	97%	79% 75C	79%	85%	97%	79% 75C
Moisture Absorption (%)	0.514	0.546	0.677	1.51	0.191	0.21	0.286	0.539	0.171	0.198	0.254	0.452
Volume Increase (%)	1.24	1.09	1.15	3.17	0.52	0.39	0.49	0.34	1.51	1.39	1.23	1.64
ILSS (ksi)	-	-	-	-	8.027	7.932	7.097	7.876	8.325	8.283	8.079	3.33
Flex Modulus (Msi)	-	-	-	-	2.598	2.576	2.504	2.628	2.603	2.509	2.52	2.529
Compressive Strength (ksi)	-	-	-	-	141.4	139.2	141.8	123.3	-	-	-	-
Compressive Modulus (Msi)	-	-	-	-	1.24	1.23	1.27	1.39	-	-	-	-
Dielectric Strength (MV/in)	-	-	-	-	2.678	2.473	2.372	2.423	-	-	-	-
Electrical Strength (MV/in^.5)	-	-	-	-	0.376	0.347	0.329	0.334	-	-	-	-
Storage Modulus T_g (°C)	193.5	193.8	193.2	186.3	-	-	-	-	-	-	-	-
Tan Delta T_g (°C)	247.8	248.6	248.7	202.2	-	-	-	-	-	-	-	-

CHAPTER V

CONCLUSIONS AND RECOMMENDATIONS

5.1 Conclusions

Cyanate-ester-based resin systems, specifically CTD-403, have been developed for use in many applications, including the advancement of insulation systems for fusion devices. Ease of processing and fabrication, increased radiation resistance, low moisture absorption and dimensional stability, and mechanical and electrical strength at cryogenic and elevated temperatures are the focus of these new insulation systems. The advancements of these properties have been validated through laboratory testing and analysis, but in order to validate the application specific use of CTD-403 in QPS further research was performed. This report summarizes the aging effects on moisture resistance, dimensional stability, and mechanical and electrical properties of CTD-403 based insulation systems under humid environments as well as elevated temperatures. The aging effects on adhesion characteristics to both metals and glass fibers are also studied.

After six months of exposure, CTD-403/S2 glass insulation systems have been shown to exhibit the necessary mechanical and electrical performance to ensure the integrity of the insulation for future fusion magnet applications. The dimensional stability and moisture absorption trends of the resin have also been shown superior compared to existing epoxy based resin systems.

The major findings of this thesis are listed below.

(1) The moisture diffusion process in CE follows the Fickian mode in the initial stages of the diffusion process but becomes non-Fickian in the later stages after a time of approximately 2 weeks of exposure. CE samples absorb more moisture with increased relative humidity. CE samples show increased absorption when exposed to higher temperatures. Composite samples involving S2 glass exhibit reduced amounts of moisture absorption when compared to neat resin specimens. An average weight gain of 0.58% was seen for the room temperature specimens, where the elevated temperature specimens saw an average weight gain of 1%.

(2) The insulation specimens showed superior dimensional stability when compared with the neat resin specimens because the S2 glass fibers provide resistance to expansion of the specimens.

(3) The interlaminar shear strength of the specimens decreased with increased humidity levels. The elevated temperature conditions showed little effect on the insulation specimens, but greatly affected the copper/insulation specimens. The interlaminar shear strength meets the performance needs of QPS.

(4) The compressive strength of the insulation specimens decreased with increasing humidity exposure. The compressive strength also decreased at elevated temperatures. The compressive strength is well above the performance needs.

(5) The dielectric strength of the specimens was affected predominately by humidity exposure as opposed to elevated temperatures.

(6) As opposed to the dielectric strength, the glass transition temperature was affected predominantly by temperature as opposed to humidity. The maximum end-use

temperature after six months exposure is seen to be well above the performance needs of 150°C for all conditions.

(7) With increased humidity exposure, the specimens became more ductile in tension and more brittle in compression. With increased temperature exposure, the specimens show more brittle behavior in both compression and tension.

5.2 Recommendations

In order to fully characterize the moisture absorption trend of cyanate ester resins, humidity testing must be carried out past the six month aging period in this research. This will help identify the saturation level of the resin. In some cases, the saturation curve is seen to level off, but not in all cases. A more accurate testing of the copper foil interface at elevated temperatures should also be performed. In this research, the machined interface allowed for moisture and heat to enter the specimens, resulting in a breakdown of the interface. In practice, this interface would not be exposed in such a way, and the performance should be evaluated likewise. Also, the resin flows into the conductor strands during the impregnation process, which further complicates a comparison to the interface as tested.

Further testing recommendations are listed below.

(1) In practice, large compressive forces are typically seen on the coils which minimize the shear forces within the insulation. Improve mechanical testing by integrating a method to measure shear strength as a function of compressive load.

(2) The insulation will be exposed to repeated cycles of heating and cooling. Perform thermal cycling tests on the copper/insulation specimens as well as the insulation specimens in order to evaluate the effects on short beam shear, compressive, and dielectric properties of the insulation as well as the adhesion properties of the copper/insulation specimens.

(3) The insulation will operate under high vacuum. In order to ensure the stability under these conditions, vacuum outgas testing should be performed. CTD-403 has never been subjected to this test, but other cyanate ester based resins have been found to exhibit very good outgassing behaviors as compared to epoxy based materials.

(4) Thermal conductivity and specific heat data are needed in order for fusion magnet designers to model the thermal performance of fusion magnets. These properties can be measured using a flash diffusivity model. The coefficient of thermal expansion for the insulation also needs to be calculated as the test specimen is heated using a strain gauge technique [48].

(5) Increase exposure times in order to fully characterize moisture absorption trends at elevated temperatures.

REFERENCES

1. S.D. Grandlienard, et al., “Properties of Cyanate-Ester-Based Composite Insulation For Magnet Applications,” Composite Technology Development, Inc.
2. Narasimhaswami Shankar, "Cooling of QPS Modular Coils using Embedded Copper Tubes" (MA thesis, University of Tennessee, 2006), pg. 3.
3. J.F. Lyon, et al., “Status of the Quasi-Poloidal Stellarator Experiment (QPS),” presented at the 34th EPS Conference on Plasma Phys., Warsaw, July 2-6 2007.
4. “High Performance Magnet Technology for Fusion Applications,” Composite Technology Development, Inc.
5. B.E. Nelson, et al., “Design of the Quasi-Poloidal Stellarator Experiment (QPS),” presented at the Symposium on Fusion Technology, Helsinki, Finland, September 9-13, 2002.
6. Thome, R. and Heitzenroeder, P., "Engineering Features of the Fusion Ignition Research Experiment (FIRE)," presented at the 21st Symposium of Fusion Technology, Madrid, Spain, 2000.
7. Feucht, S.W., Fabian, P.E., and Munshi, N.A., "Development of Novel Radiation-Resistant Insulation Systems for Fusion Magnets," in *IEEE Transactions on Superconductivity* 13, Number 2, pp. 1516-19 (2003).
8. Nakamura, T.M., Takahashi, K., “Effects of Moisture Absorption on the Dynamic Interlaminar Fracture Toughness of Carbon/Epoxy Composites,” Journal of Composite Materials, VOL. 34, (2000) pp. 630-648.
9. Soles, C.L., Lee, A. F., “A Discussion of the Molecular Mechanisms of Moisture Transport in Epoxy Resins,” Journal of Polymer Science: Part B: Polymer Physics, VOL. 38, (2000) pp. 792-802.

10. http://www.eia.doe.gov/oiaf/ieo/pdf/world.pdf.

11. P.E. Fabian, N.A. Munshi, and R.J. Denis, "Highly Radiation-Resistant Vacuum Impregnation Resin Systems for Fusion Magnet Insulation," *Advances in Cryogenic Engineering – Materials,* VOL. 48, 2002.

12. M.W. Hooker, P.E. Fabian, S.D. Grandlienard, D.E. Codell, and M.J. Lizotte, "Shear Strengths of copper/Insulation Interfaces for Fusion Magnet Applications," *Advances in Cryogenic Engineering*, VOL 52B, pp. 306-313 (2006).

13. Peters, S. T., ed. Handbook of Composites 2nd ed. New York: Springer, 1997. 29-30.

14. Ashbee, Kenneth H. Fundamental Principles of Fiber Reinforced Composites. New York: C R C P LLC, 1993.

15. Mallick, P. K. Fiber-Reinforced Composites : Materials, Manufacturing, and Design. 3rd ed. New York: C R C P LLC, 2007.

16. Go. Goertzenertzen, W. K., and M. R. Kessler. "Thermal and mechanical evaluation of cyanate ester composites with low-temperature processability." ScienceDirect. 24 Jan. 2006. Iowa State University.

17. R. Hillermeirer and J. Seferis, "Environmental effects on thermoplastic and elastomer toughened cyanate ester composite systems", *J Appl Polym Sci* **77** (1997) (3), pp. 556–567.

18. I. Hamerton, Chemistry and technology of cyanate ester resins, Chapman and Hall, London (1994).

19. Merdas, I., Thominette, F.., Verdu, J., “Humid Aging of Polyetherimide. II. Consequences of Water Absorption on Thermomechanical Properties,” Journal Of Applied Polymer Science, Vol. 77, (2000) pp.1445-1451.
20. Y.Z. Wan et al., "Moisture sorption and mechanical degradation of VARTMed Three-dimensional braided carbon-epoxy composites,” ScienceDirect. 12 Dec. 2004. Tianjin University.
21. Vanlandingham, M.R., Eduljee, R.F., Gillespie, J. W., “Moisture Diffusion in Epoxy Systems,” Journal of Applied Polymer Science, VOL. 71, (1999) pp.787-798.
22. Fan, Xuejun., “Mechanics of Moisture for Polymers: Fundamental Concepts and Model Study”, *9th. Int. Conf. on Thermal, Mechanical and Multiphysics Simulation and Experiments in Micro-Electronics and Micro-Systems*, IEEE, 2008.
23. Springer, G. S., and Shen, C. H., Journal of Comp. Matter. 1976. pp. 102
24. Dewimille, B., and Bunsell, A. R., “The modeling of hydrothermal aging in glass Fiber reinforced epoxy composites,” J. Phys. D: Appl. Phys., 15 (1982) pp. 2079-2091.
25. D. De Kee, Q. Liu, and J. Hinestroza, “Viscoelastic (Non-Fickian) Diffusion” Department of Chemical and Biomolecular Engineering and Tulane Institute for Macromolecular Engineering and Science (TIMES), Tulane University.
26. Gdoutos, E. E., K. Pilakoutas, and Chris A. Rodopoulos. Failure Analysis of Industrial Composite Materials. New York: McGraw-Hill Professional, 2000. 121-122.

27. Fabian, P.E. et al., "Novel radiation-resistant insulation systems for fusion Magnets," ScienceDirect. Fusion Engineering and Design, 61-62 (2002) 795-799

28. R. P. Reed, P.E. Fabian, J.B. Schutz. U.S. ITER Insulation Irradiation Program, Final Report, CTD Report to MIT Plasma Fusion Center, Composite Technology Developmetn, Inc. and Cryogenic Materials, Inc., August 1995

29. J.R. Kerr and J.F. Haskins, "Effects of 50,000 h of thermal aging on graphite/epoxy and graphite/polyimide composites," AIAA J., 22:96 (1982).

30. Devine, F.E., "Polyester moulding materials in automotive underbonnet environments, Composites," 14:353 (1983).

31. Karad, Sunil K., Jones, Frank R., "Mechanisms of moisture absorption by cyanate ester modified epoxy resin matrices: the clustering of water molecules," ScienceDirect. 27 Jan. 2005. University of Sheffield.

32. Rodriquez O, Fornasiero F, Arce A, Radke CJ, Prausnitz JM. Polymer 2003;44:6323.

33. Brown GL. In: Rowland SP, editor. Water in polymers. Washington, DC: American Chemical Society; 1980. p. 441.

34. Lee, S. S., Kim, S. C., "Physical Aging of Polydimethylsiloxane-Modified Epoxy Resin," Journal of Applied Polymer Science, VOL. 69 (19980 pp. 1291-1300.

35. Cinquin, J., and Abjean, P., Proceedings of 38th International SAMPE Symposium, (1993) pp. 1539.

36. Kasehagen, L.J., Haury, I., Macosko, C.W., Shimp, D. A., "Hydrolosis and Blistering of Cyanate Ester Networks," Journal of Applied Polymer Science, Vol. 64. (1997) pp. 107-113.
37. Shimp, D. A., and Ising, S. J., 35th Int. SAMPE Symposium and Exhibition. 35, (1990) pp. 1045.
38. ASTM Test Standard ASTM E 104-02, "Standard Practice for Maintaining Constant Relative Humidity by Means of Aqueous Solutions," ASTM International, West Conshohocken, PA, 2000.
39. ASTM Test Standard D 5229/D 5229M-92, "Standard Test Method for Moisture Absorption Properties and Equilibrium Conditioning of Polymer Matrix Composite Materials," ASTM International, West Conshohocken, PA, 2000.
40. ASTM Test Standard D2344/D2344M-00e1, "Standard Test Method for Short-Beam Shear Strength of Polymer Matrix Composite Materials and Their Laminates," ASTM International, West Conshohocken, PA, 2000.
41. ASTM Test Standard D2344/D2344M-00e1, "Standard Test Method for Compressive Properties of Rigid Plastics," ASTM International, West Conshohocken, PA, 2000.
42. ASTM Test Standard D149-81, "Standard Test Method for Dielectric Breakdown Voltage and Dielectric Strength of Solid Electrical Insulating Materials at Commercial Power Frequencies," ASTM International, West Conshohocken, PA, 2000.

43. ASTM Test Standard D3755-79, "Standard Test Method for Dielectric Breakdown Voltage and Dielectric Strength of Solid Electrical Insulating Materials Under Direct-Voltage Stress," ASTM International, West Conshohocken, PA, 2000.

44. Daniels, Carole A. Polymers : Structure and Properties. New York: C R C P LLC, 1989. 34-35.

45. Winkeler, Mark. "A Review of Electrical Tests for Insulating Resins," P.D. George Company. http://ieeexplore.ieee.org/iel2/855/5322/00208222.pdf

46. Edward R. Salmon,"Dielectric Strength of an Insulation Material - Is It a Constant?" Electrical Insulation Magazine, Vol. 5, No. 1, pp. 36-38, January/February 1989.

47. Discussions with Matthew W. Hooker, Ph.D. Senior Program Manager. Composite Technology Development.

48. J.A. Rice, C.S. Hazelton, and P.E. Fabian, "Reduction in the Thermal Contraction of Hybrid Ceramic Insulated Composite Stacks," Advances in Cryogenic Engineering - Materials, Vol.48, pp. 237-244, 2002.

49. Discussions with Jennifer K. Walsh, Ph.D. Senior Engineer. Composite Technology Development.

50. Discussions with Samuel Grandlienard, Ph.D. Mechanical Engineer. Composite Technology Development.

51. Discussions with Madhu S. Madhukar, Ph.D. Associate Professor. University Of Tennessee.

52 John Ivan, J. Gonzales, Manolo G. Mena, "Moisture and Thermal Degradation of Cyanate-ester-based Die Attach Material", *Electronic Composite and Technology Conference*, IEEE, 1997, pp. 525-535

53. http://web.utk.edu/~qps

54. Crank, J., 1956, *The Mathematics of Diffusion*, Clarendon Press, Oxford.

APPENDICES

Figure A.1 Constant relative humidity aging in sealed jars

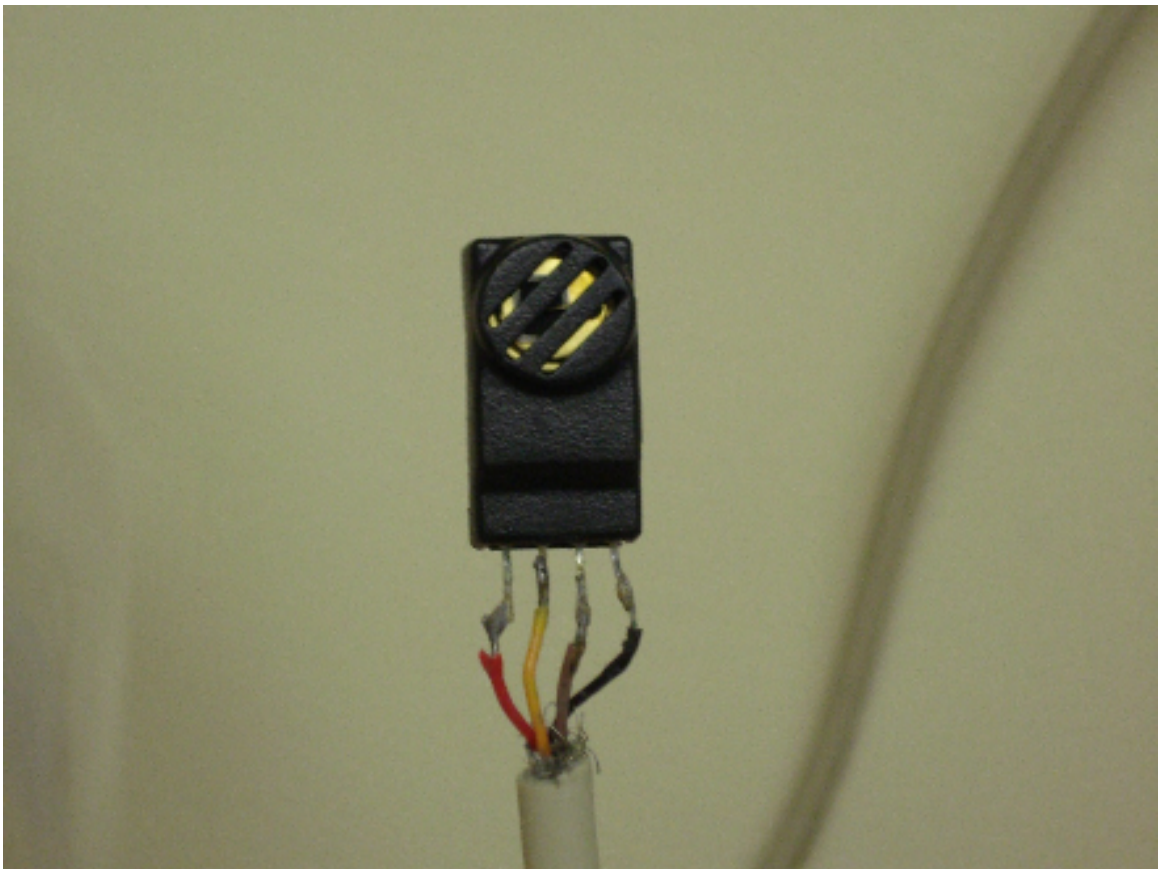

Figure A.2 HS-2000D humidity gauge used in testing

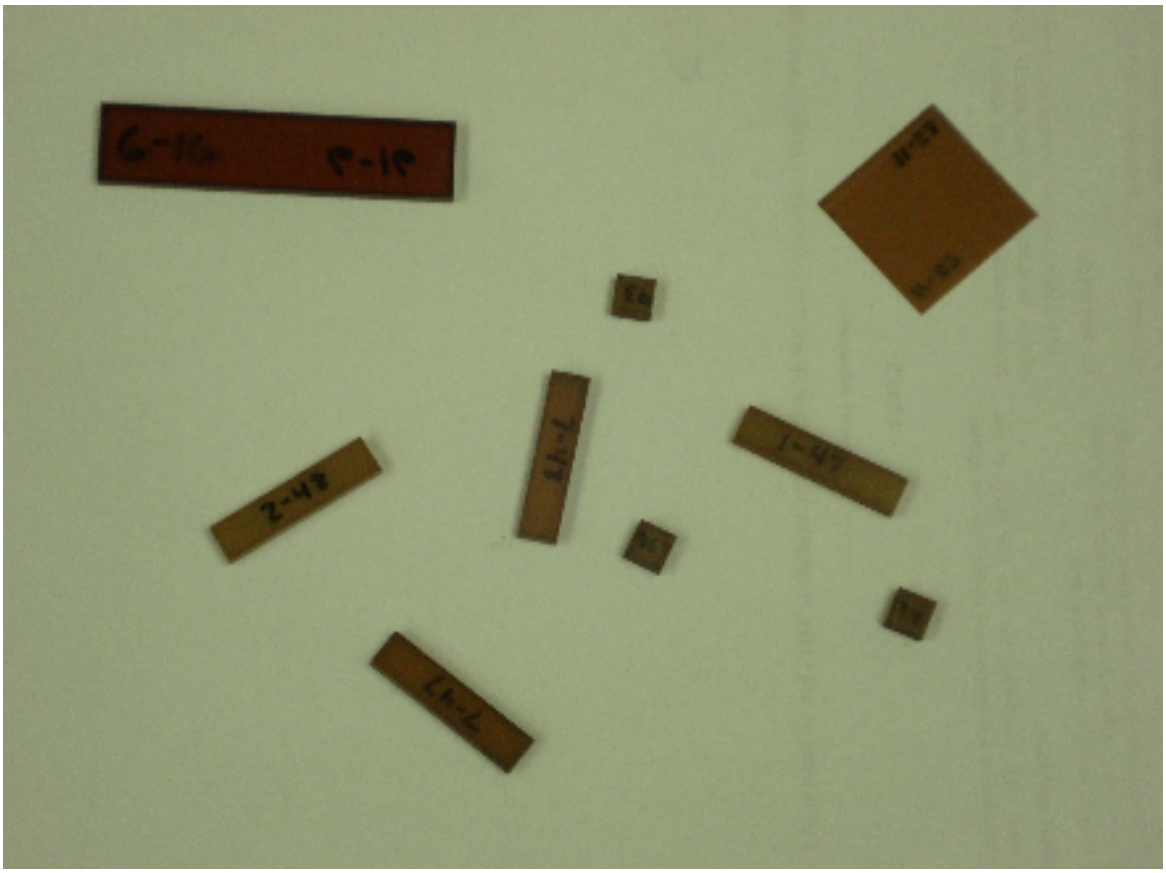

Figure A.3 Various specimens after 4 months of exposure

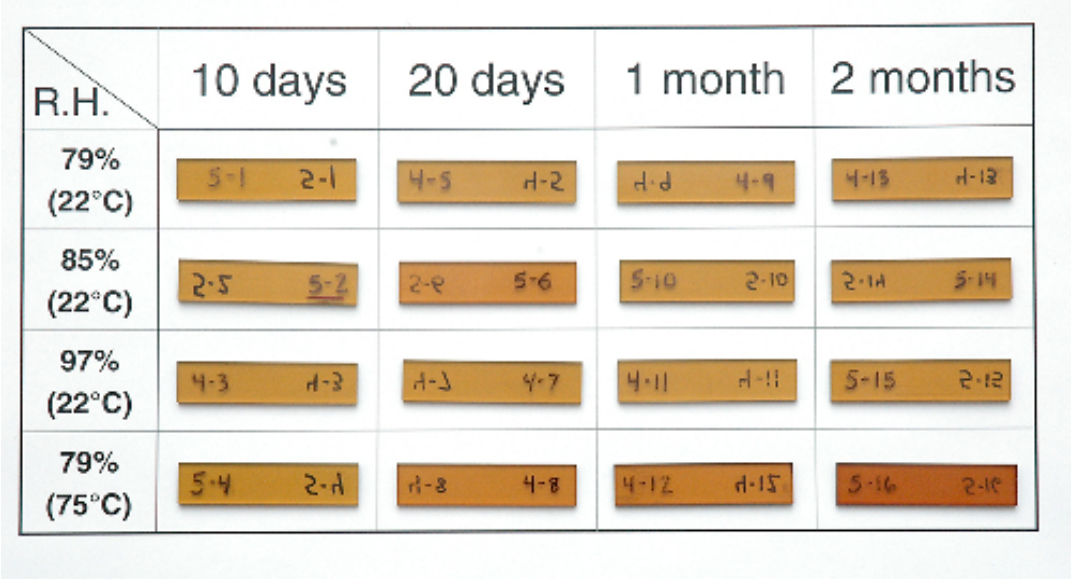

Figure A.4 Discoloration effect of elevated temperature specimens after 2 months of exposure

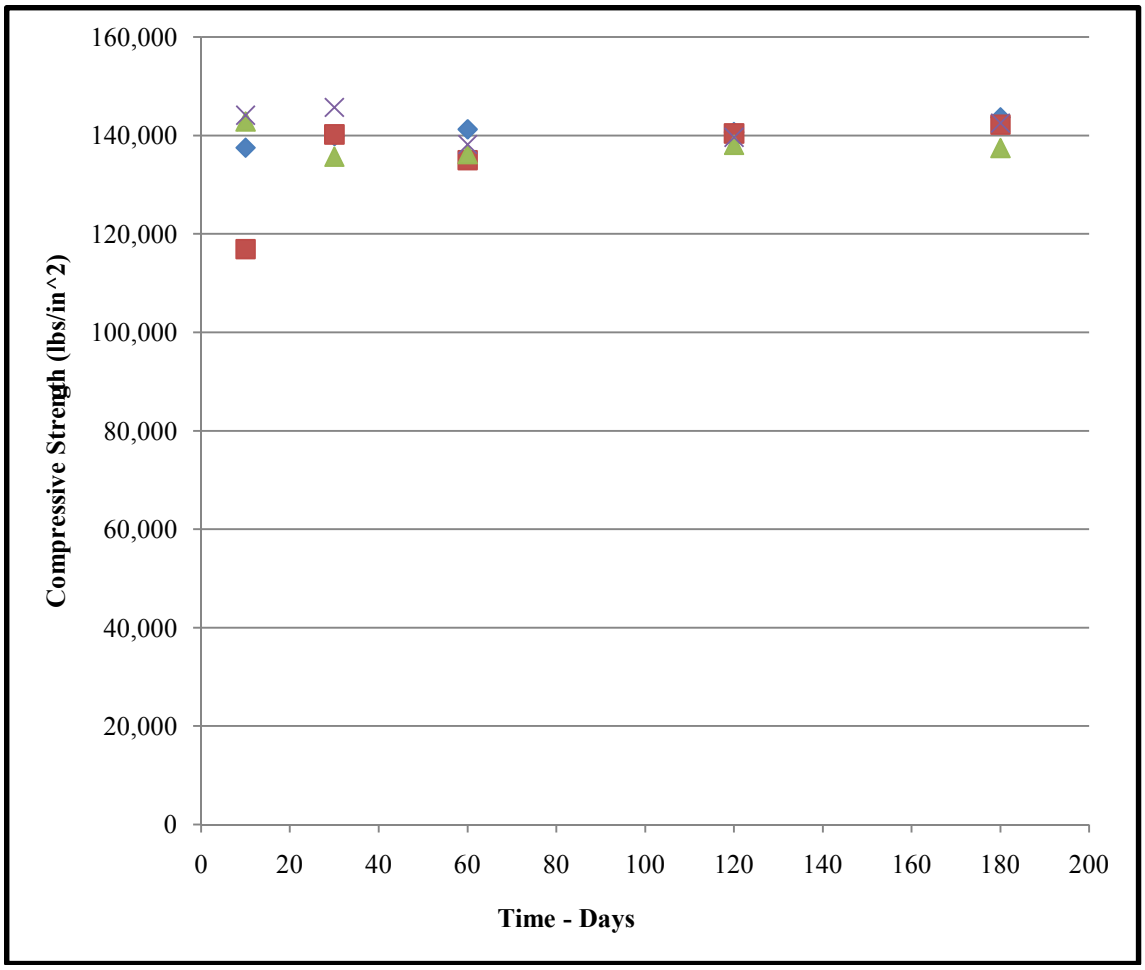

Figure A.5 Compressive strength data scatter for the 79% RH specimens

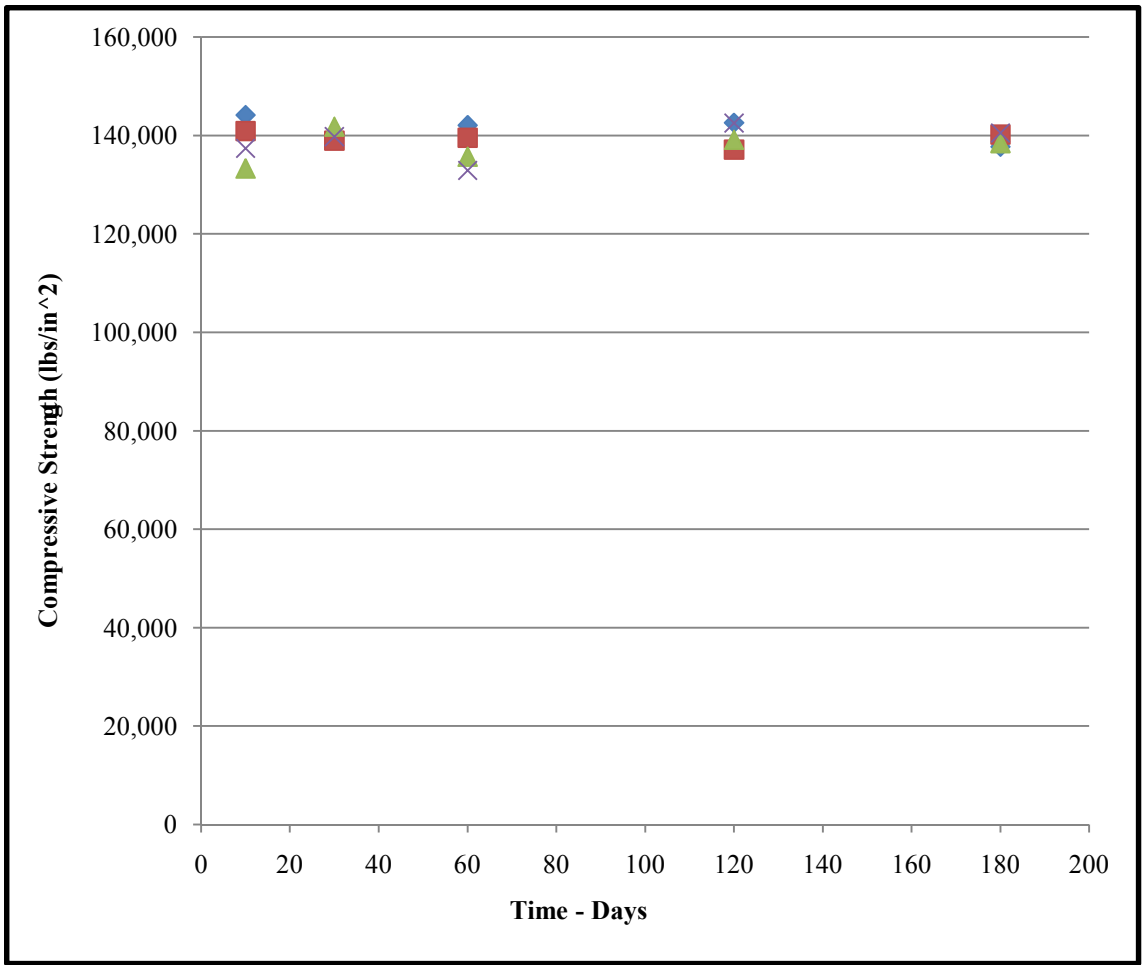

Figure A.6 Compressive strength data scatter for the 85% RH specimens

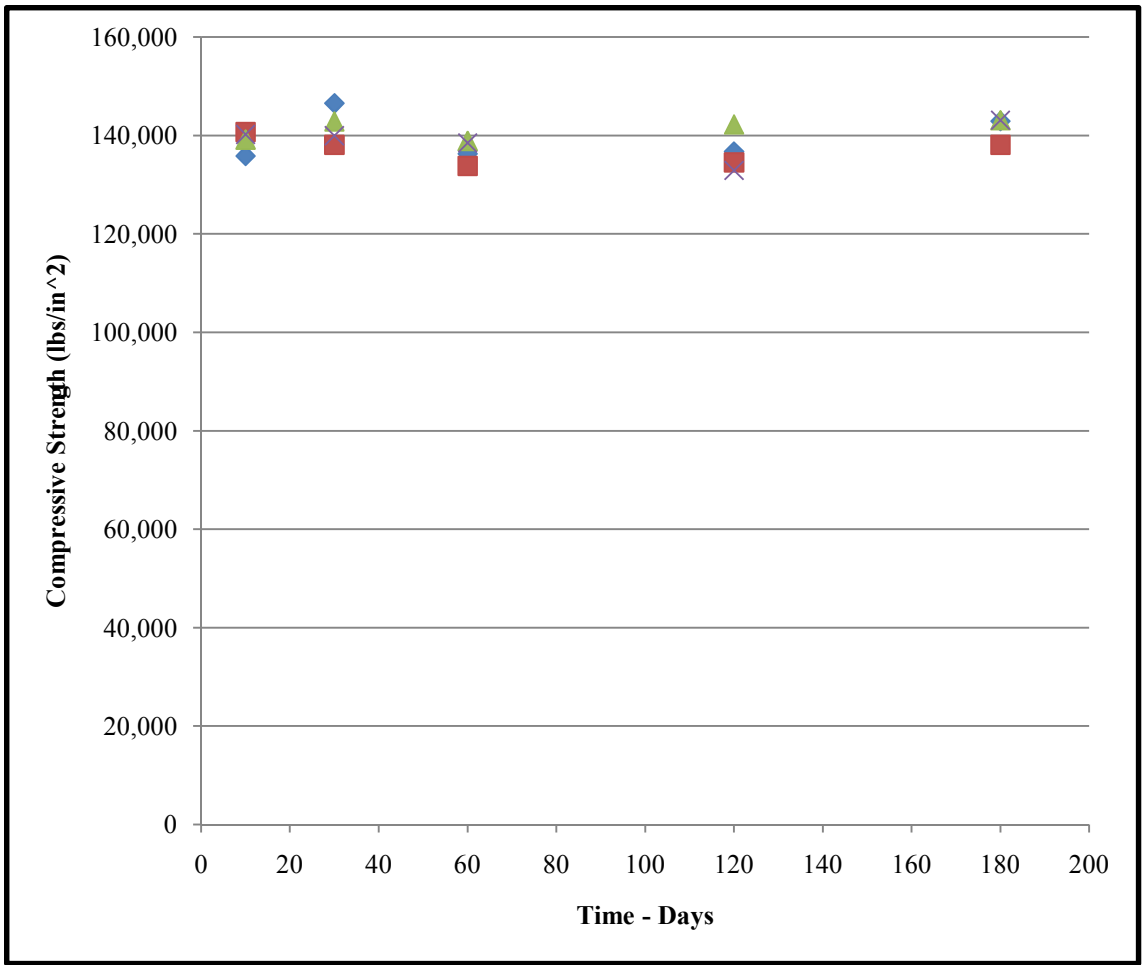

Figure A.7 Compressive strength data scatter for the 97% RH specimens

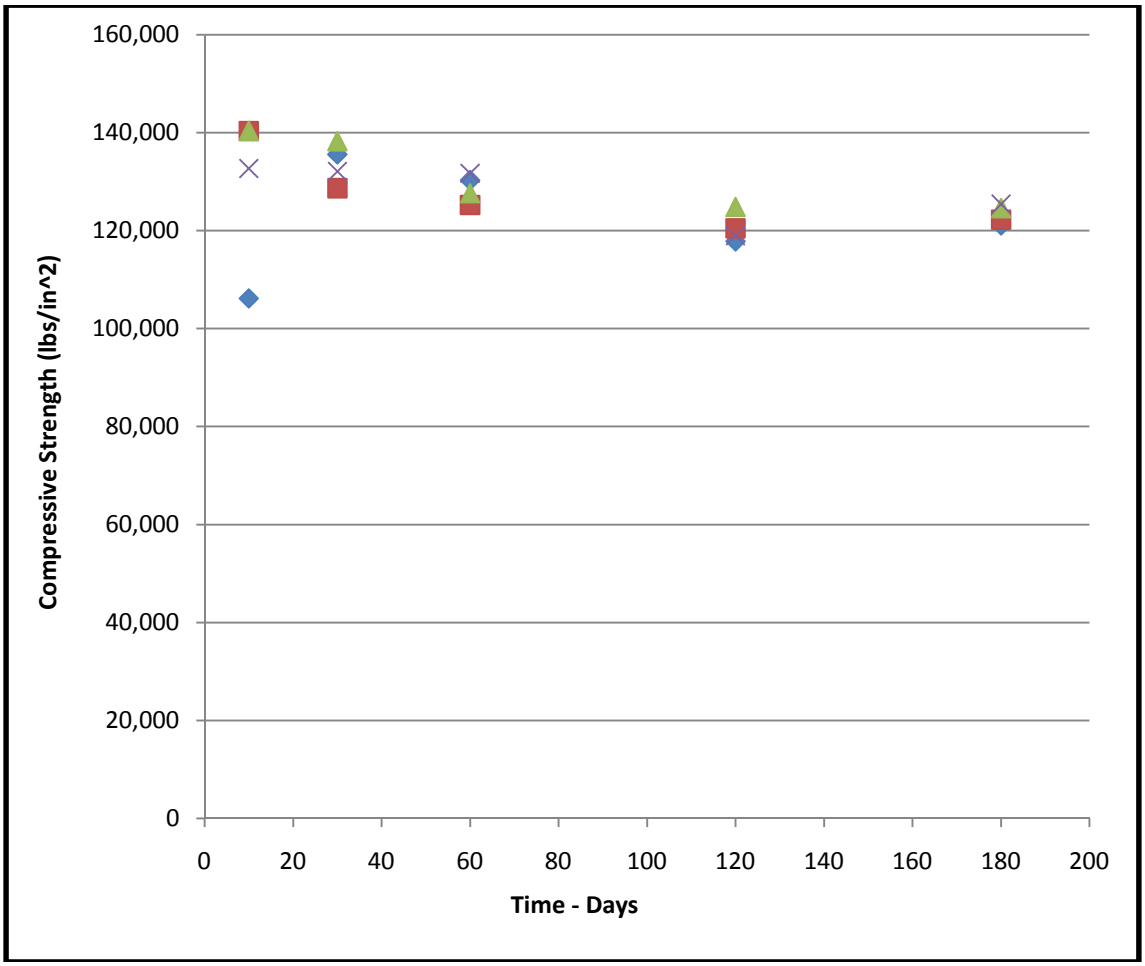

Figure A.8 Compressive strength data scatter for the 79% RH 75°C specimens

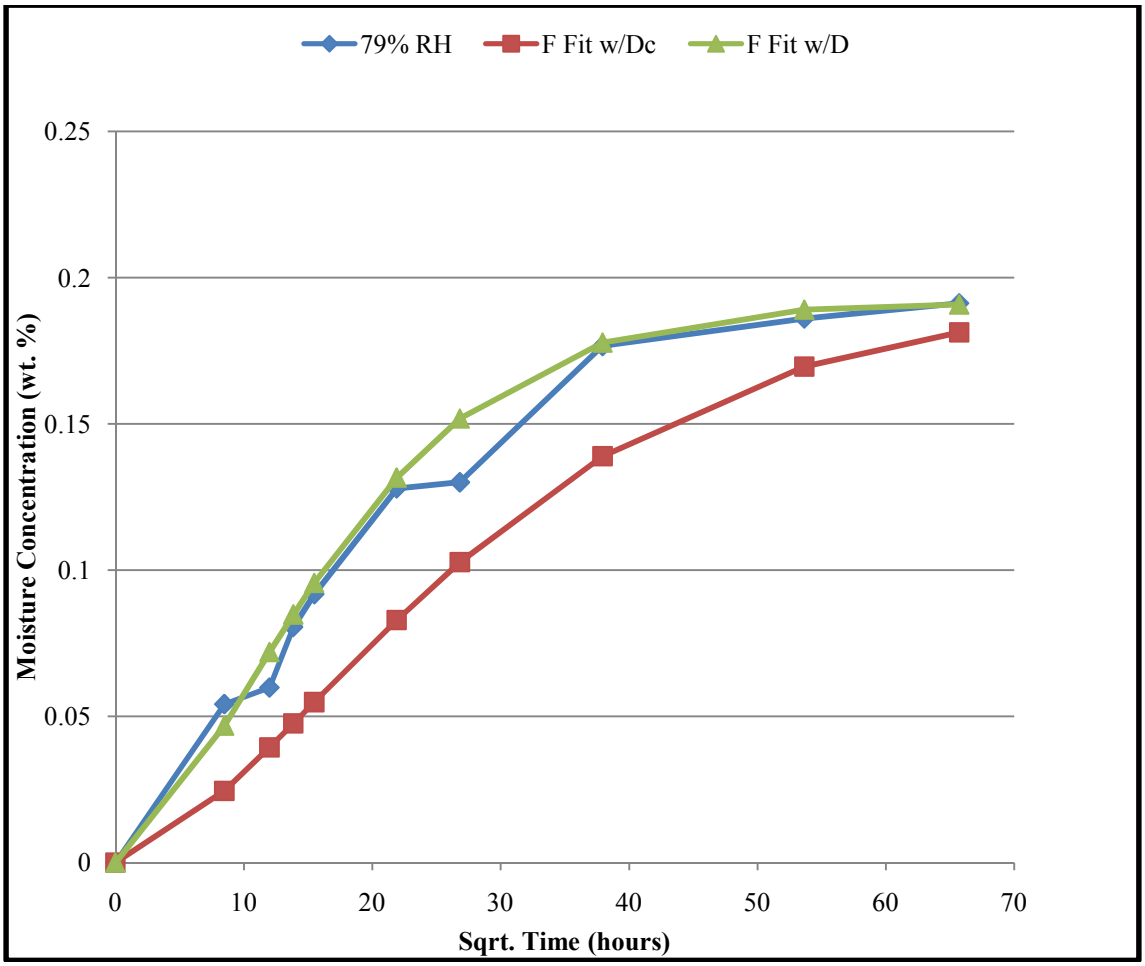

Figure A.9 Insulation Specimen Fickian curve fit at 79% RH using the diffusion coefficient and the corrected diffusion coefficient. The figure shows greater than 2% deviation from true Fickian behavior.

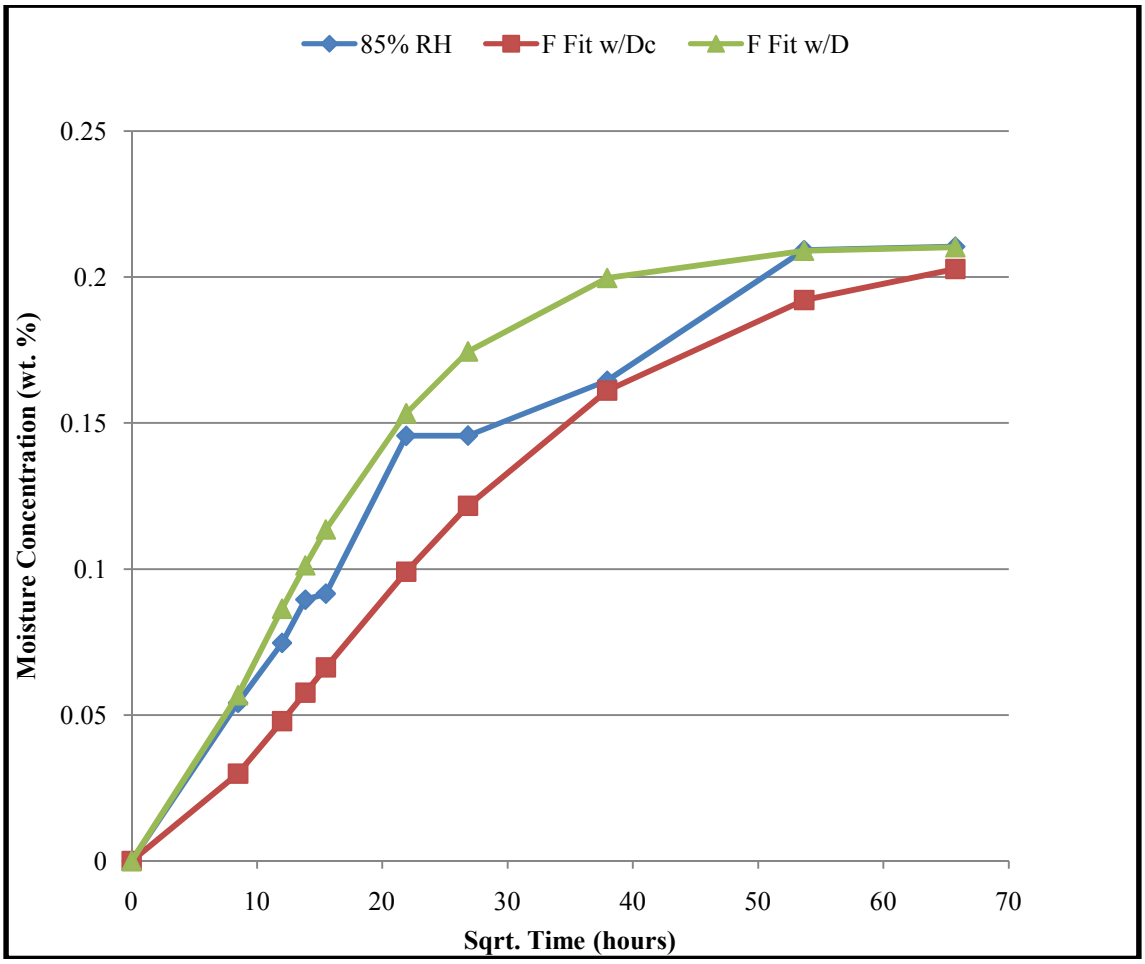

Figure A.10 Insulation Specimen Fickian curve fit at 85% RH using the diffusion coefficient and the corrected diffusion coefficient. The figure shows greater than 2% deviation from true Fickian behavior.

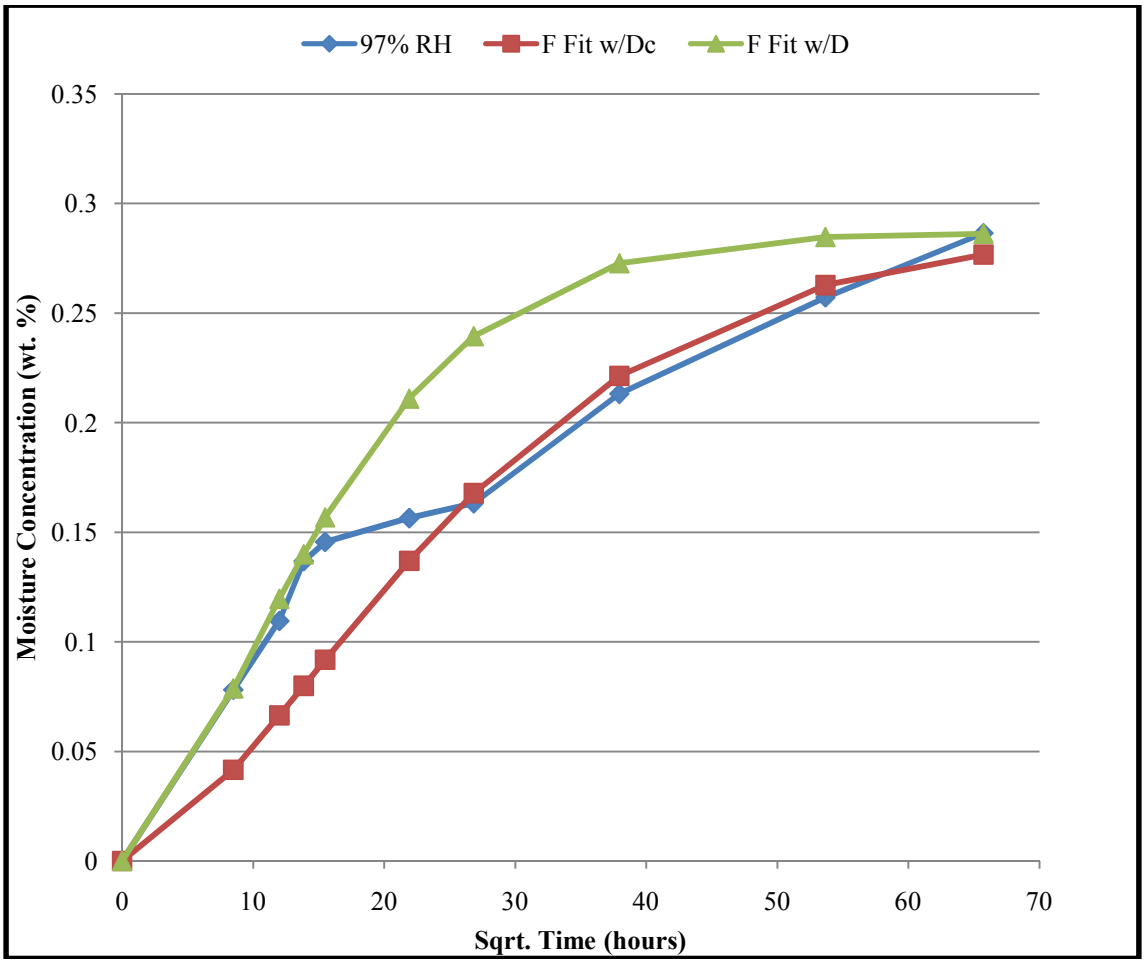

Figure A.11 Insulation Specimen Fickian curve fit at 97% RH using the diffusion coefficient and the corrected diffusion coefficient. The figure shows greater than 2% deviation from true Fickian behavior.

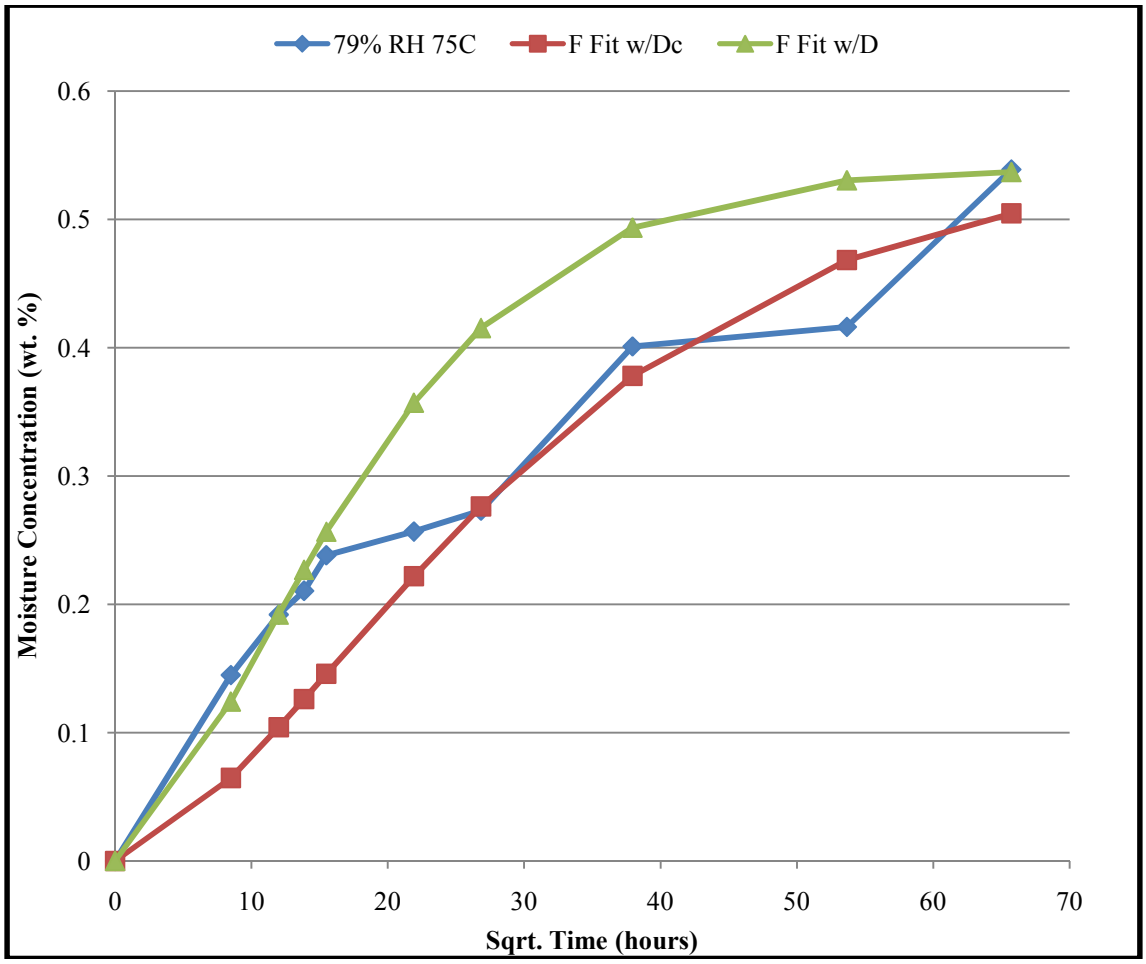

Figure A.12 Insulation Specimen Fickian curve fit at 79% RH 75°C using the diffusion coefficient and the corrected diffusion coefficient. The figure shows greater than 2% deviation from true Fickian behavior.

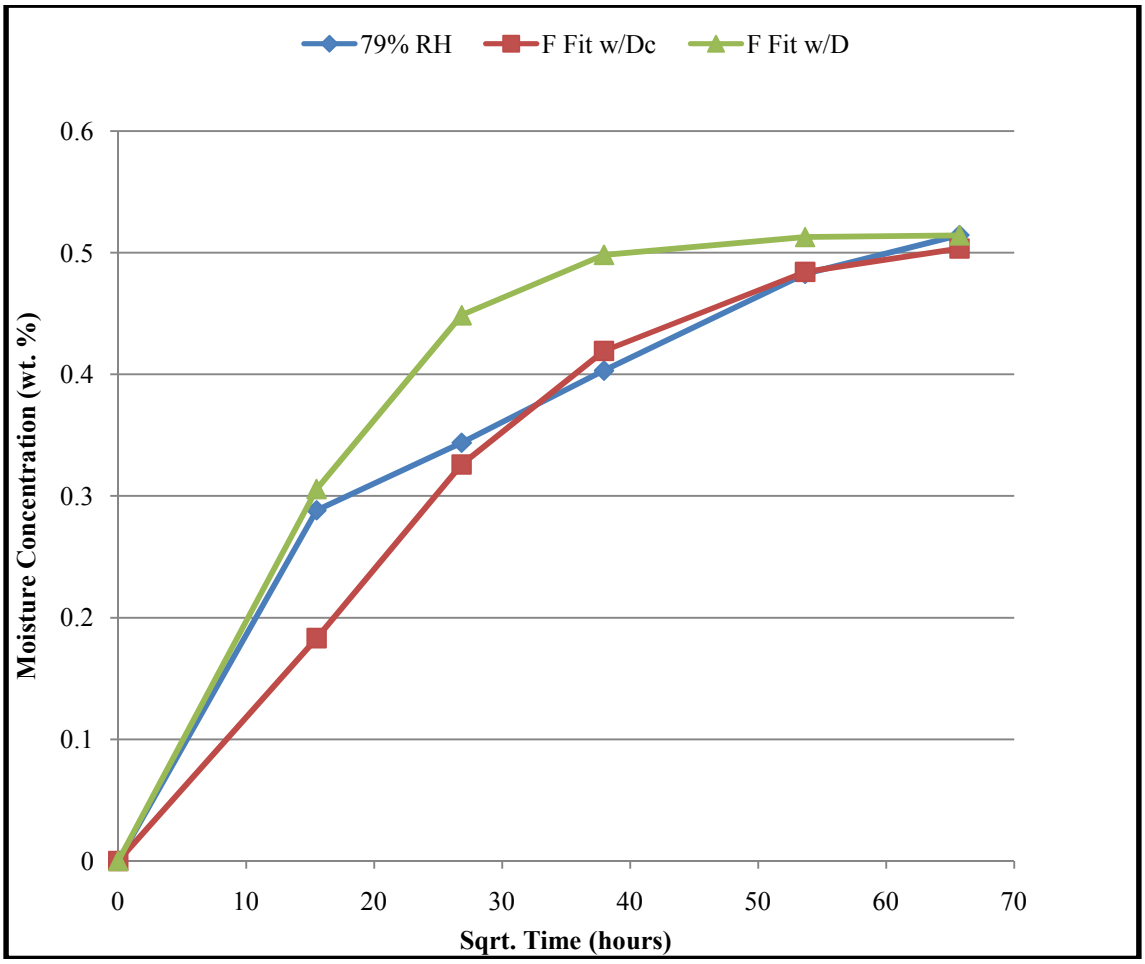

Figure A.13 Neat Resin Specimen Fickian curve fit at 79% RH using the diffusion coefficient and the corrected diffusion coefficient. The figure shows greater than 2% deviation from true Fickian behavior.

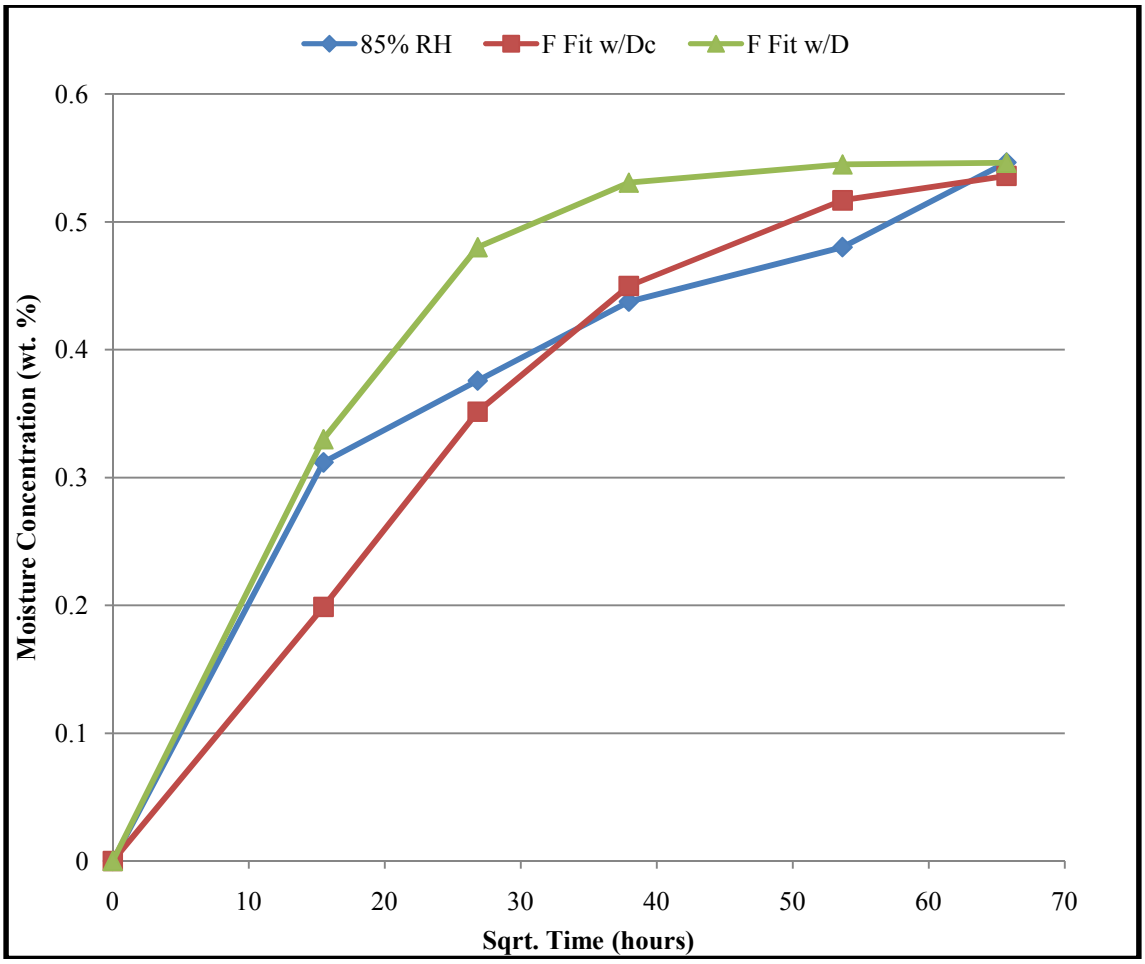

Figure A.14 Neat Resin Specimen Fickian curve fit at 85% RH using the diffusion coefficient and the corrected diffusion coefficient. The figure shows greater than 2% deviation from true Fickian behavior.

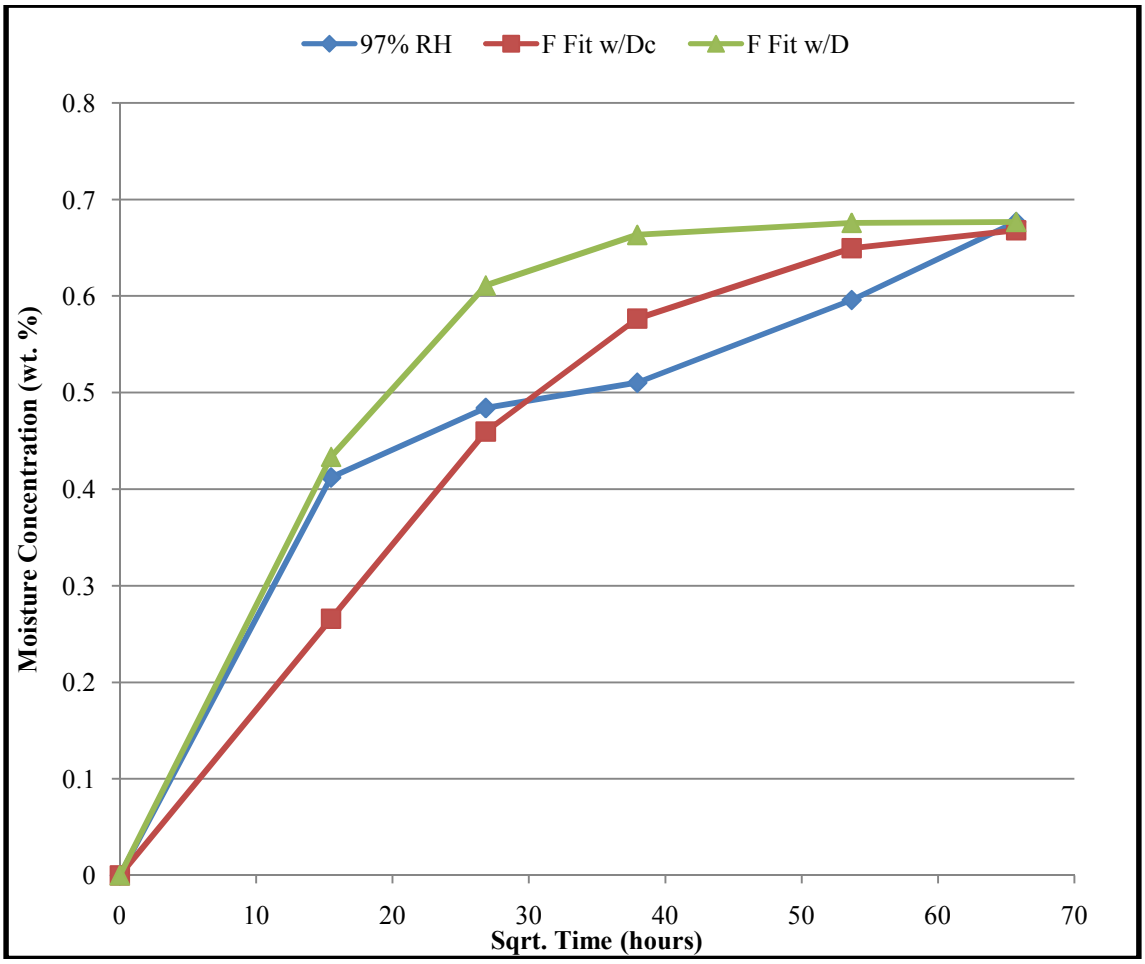

Figure A.15 Neat Resin Specimen Fickian curve fit at 97% RH using the diffusion coefficient and the corrected diffusion coefficient. The figure shows greater than 2% deviation from true Fickian behavior.

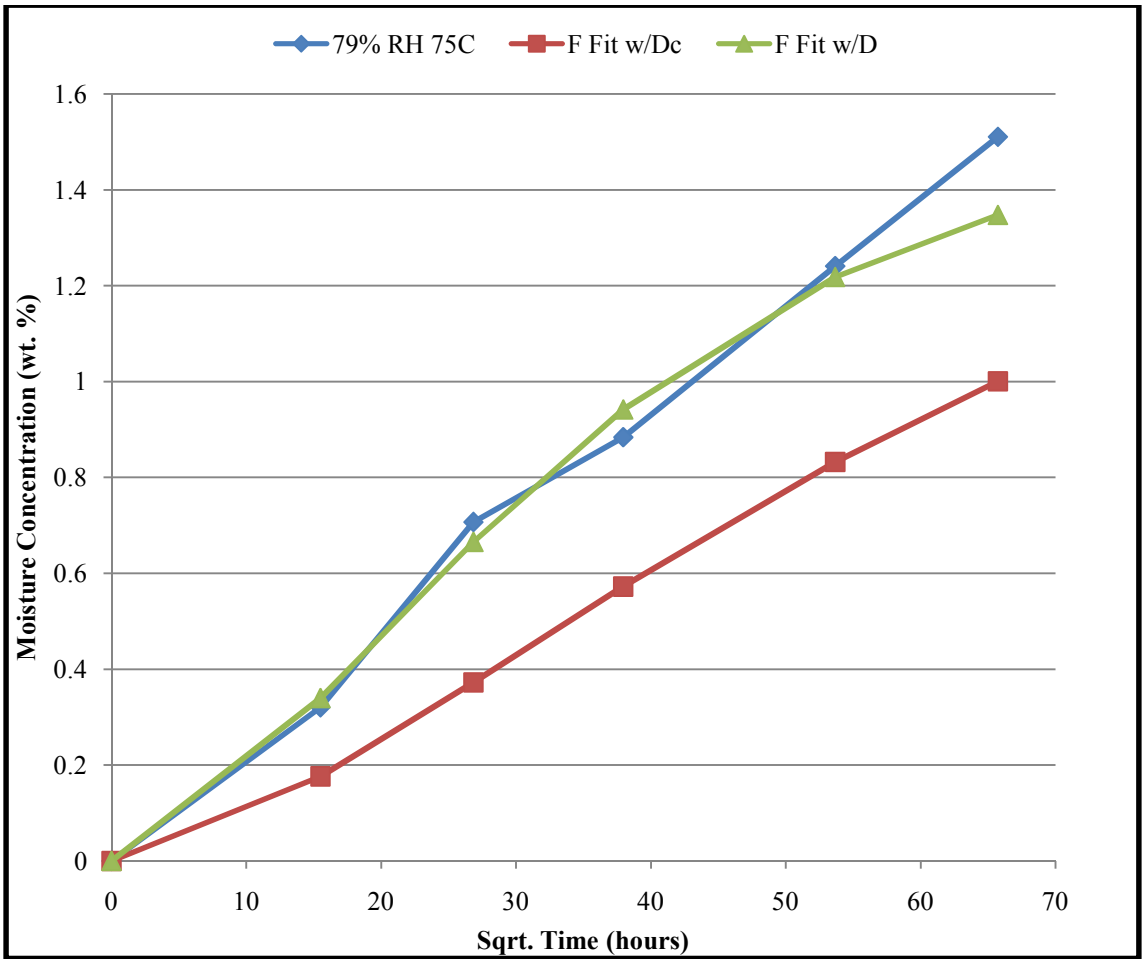

Figure A.16 Neat Resin Specimen Fickian curve fit at 79% RH 75°C using the diffusion coefficient and the corrected diffusion coefficient. The figure shows greater than 2% deviation from true Fickian behavior.

VITA

Brad Morgan was born on October 12th, 1984 in Cincinnati, Ohio. He was raised in Jackson, Tennessee, where he attended the University School of Jackson from 1st grade through high school, except for 5th and 6th grade where he attended the International School of Brussels in Brussels, Belgium. Upon graduation, he entered the Mechanical Engineering program at the University of Tennessee. During his four year study, Brad worked as an intern at Pictsweet and General Electric. Brad graduated Cum Laude May 2007 with a degree in Mechanical Engineering. He began his graduate studies in Mechanical Engineering August 2007, where he concentrated on machine design as well as polymer research. He worked as a graduate research assistant for Dr. Madhu S. Madhukar at the Magnet Development Lab on the Quasi-Poloidal Stellarator project, which is jointly carried by the Oak Ridge National Laboratory researchers and UT engineers, from May 2007 until graduation. He also worked at Procter and Gamble during his graduate studies as an intern during the summer of 2008. He will be graduating Magna Cum Laude December 2008 with his Masters of Science in Mechanical Engineering. He has accepted a job at Procter and Gamble in Cincinnati, Ohio.